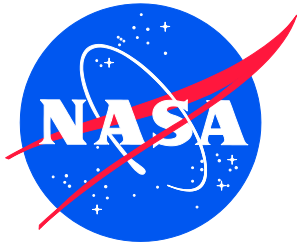


NASA/CR–2018-219800/Volume II



Methodologies for Verification and Validation of Space Launch System (SLS) Structural Dynamic Models

Appendices

Robert N. Coppolino
Measurement Analysis Corporation, Reston, Virginia

January 2018

NASA STI Program . . . in Profile

Since its founding, NASA has been dedicated to the advancement of aeronautics and space science. The NASA scientific and technical information (STI) program plays a key part in helping NASA maintain this important role.

The NASA STI program operates under the auspices of the Agency Chief Information Officer. It collects, organizes, provides for archiving, and disseminates NASA's STI. The NASA STI program provides access to the NTRS Registered and its public interface, the NASA Technical Reports Server, thus providing one of the largest collections of aeronautical and space science STI in the world. Results are published in both non-NASA channels and by NASA in the NASA STI Report Series, which includes the following report types:

- **TECHNICAL PUBLICATION.** Reports of completed research or a major significant phase of research that present the results of NASA Programs and include extensive data or theoretical analysis. Includes compilations of significant scientific and technical data and information deemed to be of continuing reference value. NASA counter-part of peer-reviewed formal professional papers but has less stringent limitations on manuscript length and extent of graphic presentations.
- **TECHNICAL MEMORANDUM.** Scientific and technical findings that are preliminary or of specialized interest, e.g., quick release reports, working papers, and bibliographies that contain minimal annotation. Does not contain extensive analysis.
- **CONTRACTOR REPORT.** Scientific and technical findings by NASA-sponsored contractors and grantees.

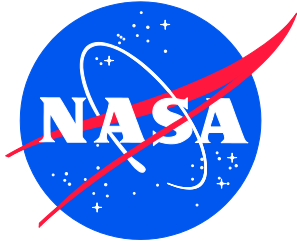
- **CONFERENCE PUBLICATION.** Collected papers from scientific and technical conferences, symposia, seminars, or other meetings sponsored or co-sponsored by NASA.
- **SPECIAL PUBLICATION.** Scientific, technical, or historical information from NASA programs, projects, and missions, often concerned with subjects having substantial public interest.
- **TECHNICAL TRANSLATION.** English-language translations of foreign scientific and technical material pertinent to NASA's mission.

Specialized services also include organizing and publishing research results, distributing specialized research announcements and feeds, providing information desk and personal search support, and enabling data exchange services.

For more information about the NASA STI program, see the following:

- Access the NASA STI program home page at <http://www.sti.nasa.gov>
- E-mail your question to help@sti.nasa.gov
- Phone the NASA STI Information Desk at 757-864-9658
- Write to:
NASA STI Information Desk
Mail Stop 148
NASA Langley Research Center
Hampton, VA 23681-2199

NASA/CR–2018-219800/Volume II



Methodologies for Verification and Validation of Space Launch System (SLS) Structural Dynamic Models

Appendices

Robert N. Coppolino
Measurement Analysis Corporation, Reston, Virginia

National Aeronautics and
Space Administration

Langley Research Center
Hampton, Virginia 23681-2199

Prepared for Langley Research Center
under Contract NNL12AA09C

January 2018

The use of trademarks or names of manufacturers in the report is for accurate reporting and does not constitute an official endorsement, either expressed or implied, of such products or manufacturers by the National Aeronautics and Space Administration.

Available from:

NASA Center for AeroSpace Information
7115 Standard Drive
Hanover, MD 21076-1320
443-757-5802

Table of Contents

Appendix A. Launch Vehicle Propellant Tank Hydroelastic Analysis (1976-2016)	1
Appendix B. Review and Recommendations regarding NESC-RP-14-00946	30
Appendix C. Evaluation of ISPE Model Sensitivities	40
Appendix D. Consolidation of Body Modes for an “Axisymmetric” Shell Structure	147
Appendix E. Verification of Experimental Modes (<i>ISPE case study using SFD modes</i>).....	187

Appendix A. Launch Vehicle Propellant Tank Hydroelastic Analysis (1976-2016)

Appendix A:
Launch Vehicle Propellant Tank
Hydroelastic Analysis (1976-2016)

Robert N. Coppolino, Consultant

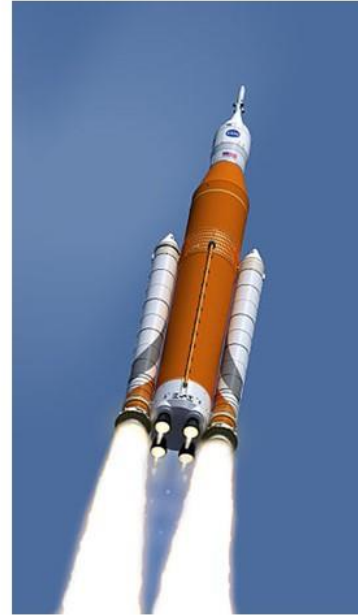
14 October 2016

Contents

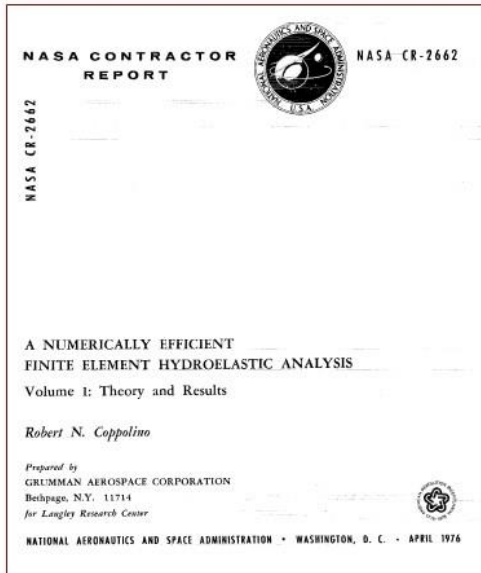
1. Introduction
2. Mathematical Foundations
3. Dynamic Behavior of Propellant Tanks
4. Efficient Hydroelastic Tank Analysis
5. Concluding Remarks

The Hydroelastic Launch Vehicle

- Typical liquid propellant launch vehicle mass distribution is ~80% fluid mass (full tanks)
- Fluid behavior in frequency band of interest is typically incompressible (except SLS, others)
- Three classes of hydroelastic normal modes
 - Slosh (low frequency, rigid structure)
 - Body (mid frequency, axial, bending, bulge)
 - Shell breathing (mid frequency, numerous!)
- Hydroelasticity plays a key role in L/V POGO
 - Propellant tank dynamics (present discussion)
 - Feedsystem (propellant line) dynamics
 - POGO suppression components



NASA CR-2662 and Subsequent Developments



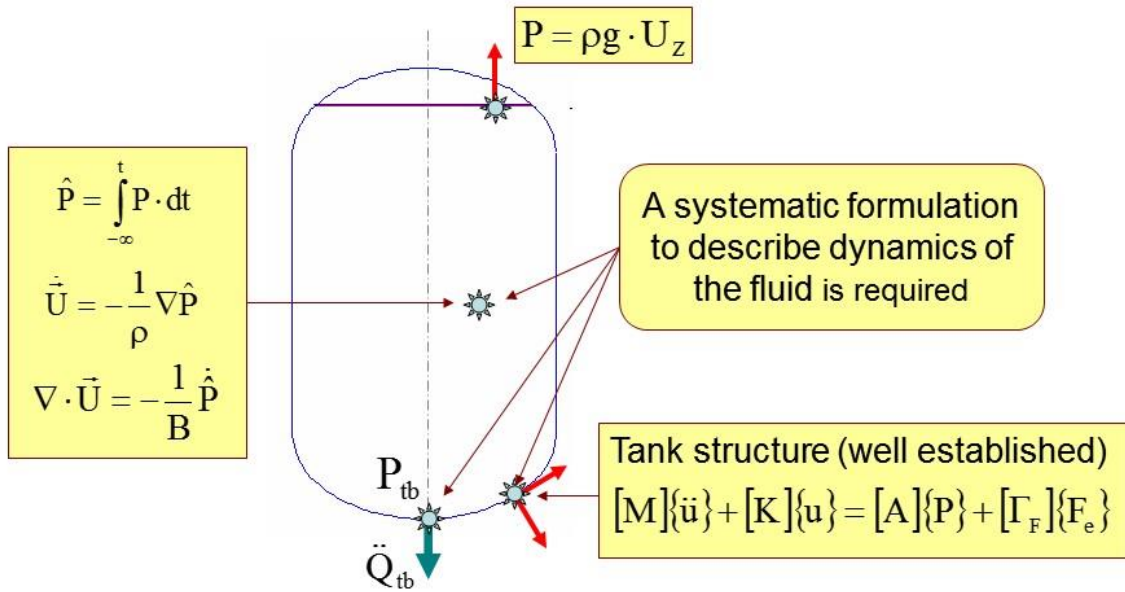
- **COSMIC NASTRAN DMAP (1976)**
- *MSC NASTRAN Code (1988)*
- *UAI NASTRAN Code (1999)*
- *Implementations by ATA & Others*
- *Current Thoughts & Suggestions*

- **Complementary Energy Principles**
- **Symmetric Matrix Formulations**
- **Model Order Reduction Strategies**
- *Selection of Significant Modes*
- *Effective, Efficient Dynamic Models*

Contents

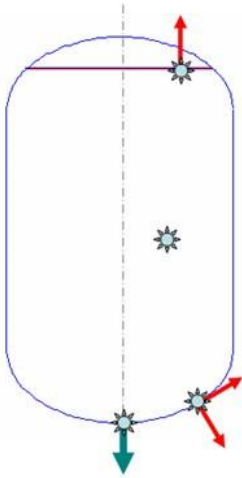
1. Introduction
2. Mathematical Foundations
3. Dynamic Behavior of Propellant Tanks
4. Efficient Hydroelastic Tank Analysis
5. Concluding Remarks

Inviscid Fluid (small displacement)



Inviscid Fluid

(based on Toupin's variational principle, 1952)



$$T_c = \frac{1}{2} \int_V \rho \cdot (\dot{\vec{U}} \cdot \dot{\vec{U}}) \cdot dV = \frac{1}{2} \int_V \frac{1}{\rho} \cdot (\nabla \hat{P} \cdot \nabla \hat{P}) \cdot dV$$

$$U_c = \frac{1}{2} \int_V B \cdot (\nabla \cdot \vec{U})^2 \cdot dV = \frac{1}{2} \int_V \frac{1}{B} \cdot (\hat{P})^2 \cdot dV$$

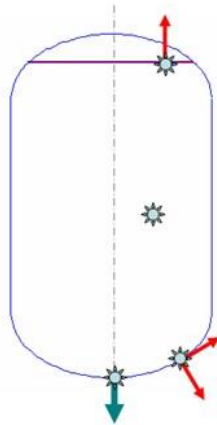
$$\delta W_c = \int_A \delta \dot{U}_n \hat{P} \cdot dA$$

$$\int_{-\infty}^{t_1} (\delta T_c - \delta U_c + \delta W_c) \cdot dt = 0$$

$$[C]\{\ddot{P}\} + [S]\{P\} = -[A]^T \{\ddot{U}\} - [\Gamma_Q] \ddot{Q}_{tb}$$

Fluid-Structure Interaction Equations

(Zienkiewicz, Herting, Cosmic Nastran)



$$\begin{bmatrix} \mathbf{M} & \mathbf{0} \\ \mathbf{A}^T & \mathbf{C} \end{bmatrix} \begin{Bmatrix} \ddot{\mathbf{U}} \\ \ddot{\mathbf{P}} \end{Bmatrix} + \begin{bmatrix} \mathbf{K} & -\mathbf{A} \\ \mathbf{0} & \mathbf{S} \end{bmatrix} \begin{Bmatrix} \mathbf{U} \\ \mathbf{P} \end{Bmatrix} = \begin{bmatrix} \Gamma_F & \mathbf{0} \\ \mathbf{0} & -\Gamma_Q \end{bmatrix} \begin{Bmatrix} \mathbf{F}_e \\ \ddot{\mathbf{Q}}_{tb} \end{Bmatrix}$$

- Unconventional, non-symmetric matrix equations
- Sparse $[\mathbf{M}]$, $[\mathbf{K}]$, $[\mathbf{C}]$, $[\mathbf{S}]$, $[\mathbf{A}]$ matrices
- Computationally difficult modal analysis (early 1970's)
- Re-cast for conventional modal analysis (1976-2016)
- Incompressible & compressible fluid forms

Fluid-Structure Interaction Equations

(Symmetric Incompressible Fluid, NASA CR-2662)



$$[C]\{\dot{\mathbf{P}}\} + [S]\{\mathbf{P}\} = -[A]^T \{\ddot{\mathbf{U}}\} - [\Gamma_Q] \ddot{\mathbf{Q}}_{tb}$$

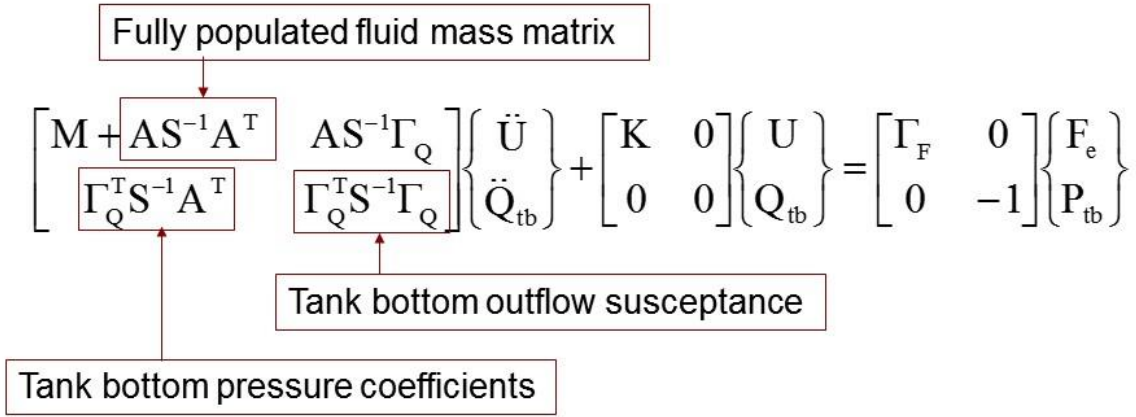
$$\{\mathbf{P}\} = -[S^{-1}A^T] \{\ddot{\mathbf{U}}\} - [S^{-1}\Gamma_Q] \ddot{\mathbf{Q}}_{tb}$$

$$\mathbf{P}_{tb} = [\Gamma_Q^T] \{\mathbf{P}\} = -[\Gamma_Q^T S^{-1} A^T] \{\ddot{\mathbf{U}}\} - [\Gamma_Q^T S^{-1} \Gamma_Q] \ddot{\mathbf{Q}}_{tb}$$

$$\begin{bmatrix} \mathbf{M} + \mathbf{A}\mathbf{S}^{-1}\mathbf{A}^T & \mathbf{A}\mathbf{S}^{-1}\mathbf{\Gamma}_Q \\ \mathbf{\Gamma}_Q^T\mathbf{S}^{-1}\mathbf{A}^T & \mathbf{\Gamma}_Q^T\mathbf{S}^{-1}\mathbf{\Gamma}_Q \end{bmatrix} \begin{Bmatrix} \ddot{\mathbf{U}} \\ \ddot{\mathbf{Q}}_{tb} \end{Bmatrix} + \begin{bmatrix} \mathbf{K} & \mathbf{0} \\ \mathbf{0} & \mathbf{0} \end{bmatrix} \begin{Bmatrix} \mathbf{U} \\ \mathbf{Q}_{tb} \end{Bmatrix} = \begin{bmatrix} \mathbf{\Gamma}_F & \mathbf{0} \\ \mathbf{0} & -\mathbf{1} \end{bmatrix} \begin{Bmatrix} \mathbf{F}_e \\ \mathbf{P}_{tb} \end{Bmatrix}$$

Fluid-Structure Interaction Equations

(Symmetric Incompressible Fluid, NASA CR-2662)



- Matrix equation set conforms to conventional structural dynamics
 - special operations required due to generally singular $[S]$
- Accommodates definition of a modal component
 - with consistent interface partitions for connection to the L/V feedsystem.

Fluid-Structure Interaction Equations (Symmetric Compressible Fluid, 2016)

Introduce the generalized volume strain variable, $[C]\{P\} = \{V\}$

$$\{P\} = [C^{-1}]\{V\} = -[S^{-1}A^T]\{\ddot{U}\} - [S^{-1}]\{\ddot{V}\} - [S^{-1}\Gamma_Q]\ddot{Q}_{tb}$$

$$P_{tb} = [\Gamma_Q^T]\{P\} = -[\Gamma_Q^T S^{-1} A^T]\{\ddot{U}\} - [\Gamma_Q^T S^{-1}]\{\ddot{V}\} - [\Gamma_Q^T S^{-1} \Gamma_Q]\ddot{Q}_{tb}$$

$$\begin{bmatrix} M + AS^{-1}A^T & AS^{-1} & AS^{-1}\Gamma_Q \\ S^{-1}A^T & S^{-1} & S^{-1}\Gamma_Q \\ \Gamma_Q^T S^{-1}A^T & \Gamma_Q^T S^{-1} & \Gamma_Q^T S^{-1}\Gamma_Q \end{bmatrix} \begin{Bmatrix} \ddot{U} \\ \ddot{V} \\ \ddot{Q}_{tb} \end{Bmatrix} + \begin{bmatrix} K & 0 & 0 \\ 0 & C^{-1} & 0 \\ 0 & 0 & 0 \end{bmatrix} \begin{Bmatrix} U \\ V \\ Q_{tb} \end{Bmatrix} = \begin{bmatrix} \Gamma_F & 0 \\ 0 & 0 \\ 0 & -1 \end{bmatrix} \begin{Bmatrix} F_e \\ P_{tb} \end{Bmatrix}$$

- Matrix equation set conforms to conventional structural dynamics
 - *fully populated mass matrix, potential computational inefficiencies*
- Accommodates definition of a modal component

Hydroelastic Tank Modal Analysis (general strategy)

$$\left[\begin{array}{cc|c} \mathbf{M} + \mathbf{A}\mathbf{S}^{-1}\mathbf{A}^T & \mathbf{A}\mathbf{S}^{-1} & \mathbf{A}\mathbf{S}^{-1}\mathbf{\Gamma}_Q \\ \mathbf{S}^{-1}\mathbf{A}^T & \mathbf{S}^{-1} & \mathbf{S}^{-1}\mathbf{\Gamma}_Q \\ \hline \mathbf{\Gamma}_Q^T\mathbf{S}^{-1}\mathbf{A}^T & \mathbf{\Gamma}_Q^T\mathbf{S}^{-1} & \mathbf{\Gamma}_Q^T\mathbf{S}^{-1}\mathbf{\Gamma}_Q \end{array} \right] \begin{Bmatrix} \ddot{\mathbf{U}} \\ \ddot{\mathbf{V}} \\ \ddot{\mathbf{Q}}_{tb} \end{Bmatrix} + \left[\begin{array}{cc|c} \mathbf{K} & \mathbf{0} & \mathbf{0} \\ \mathbf{0} & \mathbf{C}^{-1} & \mathbf{0} \\ \hline \mathbf{0} & \mathbf{0} & \mathbf{0} \end{array} \right] \begin{Bmatrix} \mathbf{U} \\ \mathbf{V} \\ \mathbf{Q}_{tb} \end{Bmatrix} = \begin{Bmatrix} \mathbf{\Gamma}_F & \mathbf{0} \\ \mathbf{0} & \mathbf{0} \\ \mathbf{0} & -\mathbf{1} \end{Bmatrix} \begin{Bmatrix} \mathbf{F}_e \\ \mathbf{P}_{tb} \end{Bmatrix}$$

↓ *this is like...*

$$\begin{bmatrix} \mathbf{M}_{UU} & \mathbf{M}_{UQ} \\ \mathbf{M}_{QU} & \mathbf{M}_{QQ} \end{bmatrix} \begin{Bmatrix} \ddot{\mathbf{U}} \\ \ddot{\mathbf{Q}}_{tb} \end{Bmatrix} + \begin{bmatrix} \mathbf{K}_{UU} & \mathbf{0} \\ \mathbf{0} & \mathbf{0} \end{bmatrix} \begin{Bmatrix} \mathbf{U} \\ \mathbf{Q}_{tb} \end{Bmatrix} = \begin{Bmatrix} \mathbf{F}_U \\ -\mathbf{P}_{tb} \end{Bmatrix}$$

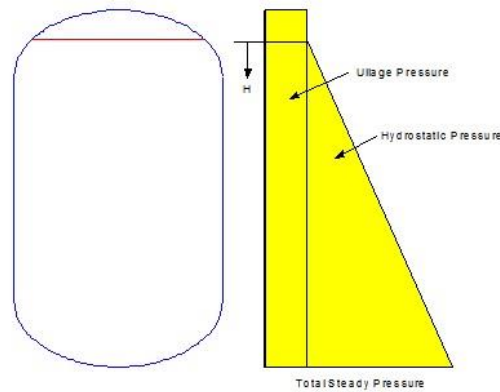
↓ $\{\mathbf{U}\} = [\mathbf{\Phi}] \{\mathbf{q}\}, [\mathbf{K}_{UU}]\{\mathbf{\Phi}\} = [\mathbf{M}_{UU}]\{\mathbf{\Phi}\}\lambda$

$$\begin{bmatrix} \mathbf{I} & \mathbf{m}_{qQ} \\ \mathbf{m}_{Qq} & \mathbf{M}_{QQ} \end{bmatrix} \begin{Bmatrix} \ddot{\mathbf{q}} \\ \ddot{\mathbf{Q}}_{tb} \end{Bmatrix} + \begin{bmatrix} \lambda & \mathbf{0} \\ \mathbf{0} & \mathbf{0} \end{bmatrix} \begin{Bmatrix} \mathbf{q} \\ \mathbf{Q}_{tb} \end{Bmatrix} = \begin{Bmatrix} \mathbf{\Phi}^T \mathbf{F}_U \\ -\mathbf{P}_{tb} \end{Bmatrix}$$

Contents

1. Introduction
2. Mathematical Foundations
3. Dynamic Behavior of Propellant Tanks
4. Efficient Hydroelastic Tank Analysis
5. Concluding Remarks

Propellant Tank Steady Load Profile (*ullage and hydrostatic pressure*)

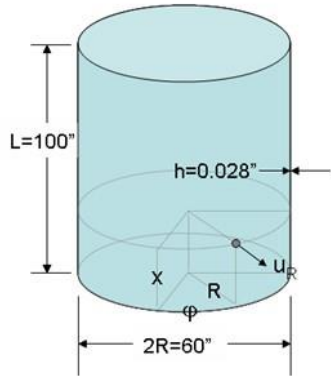


$$P_{\text{steady}} = P_{\text{ullage}} + \rho a_g H$$

- The effect of steady loading is expressed as “differential” stiffness
- Some (balloon) tank configurations have extremely thin walls
 - and “differential” stiffness from ullage pressure is necessary & dominant

Significance of Differential Stiffness

(shallow shell theory modal solution, NASA SP-106, 1966)



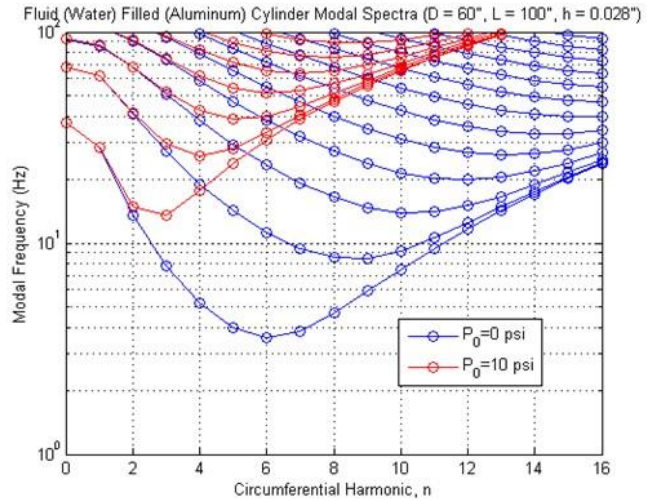
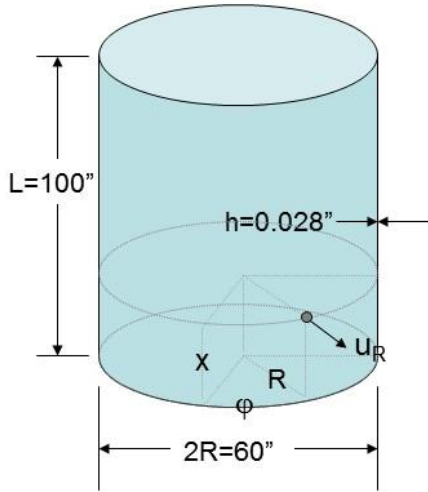
$$u_R = \sin\left(\frac{m\pi x}{L}\right) \cdot \cos(n\phi) \cdot e^{i\omega t}$$

$$m_f = \rho_f R \cdot \left[\frac{I_n\left(\frac{\pi R}{L}\right)}{\left(\frac{\pi R}{L}\right) \cdot I_n'\left(\frac{\pi R}{L}\right)} \right]$$

$$(\rho_s h + m_f) \cdot \omega^2 = \frac{Eh}{R^2} \frac{\left(\frac{m\pi}{L}\right)^2}{\left[\left(\frac{m\pi}{L}\right)^2 + \left(\frac{n}{R}\right)^2\right]} + D \cdot \left[\left(\frac{m\pi}{L}\right)^2 + \left(\frac{n}{R}\right)^2\right]^2 + p_0 R \cdot \left[\frac{1}{2}\left(\frac{m\pi}{L}\right)^2 + \left(\frac{n}{R}\right)^2\right]$$

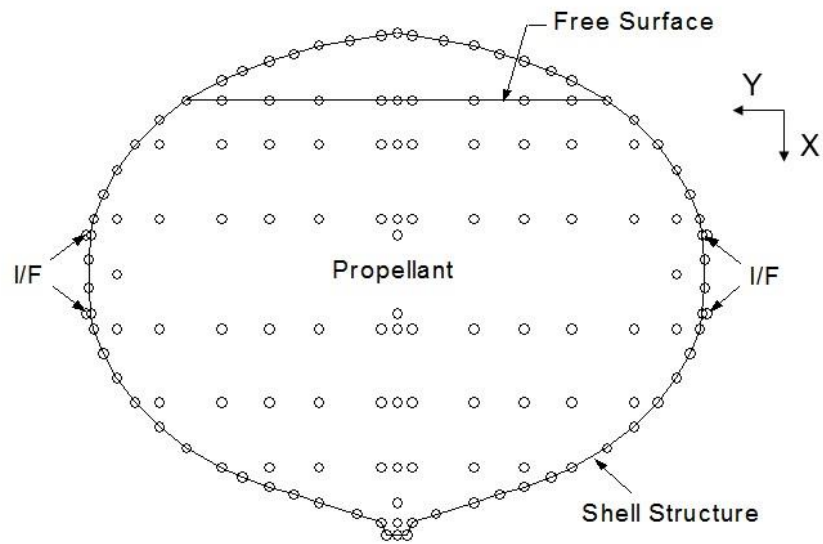
Significance of Differential Stiffness

(ullage pressure does not ordinarily affect axial & bending modes)



There are many shell breathing modes in the same frequency band as axial ($n=0$) and bending ($n=1$) modes. How significant are the shell breathing modes?

Significance of Shell Breathing Modes (*typical upper stage LOX tank*)



Significance of Shell Breathing Modes (Hurty-Craig-Bampton modal component)

- Interior & boundary dof partitions

$$\{\mathbf{u}\} = \begin{Bmatrix} \mathbf{u}_i \\ \mathbf{u}_b \end{Bmatrix} = \begin{Bmatrix} \text{Interior Motions} \\ \text{Boundary Motions} \end{Bmatrix}$$

- Partitioned dynamic equations

$$\begin{bmatrix} \mathbf{M}_{ii} & \mathbf{M}_{ib} \\ \mathbf{M}_{bi} & \mathbf{M}_{bb} \end{bmatrix} \begin{Bmatrix} \ddot{\mathbf{u}}_i \\ \ddot{\mathbf{u}}_b \end{Bmatrix} + \begin{bmatrix} \mathbf{B}_{ii} & \mathbf{B}_{ib} \\ \mathbf{B}_{bi} & \mathbf{B}_{bb} \end{bmatrix} \begin{Bmatrix} \dot{\mathbf{u}}_i \\ \dot{\mathbf{u}}_b \end{Bmatrix} + \begin{bmatrix} \mathbf{K}_{ii} & \mathbf{K}_{ib} \\ \mathbf{K}_{bi} & \mathbf{K}_{bb} \end{bmatrix} \begin{Bmatrix} \mathbf{u}_i \\ \mathbf{u}_b \end{Bmatrix} = \begin{Bmatrix} \mathbf{0} \\ \mathbf{0} \end{Bmatrix}$$

- Fixed boundary + constraint mode transformation

$$\begin{Bmatrix} \mathbf{u}_i \\ \mathbf{u}_b \end{Bmatrix} = \begin{bmatrix} \Phi_{in} & -\mathbf{K}_{ii}^{-1}\mathbf{K}_{ib} \\ \mathbf{0}_{bi} & \mathbf{I}_{bb} \end{bmatrix} \begin{Bmatrix} \mathbf{q}_n \\ \mathbf{u}_b \end{Bmatrix} = \begin{bmatrix} \Phi_{in} & \Psi_{ib} \\ \mathbf{0}_{bi} & \mathbf{I}_{bb} \end{bmatrix} \begin{Bmatrix} \mathbf{q}_n \\ \mathbf{u}_b \end{Bmatrix}$$

Hurty-Craig-Bampton component (cont'd)

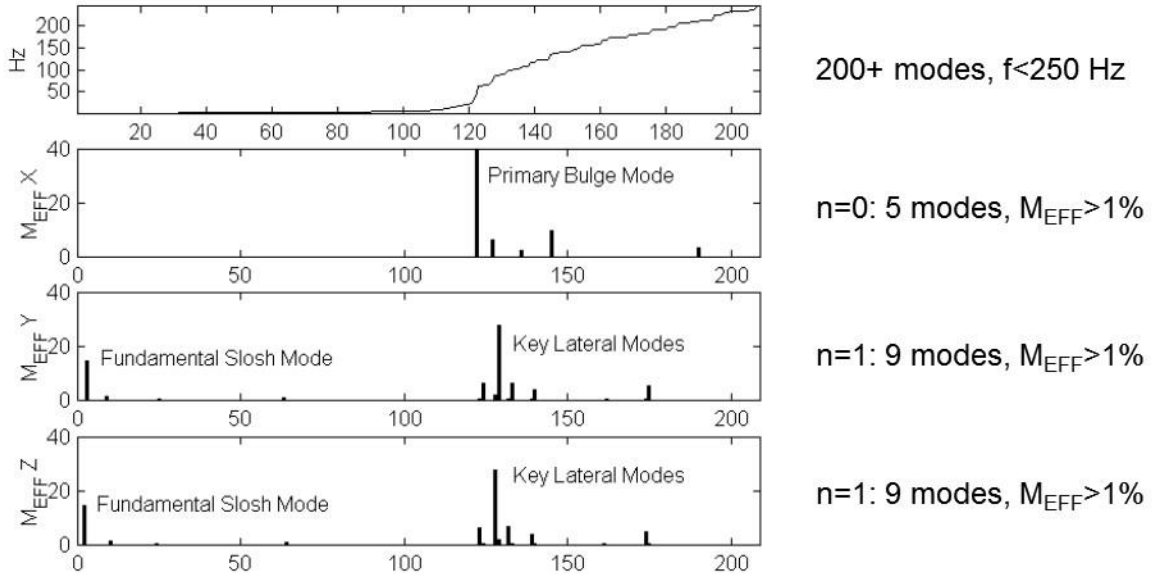
- Reduced mass and stiffness matrices

$$\begin{bmatrix} \mathbf{I}_{ii} & \mathbf{P}_{ib} \\ \mathbf{P}_{bi} & \mathbf{M}'_{bb} \end{bmatrix} \begin{Bmatrix} \ddot{\mathbf{q}}_i \\ \ddot{\mathbf{u}}_b \end{Bmatrix} + \begin{bmatrix} \omega_i^2 & \mathbf{0}_{ib} \\ \mathbf{0}_{bi} & \mathbf{K}'_{bb} \end{bmatrix} \begin{Bmatrix} \mathbf{q}_i \\ \mathbf{u}_b \end{Bmatrix} = \begin{Bmatrix} \mathbf{0} \\ \mathbf{0} \end{Bmatrix}$$

- Modes with low modal participation factors (or modal effective mass, $M_{\text{eff}} = \mathbf{P}_{ib}^2$) are self-equilibrating & do not significantly interact with other substructures.

Typical Upper Stage LOX Tank

(a few slosh, axial & lateral modes [n=0,1] are significant)



200+ modes, $f < 250$ Hz

$n=0$: 5 modes, $M_{EFF} > 1\%$

$n=1$: 9 modes, $M_{EFF} > 1\%$

$n=1$: 9 modes, $M_{EFF} > 1\%$

Note: Employment of P=0 on the free surface will eliminate slosh modes

Hydroelastic Tank Behavior and Challenges

- Behavior
 - Many component modes (slosh, axial, lateral, shell breathing)
 - Ullage & fluid inertia loading affects only shell breathing modes
 - Selected slosh, axial & lateral ($n=0,1$) modes are of significance
- Challenges
 - Large-Order Symmetric Hydroelastic Mass Matrices
 - Many non-significant modes in the frequency band of interest
 - Need for Efficient Modal Analysis Techniques
 - Verification and Validation of Hydroelastic Systems

Contents

1. Introduction
2. Mathematical Foundations
3. Dynamic Behavior of Propellant Tanks
4. Efficient Hydroelastic Tank Analysis
5. Concluding Remarks

Hydroelastic Tank Modal Analysis

(Symmetric Incompressible Fluid, NASA CR-2662)

- System dynamic equations with tank bottom outflow

$$\begin{bmatrix} \mathbf{M} + \mathbf{A}\mathbf{S}^{-1}\mathbf{A}^T & \mathbf{A}\mathbf{S}^{-1}\mathbf{\Gamma}_Q \\ \mathbf{\Gamma}_Q^T\mathbf{S}^{-1}\mathbf{A}^T & \mathbf{\Gamma}_Q^T\mathbf{S}^{-1}\mathbf{\Gamma}_Q \end{bmatrix} \begin{Bmatrix} \ddot{\mathbf{U}} \\ \ddot{\mathbf{Q}}_{tb} \end{Bmatrix} + \begin{bmatrix} \mathbf{K} & \mathbf{0} \\ \mathbf{0} & \mathbf{0} \end{bmatrix} \begin{Bmatrix} \mathbf{U} \\ \mathbf{Q}_{tb} \end{Bmatrix} = \begin{bmatrix} \mathbf{\Gamma}_F & \mathbf{0} \\ \mathbf{0} & -\mathbf{1} \end{bmatrix} \begin{Bmatrix} \mathbf{F}_e \\ \mathbf{P}_{tb} \end{Bmatrix}$$

- Closed-bottom tank modes

$$[\mathbf{K}]\{\Phi\} = [\mathbf{M} + \mathbf{A}\mathbf{S}^{-1}\mathbf{A}^T]\{\Phi\}\lambda$$

- numerical inefficiency due to the full fluid mass matrix

Hydroelastic Tank Modal Analysis (Symmetric Incompressible Fluid, NASA CR-2662)

- Closed tank bottom modes

$$[\mathbf{K}]\{\Phi\} = [\mathbf{M} + \mathbf{A}\mathbf{S}^{-1}\mathbf{A}^T]\{\Phi\}\lambda$$

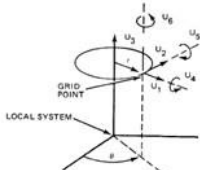
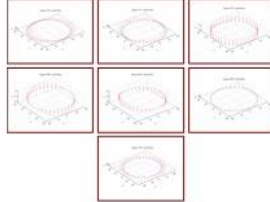
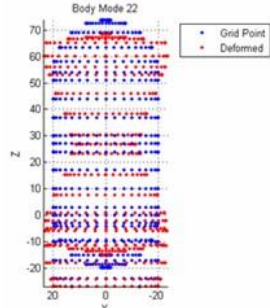
- Efficient shape function reduction
 - Harmonic reduction (NASA CR-2662, 1976)
 - Modern “load-patch” shape vectors (recent IMAC papers)

$$\{\Phi\} = [\Psi]\{\phi\} \quad (\text{reduction transformation})$$

$$[\mathbf{k}] = [\Psi^T \mathbf{K} \Psi] \quad [\mathbf{m}] = [\Psi^T \mathbf{M} \Psi] + [\Psi^T \mathbf{A}] [\mathbf{S}^{-1}] [\mathbf{A}^T \Psi]$$

$$[\mathbf{k}]\{\phi\} = [\mathbf{m}]\{\phi\}\lambda \quad (\text{reduced order eigenvalue problem})$$

Reduction Transformations (1976, 2016)

Harmonic Reduction (1976)	Load Patches (2016)
<div style="text-align: center;">  </div> $U_1(r_1, \theta_1, z_1) = \sum_{k=0}^N \left[U_{1k}^*(r_1, z_1) \cos k \theta_1 + U_{1k}^*(r_1, z_1) \sin k \theta_1 \right]$ $U_2(r_1, \theta_1, z_1) = \sum_{k=0}^N \left[U_{2k}^*(r_1, z_1) \sin k \theta_1 + U_{2k}^*(r_1, z_1) \cos k \theta_1 \right]$ $U_3(r_1, \theta_1, z_1) = \sum_{k=0}^N \left[U_{3k}^*(r_1, z_1) \cos k \theta_1 + U_{3k}^*(r_1, z_1) \sin k \theta_1 \right]$ $U_4(r_1, \theta_1, z_1) = \sum_{k=0}^N \left[U_{4k}^*(r_1, z_1) \sin k \theta_1 + U_{4k}^*(r_1, z_1) \cos k \theta_1 \right]$ $U_5(r_1, \theta_1, z_1) = \sum_{k=0}^N \left[U_{5k}^*(r_1, z_1) \cos k \theta_1 + U_{5k}^*(r_1, z_1) \sin k \theta_1 \right]$ $U_6(r_1, \theta_1, z_1) = \sum_{k=0}^N \left[U_{6k}^*(r_1, z_1) \sin k \theta_1 + U_{6k}^*(r_1, z_1) \cos k \theta_1 \right]$	<div style="text-align: center;">  </div> <div style="text-align: center;">  </div>
<p>A displacement transformation ($[U]=[G][U^*]$) does not readily describe stiffness non-symmetries, while load patches ($[\Psi]=[K^{-1}][F]$) are more accommodating.</p>	

Hydroelastic Tank Modal Analysis (Symmetric Compressible Fluid, 2016)

Introduce the generalized volume strain variable, $[C]\{P\} = \{V\}$

$$\{P\} = [C^{-1}]\{V\} = -[S^{-1}A^T]\{\ddot{U}\} - [S^{-1}]\{\ddot{V}\} - [S^{-1}\Gamma_Q]\ddot{Q}_{tb}$$

$$P_{tb} = [\Gamma_Q^T]\{P\} = -[\Gamma_Q^T S^{-1} A^T]\{\ddot{U}\} - [\Gamma_Q^T S^{-1}]\{\ddot{V}\} - [\Gamma_Q^T S^{-1} \Gamma_Q]\ddot{Q}_{tb}$$

$$\begin{bmatrix} M + AS^{-1}A^T & AS^{-1} & AS^{-1}\Gamma_Q \\ S^{-1}A^T & S^{-1} & S^{-1}\Gamma_Q \\ \Gamma_Q^T S^{-1}A^T & \Gamma_Q^T S^{-1} & \Gamma_Q^T S^{-1}\Gamma_Q \end{bmatrix} \begin{Bmatrix} \ddot{U} \\ \ddot{V} \\ \ddot{Q}_{tb} \end{Bmatrix} + \begin{bmatrix} K & 0 & 0 \\ 0 & C^{-1} & 0 \\ 0 & 0 & 0 \end{bmatrix} \begin{Bmatrix} U \\ V \\ Q_{tb} \end{Bmatrix} = \begin{bmatrix} \Gamma_F & 0 \\ 0 & 0 \\ 0 & -1 \end{bmatrix} \begin{Bmatrix} F_e \\ P_{tb} \end{Bmatrix}$$

- Matrix equation set conforms to conventional structural dynamics
 - *fully populated mass matrix, potential computational inefficiencies*
- Accommodates definition of a modal component

Hydroelastic Tank Modal Analysis (Symmetric Compressible Fluid, 2016)

- Closed tank bottom (unsymmetric eigenvalue problem)
 - Solved via sparse “complex” Lanczos or other modern algorithm

$$\begin{bmatrix} \mathbf{K} & -\mathbf{A} \\ \mathbf{0} & \mathbf{S} \end{bmatrix} \begin{Bmatrix} \Phi_U \\ \Phi_P \end{Bmatrix} = \begin{bmatrix} \mathbf{M} & \mathbf{0} \\ \mathbf{A}^T & \mathbf{C} \end{bmatrix} \begin{Bmatrix} \Phi_U \\ \Phi_P \end{Bmatrix} \lambda$$

- Introduce the “dilatational” transformation

$$[\mathbf{C}] \{\Phi_P\} = \{\Phi_V\}$$

- Normalize and verify “real” modes (using sparse calcs)

$$\begin{bmatrix} \Phi_U \\ \Phi_V \end{bmatrix}^T \begin{bmatrix} \mathbf{M} + \mathbf{A}\mathbf{S}^{-1}\mathbf{A}^T & \mathbf{A}\mathbf{S}^{-1} \\ \mathbf{S}^{-1}\mathbf{A}^T & \mathbf{S}^{-1} \end{bmatrix} \begin{bmatrix} \Phi_U \\ \Phi_V \end{bmatrix} = [\mathbf{I}] \quad \begin{bmatrix} \Phi_U \\ \Phi_V \end{bmatrix}^T \begin{bmatrix} \mathbf{K} & \mathbf{0} \\ \mathbf{0} & \mathbf{C}^{-1} \end{bmatrix} \begin{bmatrix} \Phi_U \\ \Phi_V \end{bmatrix} = [\lambda]$$

Hydroelastic Tank Modal Analysis

(Practical Engineering Options)

Sparse Matrix Computation

1. Compute all modes for the sparse, unsymmetric system.
2. Transform modal pressure dofs: $[\Phi_V] = [C][\Phi_P]$.
3. Normalize system modes to unit modal mass.
4. Select significant system modes based on modal effective mass (generally “tens” of modes among “thousands”).

Reduced Order Models

1. Impose an appropriate dof reduction transformation on the structure.
2. Compute system modes via:
 - a. Symmetric modal analysis for incompressible fluid.
 - b. Unsymmetric modal analysis for compressible fluid.
3. Select few significant “slosh” modes based on modal effective mass.

5. Concluding Remarks

1. Mixed fluid pressure-structural displacement equations transform to a symmetric structural dynamic form.
2. Hydroelastic tank axial & bending modes are generally not affected by steady loading (differential stiffness)
3. A small subset of hydroelastic modes are identified as “significant” on the basis of modal effective mass.
4. Numerically efficiency in modal analysis is realized via (a) sparse matrix operations and/or (b) application of reduction transformations.
5. Suggested topics for academic research include (a) evaluation of effects of non-axisymmetry on significant “body modes” and (b) hydroelastic modal test-analysis correlation.

Appendix B. Review and Recommendations regarding NESC-RP-14-00946

Robert N. Coppolino
Measurement Analysis Corporation
December 5, 2016

Executive Summary

Based on review of NESC-RP-14-00946, a series of recommendations are made with regard to finite element modeling, modal testing, and sensitivity analyses focusing on SLS core vehicle stage IV&V. They are:

1. Include appropriate subassembly interconnection detail (joints) in the system dynamic model. A common deficiency in modern structural dynamic models is the result of naïve oversimplification of interconnecting joints between structural components and subassemblies. It is all too easy to simply “join” parts without provision for local flexibilities (e.g., riveted, bolted and welded connections). This lack of essential parametric flexibility commonly leads to unrealistic model adjustments that vary a component’s elastic modulus in order to meet IV&V goals. Incorporation of “right-sized” model sophistication at joints has produced satisfying results in recent projects.

2. Focus on Core Vehicle Stage Target Modes. One opinion suggests that mapping of virtually all modes in a selected frequency band (e.g., $0 \leq f \leq 50$ Hz) be measured and validated using standard criteria (Ref 5). This approach incurs a severe instrumentation penalty to map all circumferential harmonic breathing modes in the selected frequency band. An alternative opinion (the writer’s) suggests mapping of body modes that are relevant to IV&V of core vehicle stage dynamics (for all propellant loading conditions) in the $0 \leq f \leq 50$ Hz frequency band. Adoption of the alternative opinion requires some rethinking of core vehicle modal testing requirements. The benefit of focus on body modes (a) drastically reduces the number of modes for IV&V and (b) eliminates the need to identify highly sensitive shell breathing modes.

3. Selection of Core Stage Vehicle Target Modes. Selection of core stage vehicle target modes becomes an effective, systematic process when modes are categorized on the basis of class (lateral, axial, torsion, shell breathing, localized appendage, etc.) by evaluation of subassembly kinetic and strain energy distributions, directional kinetic and strain energy distributions, and modal effective mass.

4. Extend the Empty Core Stage Modal Frequency Band. By tracking the anticipated natural frequencies of fully fueled and corresponding empty core vehicle stage body modes, the frequency band of target modes expands from 0-50 Hz to 0-170 Hz (TBR). The extended frequency band offers an acceptable level of assurance that target modes will exercise structural deformations that relate to vehicle system dynamics for the spectrum of flight times (propellant fill levels) within the 0-50 Hz frequency band.

5. Instrumentation Requirements for Core Vehicle Stage Modal Testing (the Shell).

The response of shell breathing modes may not be totally suppressed by orienting applied excitation loads tangential to the shell surface (a common practice). Therefore, accelerometer allocation must be sufficient to separate body modes from breathing modes; placement of tri-axial accelerometers 90 degrees apart around the core shell circumference (TBR) may suffice for satisfaction of standard NASA criteria. Additional accelerometers (or alternative strain gage sensors) are recommended to at least separate shell breathing modes from body modes.

6. Instrumentation Requirements for Core Vehicle Stage Appendages.

Pitch, yaw, roll and axial dynamics of the four engine bells must be appropriately instrumented to discern localized motions, which may couple with overall body dynamics (lateral, axial, torsion) of the shell subassembly. An appropriate accelerometer array to capture LOX feedline structural dynamics in the frequency band of the modal test must also be allocated. Past experience indicates that apparent multiple or repeated body modes need to be mapped with local appendage accelerometers in order to (a) understand and separate apparently repeated mode families while (b) satisfying test mode orthogonality criteria.

7. Core Vehicle Stage Sensitivity and Reconciliation Analysis for IV&V.

At the present time, the SLS contractor's parameterized variations on core vehicle stage modes are intended as specific, fixed candidates for correlation with modal test data. The modal sensitivity formulation introduced in 2002 and further refined in 2013 provides the means to efficiently conduct concurrent sensitivity and test-analysis correlation (and with "luck", optimal reconciliation) evaluations.

8. The present report offers a first-cut set of recommendations by the writer.

Further Loads and Dynamics TDT discussions and additional SLS program information will certainly lead to expansion and refinement of recommendations.

Introduction

Review of NESC-RP-14-00946 indicates the following consensus:

1. System models will be assembled employing Hurty-Craig-Bampton (HCB) components (which are commonly called modal substructures or superelements).
2. Full-scale modal tests will be planned to map modes to about 50 Hz.
3. Core vehicle stage modal tests will be conducted with empty propellant tanks.
4. Employment of orthogonality, cross-orthogonality & frequency correlation criteria are expected to be very challenging.

There appears to be a lack of consensus on the general approach to core vehicle modal testing, specifically:

5. Should all modes or some target modes below 50 Hz (TBR) be mapped in modal tests?
6. Is pressurization important in modal testing?
7. Definition of an appropriate instrumentation array is highly dependent on (5 & 6),

Conversations with Dr. Alvar Kabe indicate that the SLS contractor is building core stage mathematical models, which differ from one-another in parametrically sensitized zones. Those specific zones are sensitized by variation of basic material properties (e.g. elastic modulus). This commonly employed approach is (in this reviewer's opinion) both naïve and physically unrealistic. A more appropriate strategy for parametric sensitivity focuses on uncertainty at interconnecting joints (especially between substructures and subassemblies). In order to enable exercise of joint sensitivities, interfaces must include sufficiently realistic features to include those sensitivities.

It appears prudent to review the intent of IV&V from the viewpoints of separate engineering sub-disciplines, namely (a) flight structural loads, (b) control stability, (c) pogo stability, and (d) aeroelasticity. Each of these sub-disciplines requires differing subsets of modal information to conduct reliable engineering evaluations. It is noteworthy to recall that the past 60 years of space launch experience has generally succeeded while employing less sophisticated dynamic models than those envisioned in the present endeavor.

Relevant Structural Dynamic Models

The dynamic frequency band ($0 \leq f \leq f^*$) for a relevant structural dynamic model (assumed linear for the present) is governed by the SRS of its anticipated loading environments (Ref 1). Based on f^* (typically 50 Hz), minimum grid spacing of structural components may be defined; however, employment of modern CAE tools generally produces refined finite element models that exceed minimum grid spacing requirements. It should be noted that strict adherence to engineering drawings (as emphasized in of NESC-RP-14-00946), while avoiding ill-advised modeling liberties (often employing RBE2 & RBE3 constraints) minimizes the occurrence of severe modeling deficiencies.

A common deficiency in modern structural dynamic models is the result of naïve oversimplification of interconnecting joints between structural components and subassemblies. It is all too easy to simply “join” parts without provision for local flexibilities (e.g., riveted, bolted and welded connections). This lack of essential parametric flexibility commonly leads to unrealistic model adjustments that vary a component’s elastic modulus in order to meet IV&V goals. Incorporation of “right-sized” model sophistication at joints has produced satisfying results in recent projects.

The core vehicle stage presents a particular challenge for IV&V in that (a) its primary structure is a shell (with many shell breathing modes within the band of classically significant body modes), (b) propellant constitutes the majority of the system’s mass when it is fully loaded, and (c) core stage modal testing will be limited to the empty condition. Classical shell theory (Ref 2) and laboratory experience (Ref 3) indicate that shell breathing modes are sensitive to static pressure and weight loading as well as flexural stiffness of shell segment transitions and boundary conditions. The body modes, however, are relatively insensitive to static pressure and weight loading (the exceptional case occurs for balloon-type propellant tanks typical of earlier Atlas and Centaur vehicles). In addition, theoretical analyses (Ref 4) and past launch vehicle experiences strongly indicate that structural loads and system dynamics are primarily influenced by “body” modes (axial, lateral, torsion). While modern finite element models include all body and breathing modes of shell structures, it is highly recommended that the core stage vehicle IV&V process should focus on body modes only.

Focus on Core Vehicle Stage Target Modes

There are differing opinions on IV&V for the core vehicle stage:

1. One opinion suggests that mapping of virtually all modes in a selected frequency band (e.g., $0 \leq f \leq 50$ Hz) be measured and validated using standard criteria (Ref 5). This approach incurs a severe instrumentation penalty to map all circumferential harmonic breathing modes in the selected frequency band.
2. An alternative opinion (the writer’s) suggests mapping of body modes that are relevant to IV&V of core vehicle stage dynamics (for all propellant loading conditions) in the $0 \leq f \leq 50$ Hz frequency band.

Adoption of the alternative opinion requires some rethinking of core vehicle modal testing requirements.

Selection of Core Vehicle Stage IV&V Target Body Modes

The theoretical modes of a fixed-base core stage dynamic model with selected propellant fill levels may be categorized in terms of (a) sub-component kinetic and strain energy distributions, (b) directional kinetic and strain energy distributions, and (c) modal effective mass (Ref 4). Prominent body modes are readily identified by employing the above cited energy and modal effective mass metrics. Tracking of the frequency

migration of important body modes with decreasing propellant levels (using cross-orthogonality or modal assurance criteria (MAC)) will indicate which set of empty body modes should be included in the target mode set.

A very preliminary estimate of the target body mode frequency band results from the ratio of fully loaded (~2,159,000 lb) to empty (~188,000 lb) weights. The ratios of natural frequencies for corresponding empty and fully loaded system body modes are on the order of 3.4 (square root of 11.5). This increases the frequency band for empty core stage target modes from 50 Hz to about 170 Hz (TBR). A more refined estimate of the frequency range of core stage target modes for IV&V must be the result of rigorous core stage vehicle (mathematical model) modal tracking. It should be noted that the only type of body mode that should not be affected by fuel mass loading is torsion, since no propellant mass should be moved during pure torsion activity.

A relatively simple example shell structure (taken from Ref 4) illustrates how target modes may roughly scale with respect to fuel level. The original model consists of a 20” radius, 100” long, 0.5” wall thickness aluminum shell and skirt assembly composed of five (5) subassemblies, as illustrated below in Figure 1.

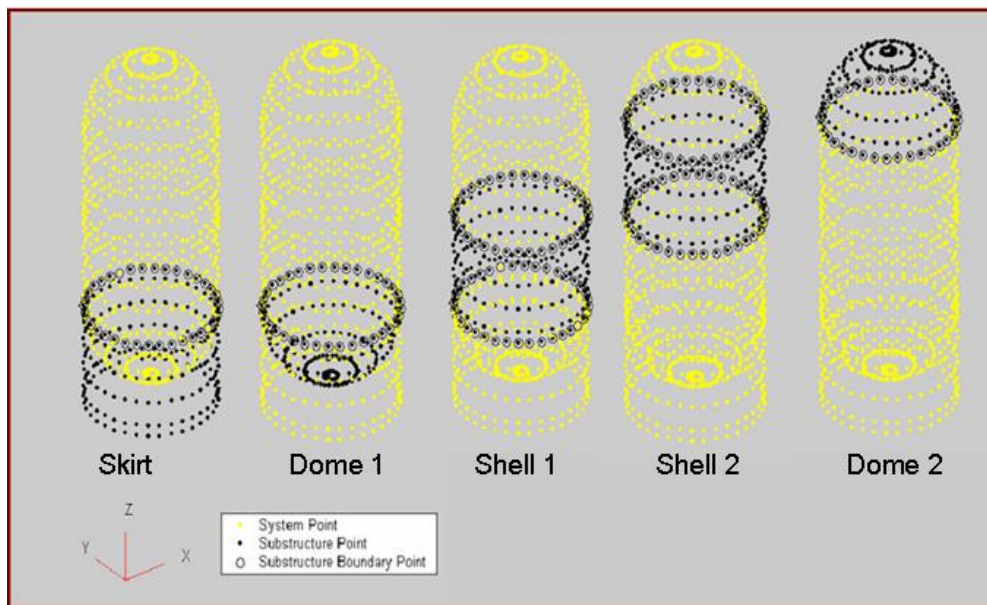


Figure 1: Illustrative Example Shell Structure

In order to “up-scale” this example from 20” radius (40” diameter) to SLS scale, which is (27’ diameter), the empty shell frequencies will reduce by a length factor of 8.1. The empty full-scale frequencies are subsequently scaled by a reduction factor of 3.4 (corresponding to the SLS “weight factor”); torsion modes are not subjected to the mass factor. Results of this process are summarized below in Table 1.

Table 1: Illustrative Example Base-Fixed Body Modes (with scaling)

Mode	N	Frequency (Hz)			Component Kinetic Energy (%)				Directional Kinetic Energy (%)			Modal Effective Mass (%)					
		Empty		100% Fueled	SKIRT	DOME1	SHELL	DOME2	X	Y	Z	X	Y	Z	RX	RY	RZ
		1/8.1 Scale	Full Scale	Full Scale													
1Y	1	122.21	15.09	4.44	1.1	1.4	46.7	50.8	0.0	96.2	3.8		61.6		98.4		
2X	1	122.21	15.09	4.44	1.1	1.4	46.7	50.8	96.2	0.0	3.8	61.6			98.4		
11T	0	316.86		38.92	3.9	5.7	64.6	25.8	50.0	50.0	0.0						82.1
14Y	1	377.59	46.57	13.70	11.9	35.6	36.6	16.0	0.0	91.0	8.9		29.8				
15X	1	377.62	46.57	13.70	11.9	35.6	36.6	15.9	91.1	0.0	8.9	29.8				0.4	
24Z	0	469.44	57.75	16.99	3.4	7.3	52.7	36.6	0.4	0.4	99.1			80.8			
49Y	1	708.88	87.24	25.66	3.1	36.9	41.0	18.9	0.5	89.9	9.6		1.0	1.0		0.0	
50X	1	709.27	87.24	25.66	3.1	37.0	41.2	18.7	90.1	0.5	9.4	1.0				0.0	
65T	0	860.54		103.87	16.4	31.7	29.5	22.4	50.0	50.0	0.0						9.2
76Y	1	1005.70	123.15	36.22	17.5	18.9	51.1	12.6	1.8	61.3	36.9		0.5	0.4		0.3	
77X	1	1011.50	123.15	36.22	18.4	18.4	52.3	10.9	63.3	1.9	34.8					0.3	
86Z	0	1036.20	127.15	37.40	7.7	51.9	13.6	26.9	7.7	7.7	84.6			7.7			
99Y	1	1183.30	144.40	42.47	27.4	15.6	30.1	26.9	3.0	57.3	39.7		1.6	1.6		0.0	
100X	1	1189.60	144.40	42.47	28.0	15.5	31.1	25.4	56.0	2.9	41.1	1.6				0.0	

The mode numbers in the first column are associated with 14 body modes out of a total of 100 modes (all modes that are not listed are associated with shell breathing). The letter after each body mode number designates the body mode type (Y, X represent lateral bending, T represents torsion, and Z represents axial). Plots of four body modes are illustrated below in Figure 2.

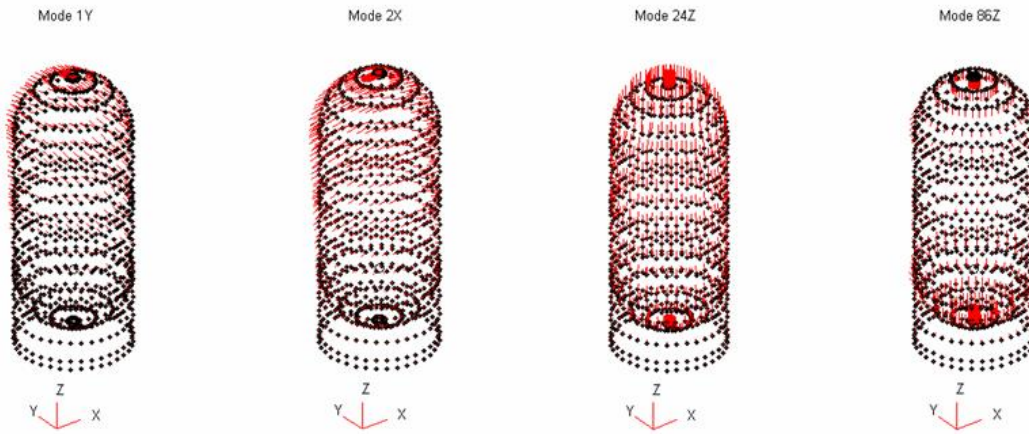


Figure 2: Illustrative Example Body Modes

Note that modes 24Z and 86Z may be significant for a hypothetical Pogo stability evaluation. Based on examination of the frequency shifts in lateral and axial body modes, it is clear that empty structure body modes in the $0 \leq f \leq 50$ Hz frequency band are not representative of important fuel-loaded body modes in the same frequency band.

The illustrative example shell structure offers rationale for (a) selection of target IV&V modes, and (b) expansion of the modal test frequency band to include significant hydroelastic modes. In addition, elimination of shell breathing modes from the target mode set, simplifies prospects for satisfaction of test-analysis correlation goals (Ref 5).

Instrumentation Requirements for Core Vehicle Stage Modal Testing (the Shell)

The response of shell breathing modes may not be totally suppressed by orienting applied excitation loads tangential to the shell surface (a common practice). Therefore, accelerometer allocation must be sufficient to separate body modes from breathing modes. A recently published paper (Ref 6) introduces an extended RKE strategy for allocation of accelerometers and development of a TAM mass matrix for orthogonality and cross-orthogonality calculations (to satisfy Ref 5 standards). However, additional accelerometers (or alternative strain gage sensors) are recommended to at least separate shell breathing modes from body modes. An array of the type illustrated below in Figure 3 provides a way forward for effecting separation of shell breathing and body modes.

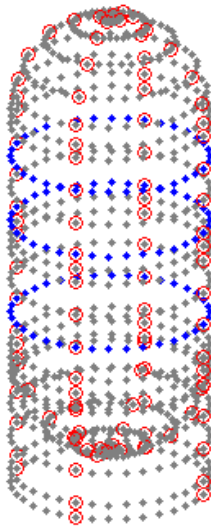


Figure 3: Accelerometer Array for Illustrative Example Shell Structure

The tri-axial accelerometer locations denoted by red circles (90 degree circumferential separation) correspond to the allocation deemed prudent for mapping of body modes (employing an opportune reduction transformation for body modes). The additional blue point tri-axial accelerometer (or NASA AFRC type fiber optic strain string) bands correspond to additional arrays, which are intended to identify the presence of shell breathing modes (to be eliminated from the measured target mode set).

Instrumentation Requirements for Core Vehicle Stage Appendages

On the assumption that the propellant tank and intertank subassemblies will be instrumented following the above recommendations, there are additional practical matters that should be addressed related to appendages (e.g., engines, long LOX feedline). General construction of the core vehicle stage is illustrated below in Figure 4.

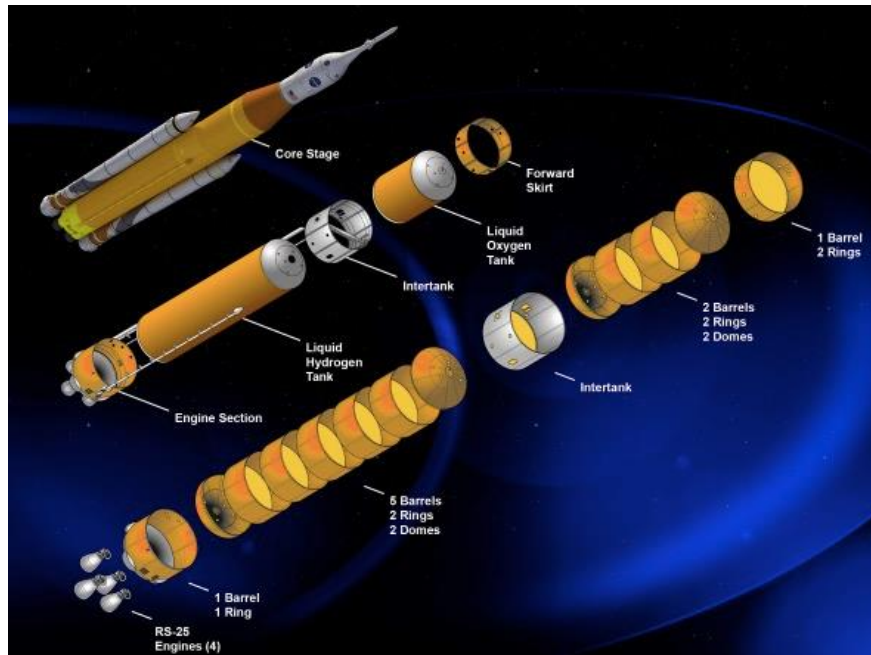


Figure 4: Core Vehicle Stage Construction

Pitch, yaw, roll and axial dynamics of the four engine bells must be appropriately instrumented to discern localized motions, which may couple with overall body dynamics (lateral, axial, torsion) of the shell subassembly. In addition, the long LOX feedline (empty) may be subject to localized flexural and axial dynamics that couple with the shell subassembly. An appropriate accelerometer array to capture LOX feedline structural dynamics in the frequency band of the modal test must be allocated. Past experience (e.g., automobile modal testing, Ref 7) has indicated that apparent multiple or repeated body modes need to be mapped with local appendage accelerometers in order to (a) understand and separate apparently repeated modes families while (b) satisfying test mode orthogonality criteria.

Core Vehicle Stage Sensitivity and Reconciliation Analysis for IV&V

Conversations with Dr. Alvar Kabe indicate that the SLS contractor is building core stage mathematical models, which differ from one-another in parametrically sensitized zones. Those specific zones are sensitized by variation of basic material properties (e.g. elastic modulus). This commonly employed approach is (in this reviewer's opinion) both naïve and physically unrealistic. A more appropriate strategy for parametric sensitivity focuses on uncertainty at interconnecting joints (especially between substructures and subassemblies). In order to enable exercise of joint sensitivities, interfaces must include realistic enough features to include those sensitivities.

At the present time, the SLS contractor's parameterized variations on Core Vehicle Stage modes are intended as specific candidates for correlation with modal test data. The modal sensitivity formulation introduced in 2002 (Ref 8-9) and further refined in 2013 (Ref 10) provides the means to efficiently conduct concurrent sensitivity and test-analysis correlation (and with "luck", optimal reconciliation) evaluations.

The key to the sensitivity formulation is collection of baseline model and individual parametric variants (finite change in regions of a system, e.g., group of joints), as described by the sensitized dynamic equation set,

$$\left[M_0 + \sum_{i=1}^N p_i \cdot \Delta M_i \right] \{\ddot{u}\} + \left[K_0 + \sum_{i=1}^N p_i \cdot \Delta K_i \right] \{u\} = \{0\} \quad (1)$$

When all “ p_i ” are null, the system is “baseline”. The low frequency undamped modes of the baseline system are solutions of the eigenvalue problem

$$[K_0][\Phi_{0L}] - [M_0][\Phi_{0L}][\lambda_{0L}] = [0] \quad (2)$$

Definition of residual vectors describing parametric variations in Equation 1 is accomplished utilizing the lowest frequency mode shapes of the baseline structure as well as the lowest mode shapes associated with each independent alteration of the structure

$$[K_0 + \bar{p}_i \Delta K_i][\Phi_{iL}] - [M_0 + \bar{p}_i \Delta M_i][\Phi_{iL}][\lambda_{iL}] = [0] \quad (\text{for } i=1, \dots, N), \quad (3)$$

where \bar{p}_i is a finite (rather than infinitesimal parametric perturbation). An initial set of trial vectors that redundantly encompass all low frequency altered system mode shapes is

$$[\Psi] = [\Phi_{1L} \quad \Phi_{2L} \quad \dots \quad \Phi_{NL}] \quad (4)$$

The redundant set of trial vectors is reduced to a linearly independent “modal” set, $[\bar{\Phi}_{OL}]$, by following the methodology described in Ref 9. $[\bar{\Phi}_{OL}] = [\Phi_{OL} \quad \Psi_p]$ is the trial vector set (sensitivity vectors) to be used for expansion of measured operating deflection shapes.

It is of interest to note that the resulting approximate generalized sensitivity model (that may be employed in a more complete system identification exercise) is

$$\left[k_0 + \sum_{i=1}^N p_i [\Delta k_i] \right] [\varphi] - \left[m_0 + \sum_{i=1}^N p_i [\Delta m_i] \right] [\varphi][\lambda] = [0] \quad , \quad (5)$$

where the reduced stiffness and mass matrix components are

$$[k_0] = [\bar{\Phi}_{OL}^T K_0 \bar{\Phi}_{OL}], \quad [m_0] = [\bar{\Phi}_{OL}^T M_0 \bar{\Phi}_{OL}], \quad [\Delta k_i] = [\bar{\Phi}_{OL}^T \Delta K_i \bar{\Phi}_{OL}], \quad [\Delta m_i] = [\bar{\Phi}_{OL}^T \Delta M_i \bar{\Phi}_{OL}] \quad (6)$$

The low frequency physical modes for the altered dynamic system are recovered using the relationship

$$[\Phi_L] = [\bar{\Phi}_{OL}][\varphi] \quad (7)$$

Further operations, successfully employed in modal tests (e.g., Ref 7) have resulted in post-test system models (with specific parameter values) that closely agree with modal test data.

References

- [1] Harris' Shock and Vibration Handbook, 6th Ed, A. Piersol and T. Paez (Ch. 23, R. Coppelino), McGraw-Hill, 2010
- [2] "The Dynamic Behavior of Liquids in Moving Containers", H.N. Abrahamson, NASA SP-106, 1966
- [3] "A Numerically Efficient Finite Element Hydroelastic Analysis, Vol. 1: Theory and Results", .R. Coppelino, NASA CR-2662, 1976
- [4] "Understanding Large Order Finite Element Model Dynamic Characteristics", R. Coppelino, IMAC XXIX, 2011
- [5] "Loads Analyses of Spacecraft and Payloads", NASA-STD-5002, 1996
- [6] "Response DOF Selection for Mapping Experimental Normal Modes-2016 Update", R. Coppelino, IMAC XXXIV, 2016
- [7] "Integrated Modal Testing and Analysis of a Body-on-Frame Automobile", R. Coppelino and V. Borowski, IMAC XV, 1997
- [8] "International Space Station P5 Modal Survey: Test Planning through FEM Reconciliation", R. Coppelino, IMAC XX, 2002
- [9] "Modal Test Data to FEM Reconciliation using Balanced Cost Functions", R. Coppelino, IMAC XX, 2002
- [10] "FEM Sensitivity Vector Basis for Measured Mode Expansion", R. Coppelino, IMAC XXXI, 2013

Appendix C. Evaluation of ISPE Model Sensitivities

Appendix C: Evaluation of ISPE Model Sensitivities

Bob Coppolino
16 March 2017

Sensitivity Road Map

/ ICPS

- Keeping 12 variables
- LH2 'top' MSA (diagonal)
- LH2 Tank Forward Skirt (light blue)
- IT Forward Skirt (yellow)
- LH2 upper dome (yellow, not seen)
- LH2 middle skirt
- LH2 weldlands (cyan)
- LH2 Lower dome (green)
- Struts (orange)
- Struts-LOX IF (cyan)
- LOX upper dome (black)
- LOX middle skirt
- LOX Lower dome (red)

/ Core Simulator

- Keeping 2 variables
- Barrel (green) mat# 2000002
- Weldlands (yellow) mat# 2000001

/ MSA

- Keeping 3 variables
- Barrel region (red) geom# 302195 CID mat# 301981 mat# 321982
- Flange Material Blue mat# 302219
- Weldlands (yellow) mat# 301981

/ LVSA

- Keeping 3 variables
- FWD Barrel ring (yellow) mat# 2301000
- Aft Barrel region (orange) mat# 2301001
- FWD Ring (black) mat# 2301004
- FWD Int. Ring (red) mat# 2301007
- Weldlands (green) mat# 2301003
- Aft Ring (cyan) mat# 2301005

/ MPCV Simulator

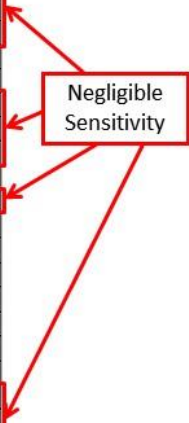
- Keeping 2 variables
- Barrel (green) mat# 2000011
- Interface Rings (yellow) mat# 2000012

/ Interfaces

- Sure Sep ring (blue-ink)
- Other interfaces modeled with springs
- Core simulator to ICPS
- ICPS to MSA
- MSA to MPCV simulator
- Axial, radial, tangential directions have stiffness of half other conditions are half zero
- Boundary conditions
- Core simulator fixed to fixed
- Connections pins with ball bearings
- Translations - full rotations to 0

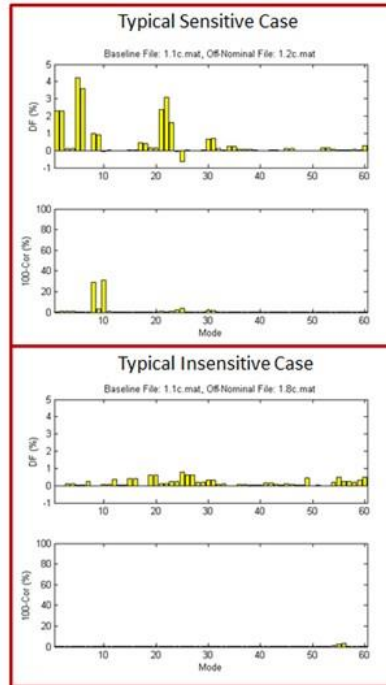
Element	Subcomponent Perturbed	Run #
Nominal Run	---	1
MSA	Barrel Region	2
	Flange Material	3
	Weldlands	4
LVSA	Aft Barrel Region	5
	FWD Barrel Region	6
	Weldlands	7
	FWD Ring	8
ICPS	Aft Ring	9
	LOX Tank Lower dome	10
	LOX Tank Middle	11
	LOX Tank Upper Dome	12
	LH2 Tank Lower dome	13
	LH2 Tank Middle	14
	LH2 Tank Middle Welds	15
	LH2 Tank Upper Dome	16
	Struts	17
	Strut-LOX IF	18
	LH2 tank Forward Skirt	19
Intertank Forward Skirt	20	
Sure Sep	Sure Sep	21
Core Simulator	Barrel	22
	Weldlands	23
MPCV Simulator	Barrel	24
Integration	Interface Rings	25
	MPCV Sim to MSA	26
	Core Sim to LVSA	27
	MSA to ICPS	28
	Core Sim to Ground	29

Negligible Sensitivity



Discrimination of Sensitive and Insensitive Cases

Case	DF (%)	100-Cor (%)	Class
1.2c.mat	4	31	Sensitive
1.3c.mat	5	30	
1.4c.mat	9	17	
1.5c.mat	13	97	
1.6c.mat	13	90	
1.7c.mat	2	35	
1.8c.mat	1	3	Insensitive
1.9c.mat	1	7	
1.10c.mat	0	0	
1.11c.mat	1	7	
1.12c.mat	1	10	Sensitive
1.13c.mat	2	81	
1.14c.mat	4	22	Insensitive
1.15c.mat	0	0	
1.16c.mat	0	1	
1.17c.mat	2	8	
1.18c.mat	23	95	Sensitive
1.19c.mat	1	6	Insensitive
1.20c.mat	6	93	Sensitive
1.21c.mat	3	89	
1.22c.mat	2	15	
1.23c.mat	23	100	
1.24c.mat	16	100	
1.25c.mat	8	2	
1.26c.mat	28	100	Insensitive
1.27c.mat	0	0	
1.28c.mat	0	0	
1.29c.mat	0	0	
1.30c.mat	0	0	



Efficient Modal Sensitivity Convergence

- Exact system modes (for each reference parameter value, p_i)

$$\left[\mathbf{K}_0 + \sum_i p_i \Delta \mathbf{K}_i \right] [\Phi_e] = \left[\mathbf{M}_0 + \sum_i p_i \Delta \mathbf{M}_i \right] [\Phi_e] [\lambda_e]$$

- Approximate system modes (for a selected value of “tol”)

$$\left[\mathbf{k}_0 + \sum_i p_i \Delta \mathbf{k}_i \right] [\varphi_a] = \left[\mathbf{m}_0 + \sum_i p_i \Delta \mathbf{m}_i \right] [\varphi_a] [\lambda_a]$$

$$[\Phi_a] = [\Psi][\varphi_a]$$

- Convergence indicator

$$[\mathbf{C}_{ea}] = [\Phi_e^T \mathbf{M}_0 \Phi_a]$$

- If cross-orthogonality is not close to $[\mathbf{I}_0]$ for all cases, reduce “tol” until this criterion is satisfied (modal frequencies will converge when this is met)

Efficient Modal Sensitivity Convergence Results

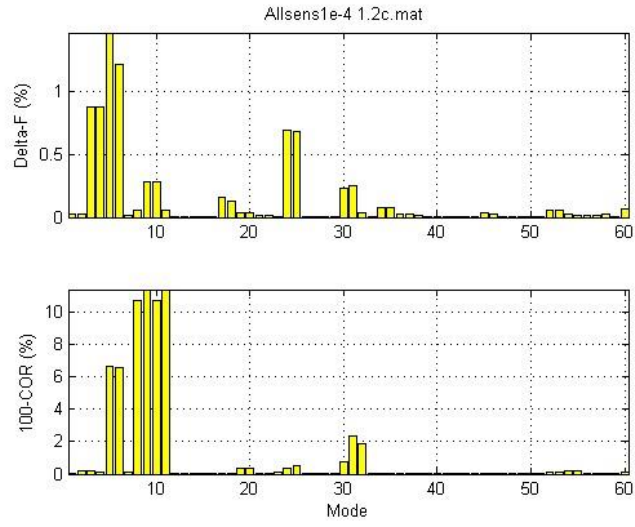
Tolerance	1.00E-04		1.00E-05		1.00E-06	
Residuals	65		160		291	
Case	Δf (%)	ΔC (%)	Δf (%)	ΔC (%)	Δf (%)	ΔC (%)
1.2c.mat	1.5	11	1.2	10	0.1	3
1.3c.mat	2.3	16	1.9	16	0.0	1
1.4c.mat	3.2	33	1.6	29	0.1	1
1.5c.mat	1.0	16	0.5	1	0.2	0
1.6c.mat	1.3	1	1.0	3	0.1	0
1.7c.mat	0.4	8	0.4	4	0.1	0
1.13c.mat	0.3	12	0.1	2	0.0	0
1.14c.mat	2.5	16	0.6	5	0.0	0
1.18c.mat	0.7	19	0.1	0	0.0	0
1.20c.mat	3.0	20	1.4	7	0.1	2
1.21c.mat	0.7	15	0.3	1	0.0	1
1.22c.mat	0.4	7	0.2	1	0.1	1
1.23c.mat	1.0	4	0.5	3	0.1	0
1.24c.mat	0.1	0	0.1	0	0.0	0
1.25c.mat	1.7	99	0.6	6	0.1	1
1.26c.mat	0.9	5	0.2	2	0.0	0

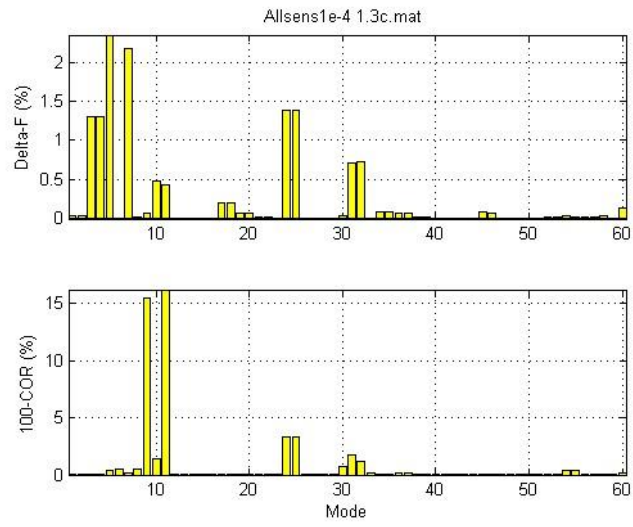
Notes:

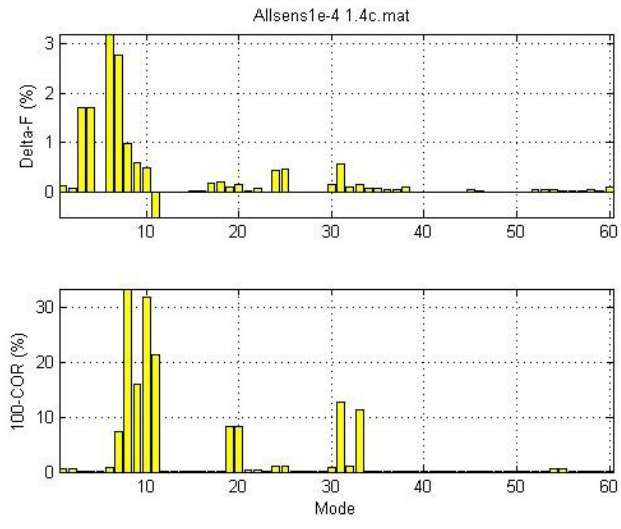
1. Δf (%) = $[\text{approximate} - \text{exact frequency}] / [\text{exact frequency}]$ (%)
2. ΔC (%) = $100\% - [\text{Cross-Orthogonality}]$ (%)

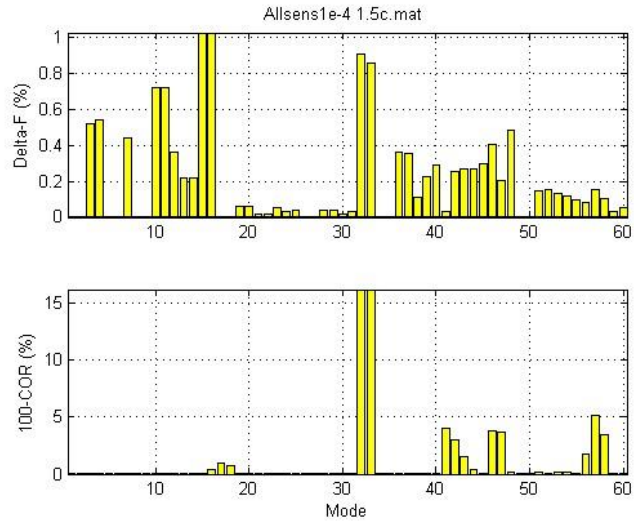
File: Allsens1e-4: Convergence Summary

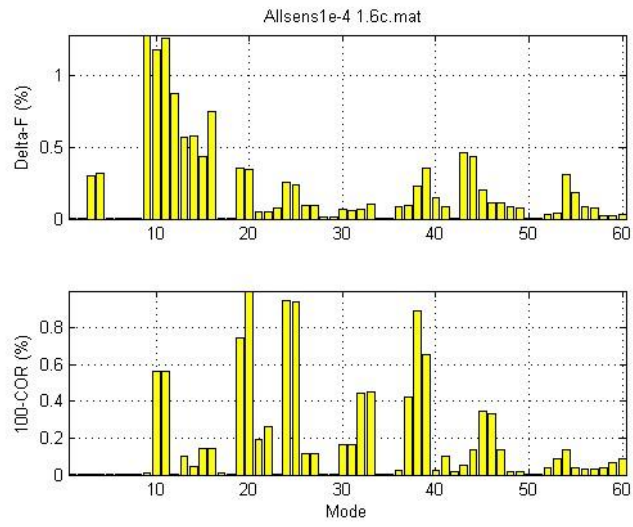
6

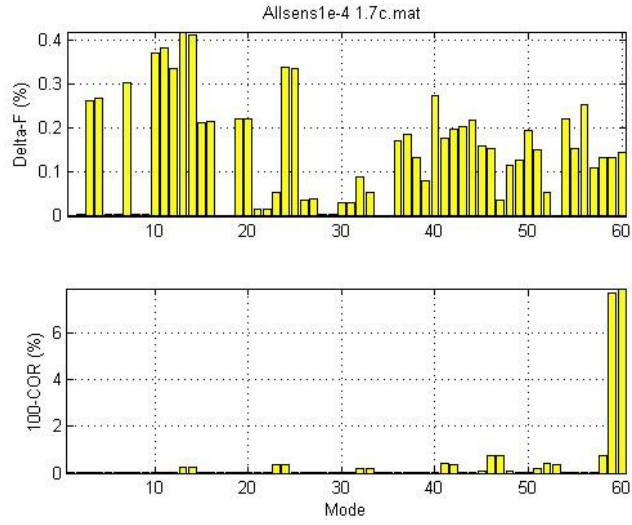


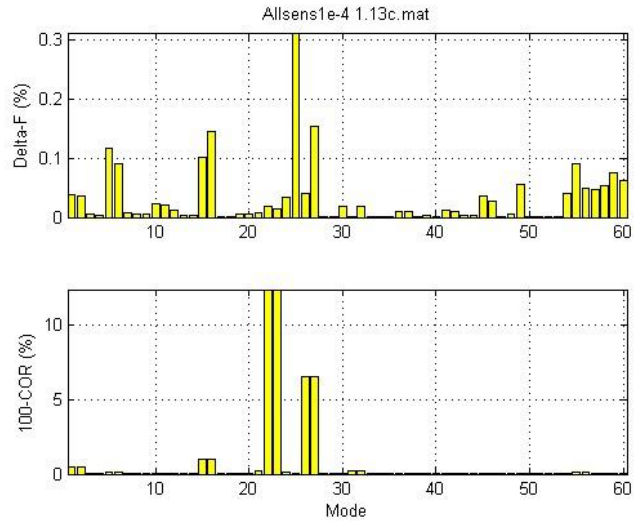


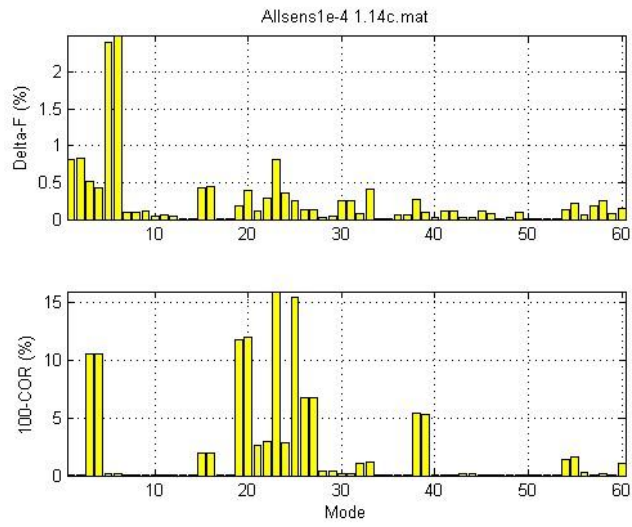


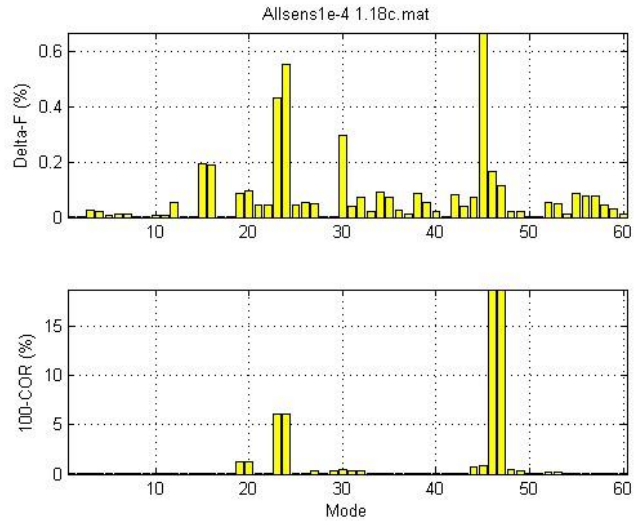


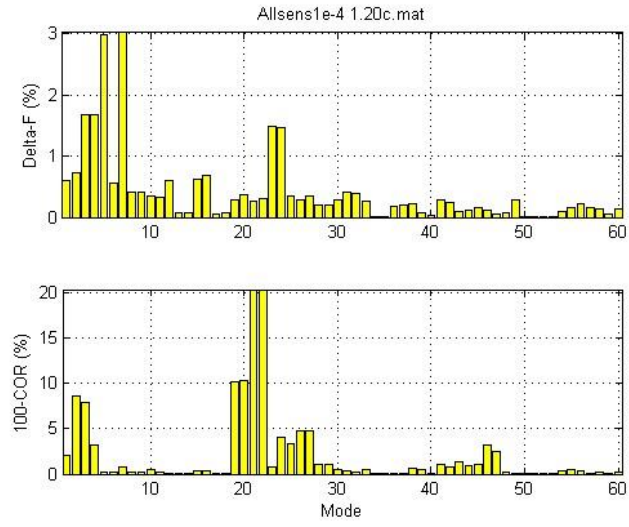


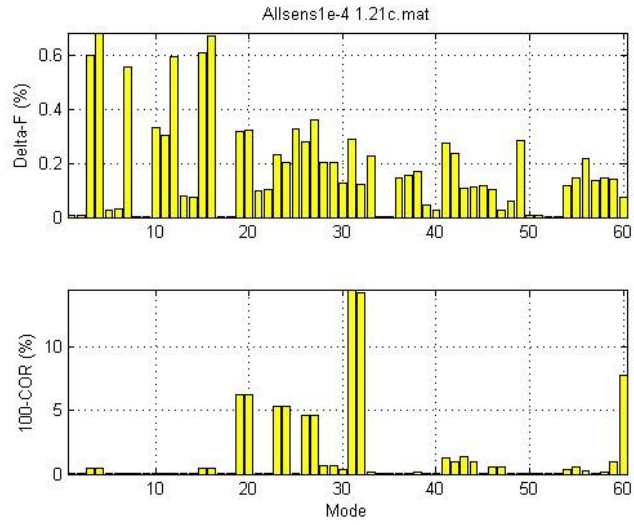


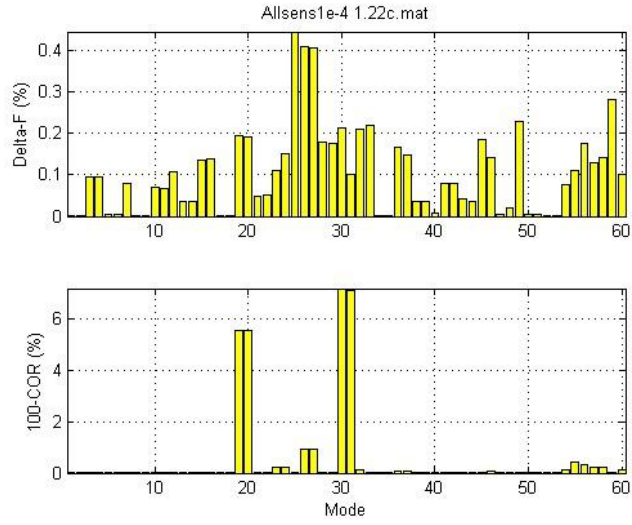


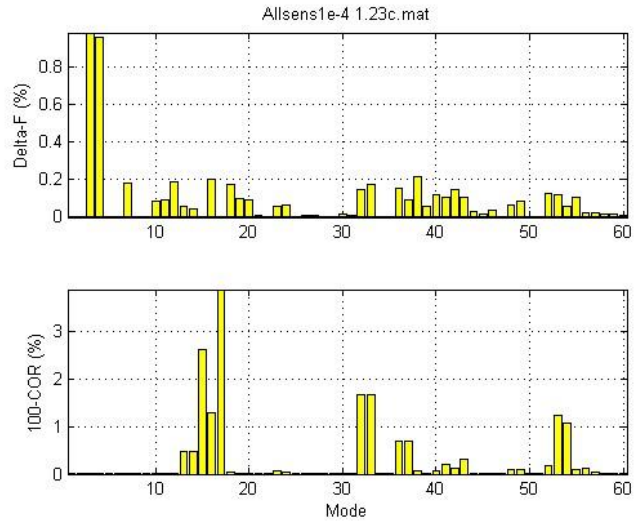


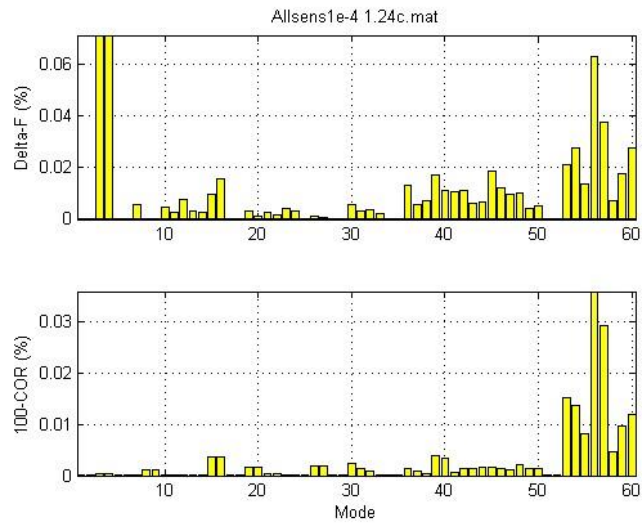


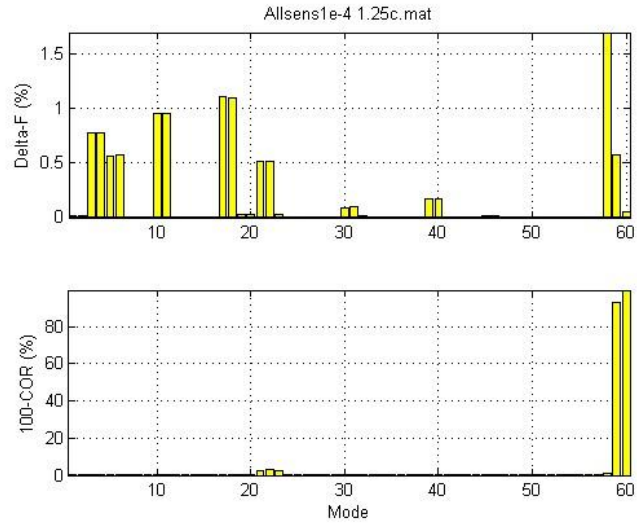


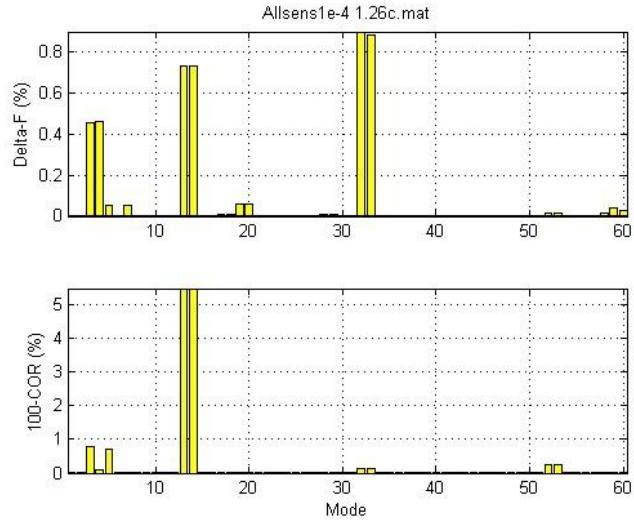






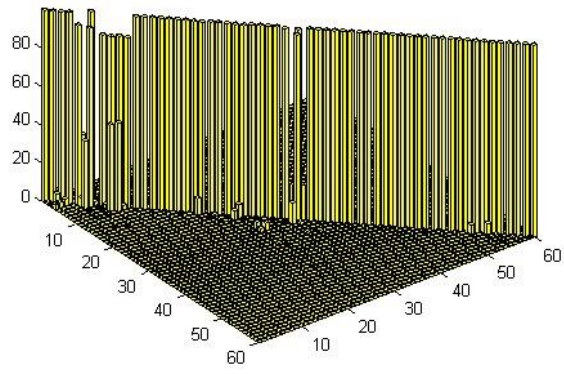




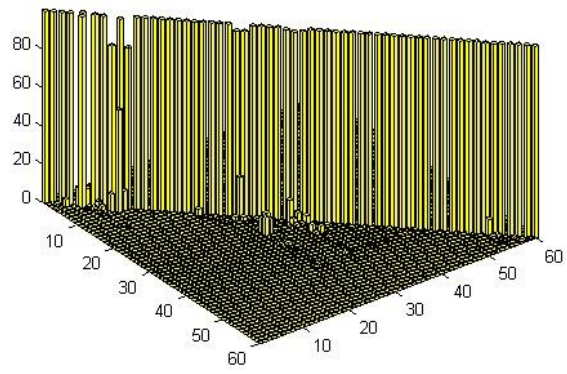


File: Allsens1e-4: Convergence Cross-Orthogonality

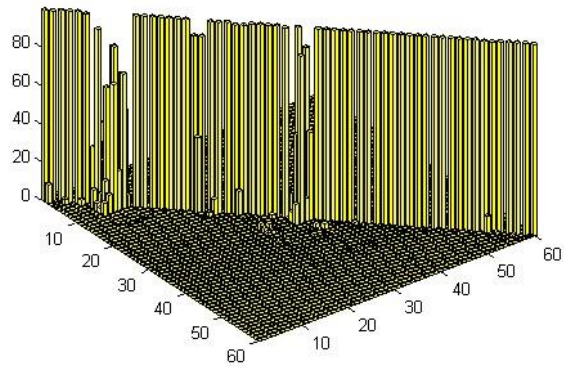
Baseline File: 1.1c.mat , Perturbed File: 1.2c.mat , tol=0.0001



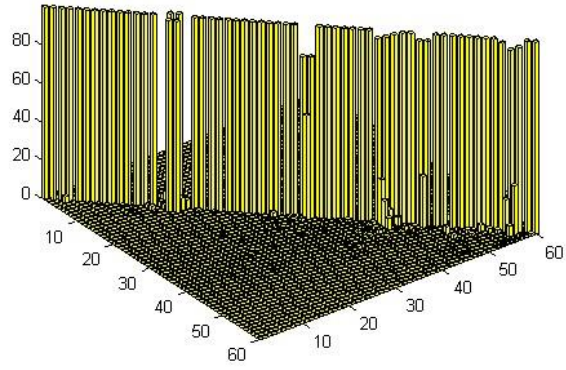
Baseline File: 1.1c.mat , Perturbed File: 1.3c.mat , tol=0.0001



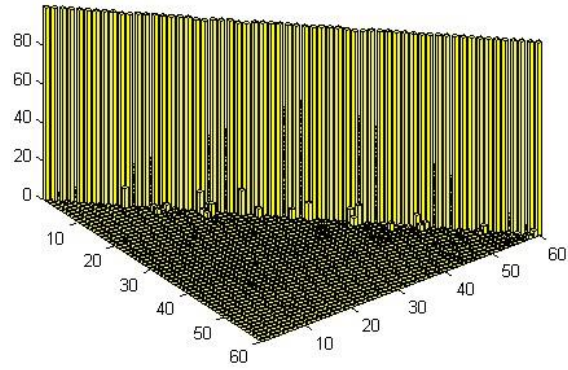
Baseline File: 1.1c.mat , Perturbed File: 1.4c.mat , tol=0.0001



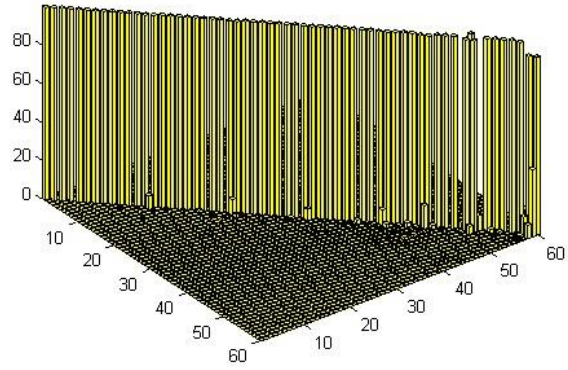
Baseline File: 1.1c.mat , Perturbed File: 1.5c.mat , tol=0.0001



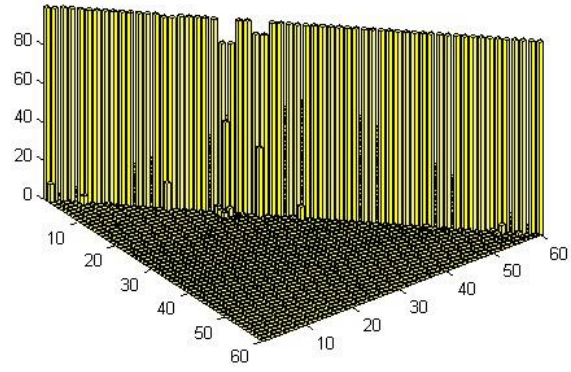
Baseline File: 1.1c.mat , Perturbed File: 1.6c.mat , tol=0.0001



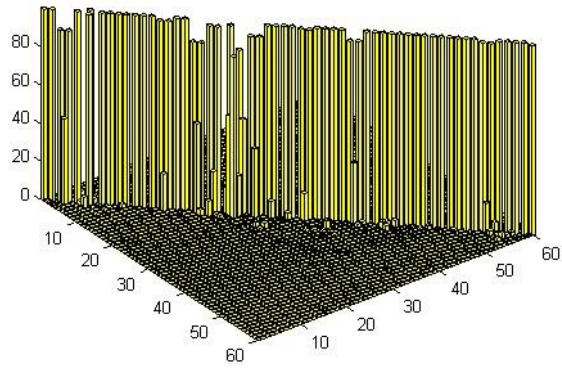
Baseline File: 1.1c.mat , Perturbed File: 1.7c.mat , tol=0.0001



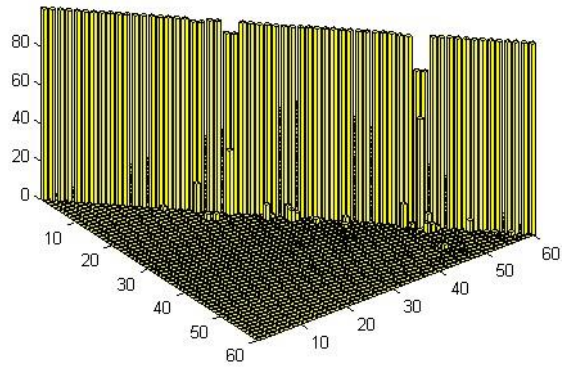
Baseline File: 1.1c.mat , Perturbed File: 1.13c.mat, tol=0.0001



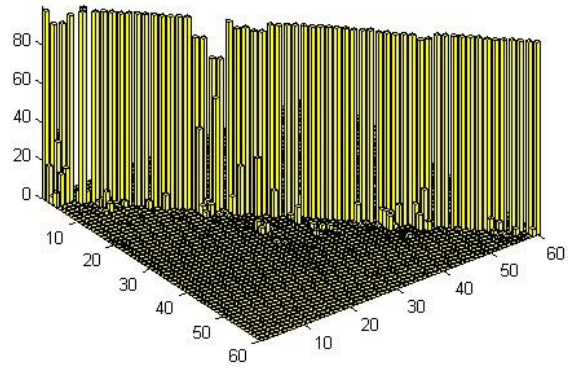
Baseline File: 1.1c.mat , Perturbed File: 1.14c.mat, tol=0.0001



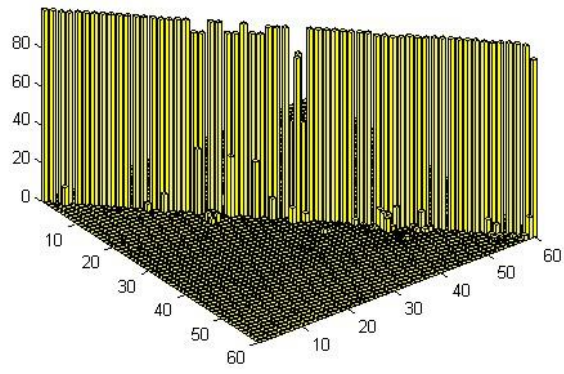
Baseline File: 1.1c.mat , Perturbed File: 1.18c.mat, tol=0.0001



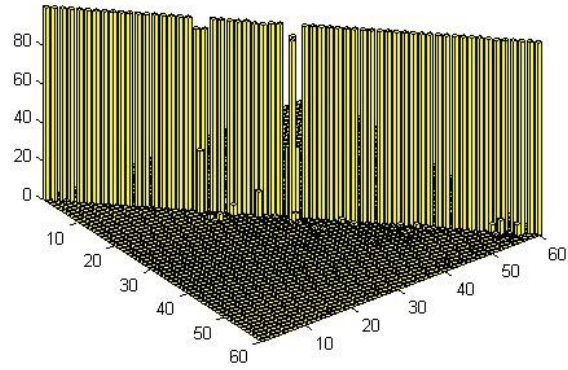
Baseline File: 1.1c.mat , Perturbed File: 1.20c.mat, tol=0.0001



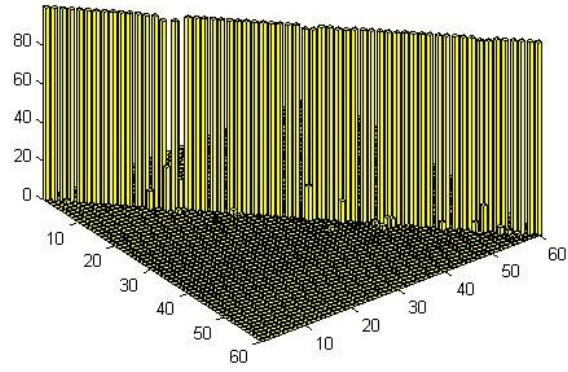
Baseline File: 1.1c.mat , Perturbed File: 1.21c.mat, tol=0.0001



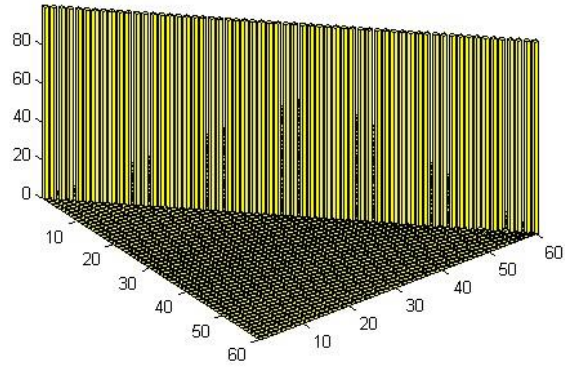
Baseline File: 1.1c.mat , Perturbed File: 1.22c.mat, tol=0.0001



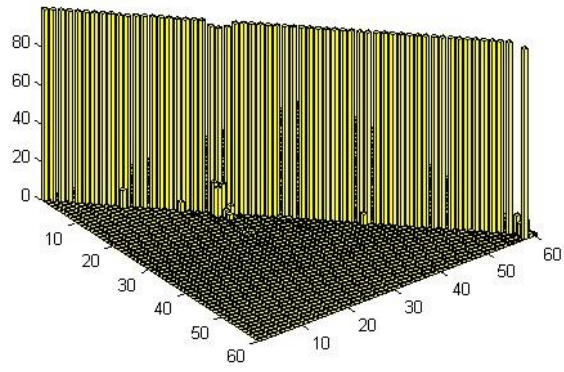
Baseline File: 1.1c.mat , Perturbed File: 1.23c.mat, tol=0.0001



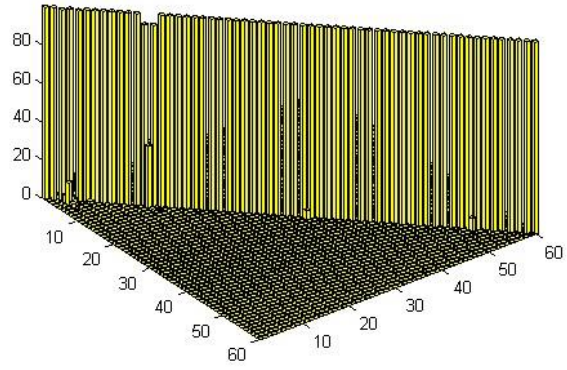
Baseline File: 1.1c.mat , Perturbed File: 1.24c.mat, tol=0.0001



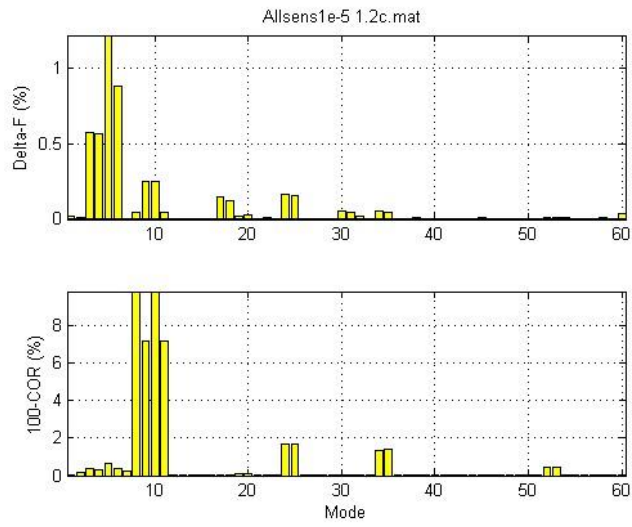
Baseline File: 1.1c.mat , Perturbed File: 1.25c.mat, tol=0.0001

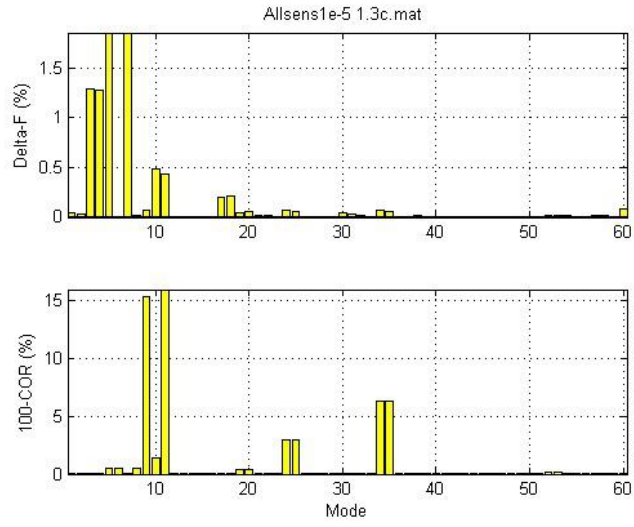


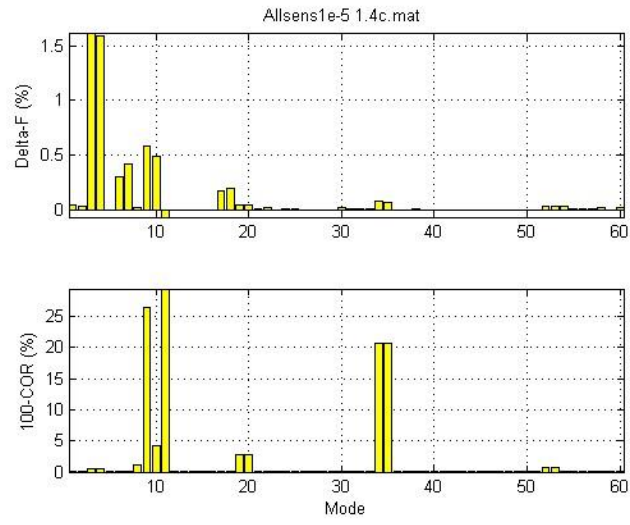
Baseline File: 1.1c.mat , Perturbed File: 1.26c.mat, tol=0.0001

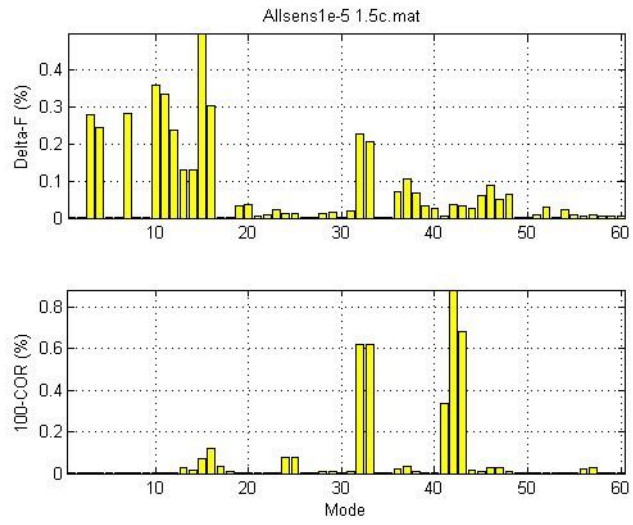


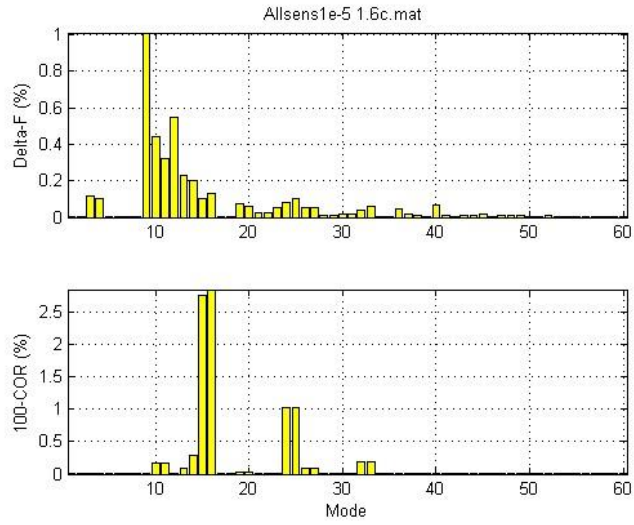
File: Allsens1e-5: Convergence Summary

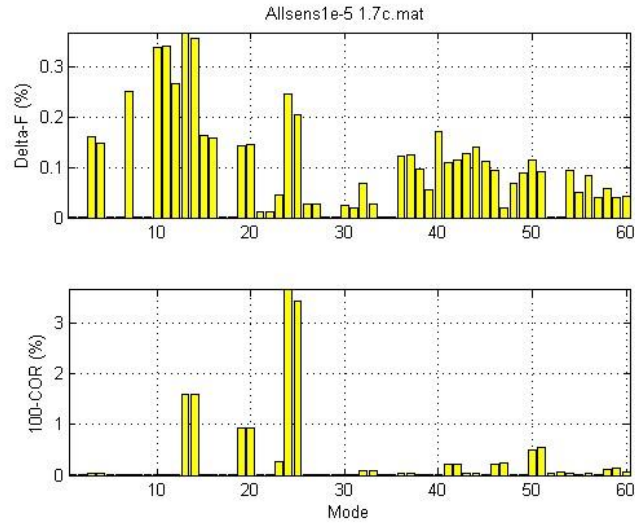


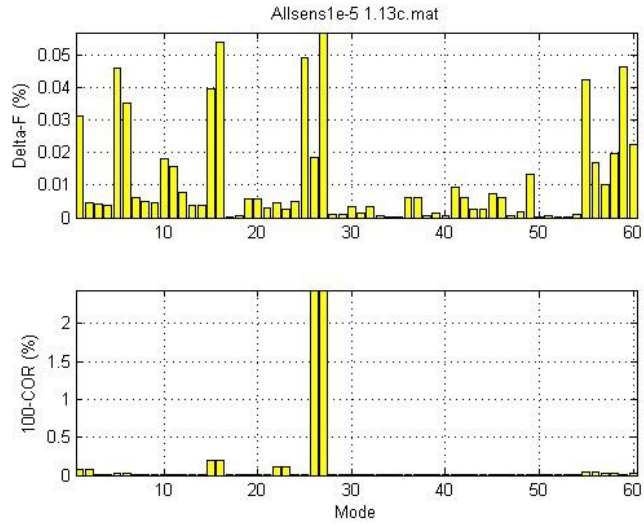


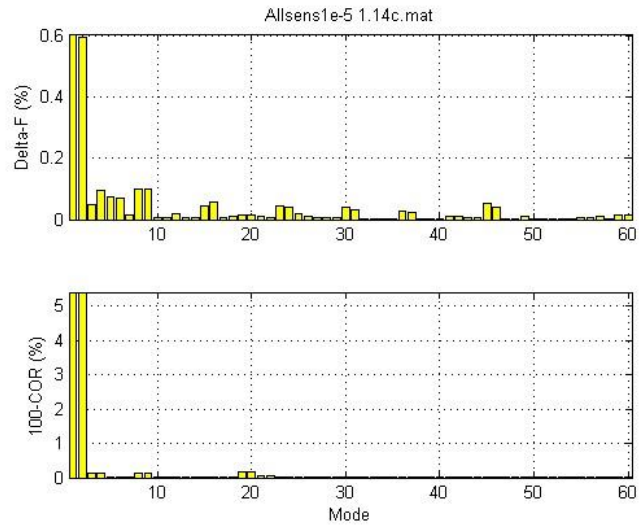


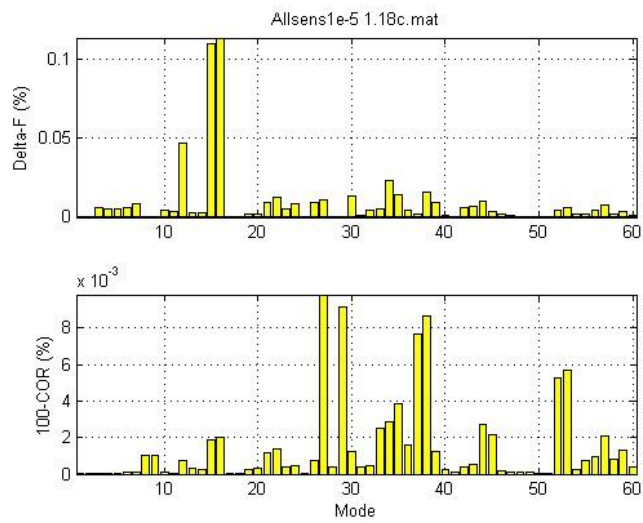


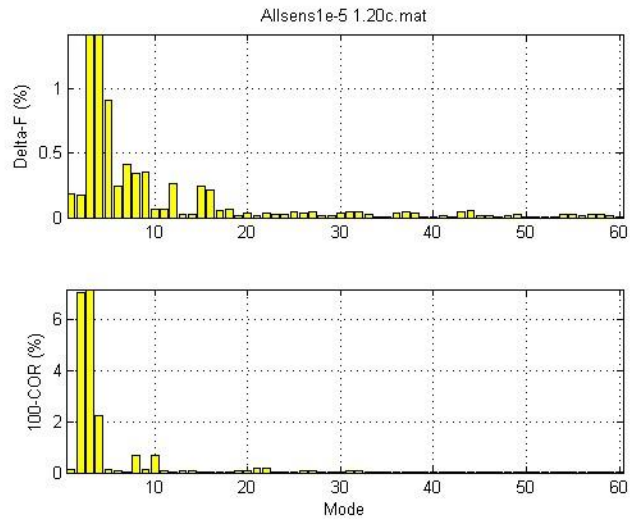


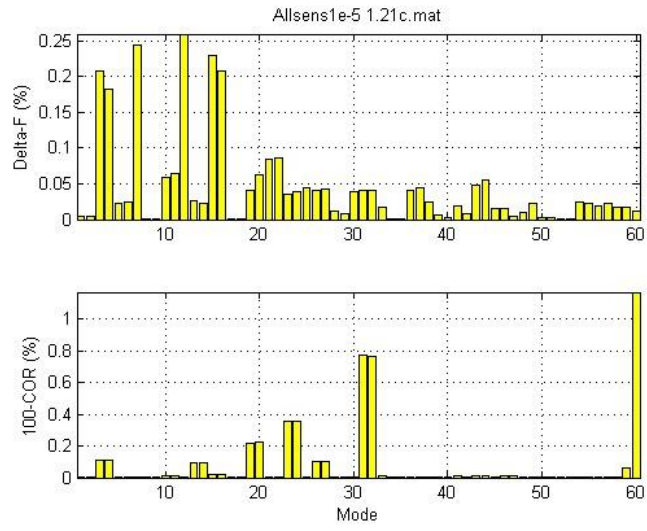


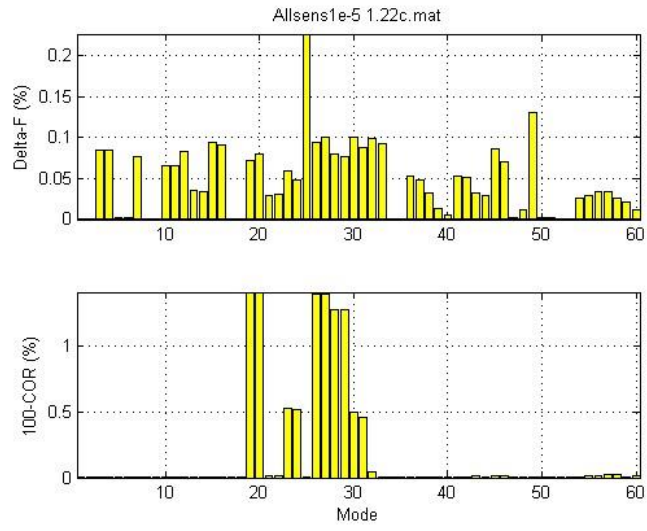


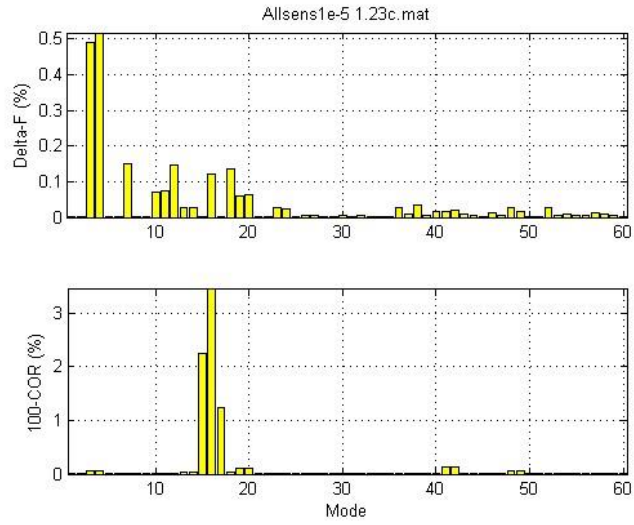


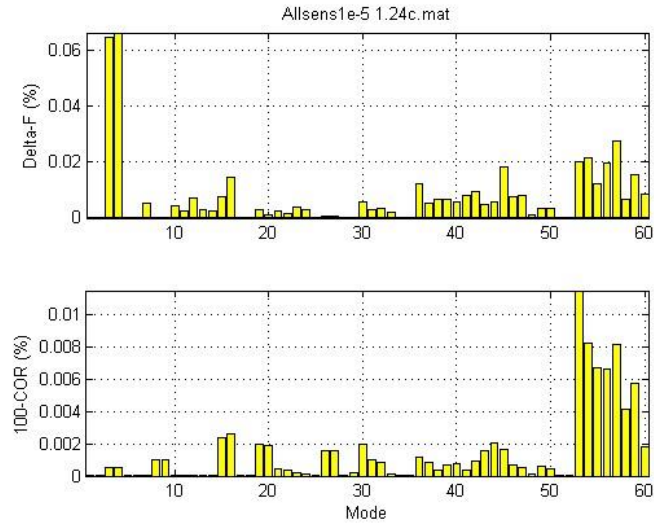


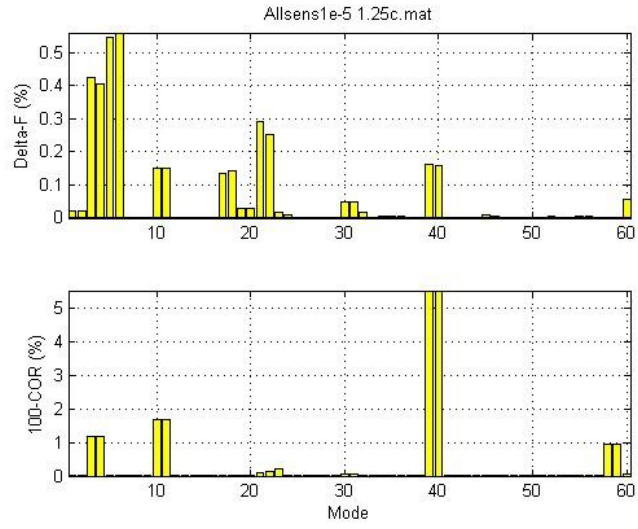


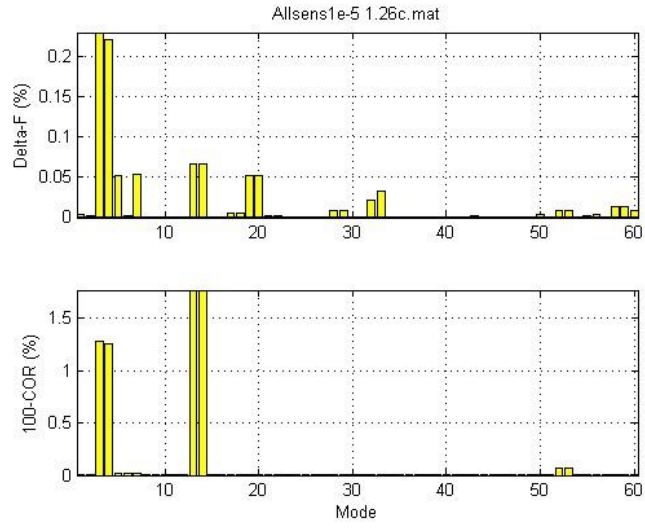








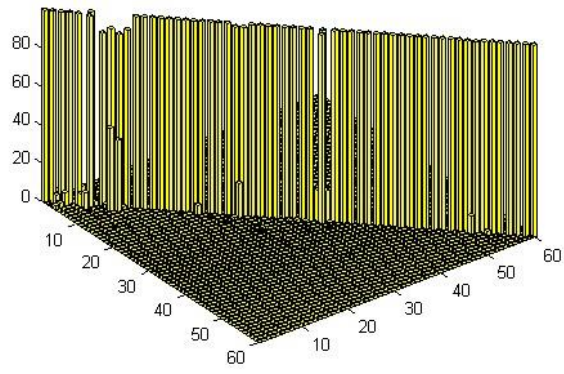




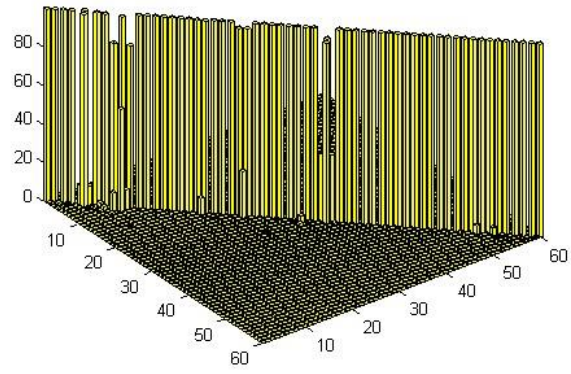
File: Allsens1e-5: Convergence Cross-Orthogonality

57

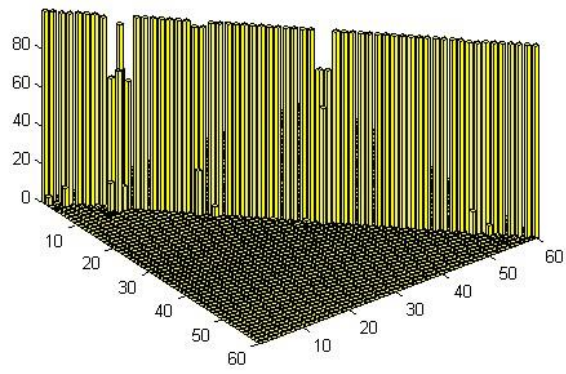
Baseline File: 1.1c.mat , Perturbed File: 1.2c.mat , tol=1e-005



Baseline File: 1.1c.mat , Perturbed File: 1.3c.mat , tol=1e-005

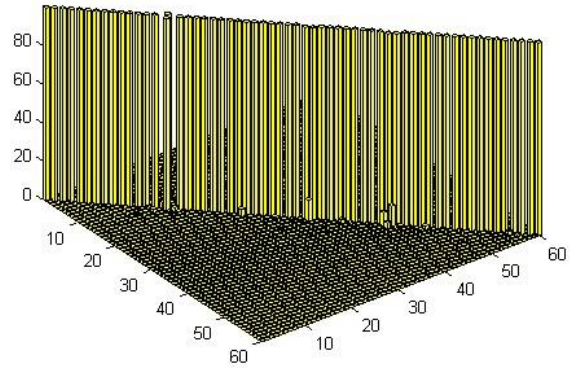


Baseline File: 1.1c.mat , Perturbed File: 1.4c.mat , tol=1e-005



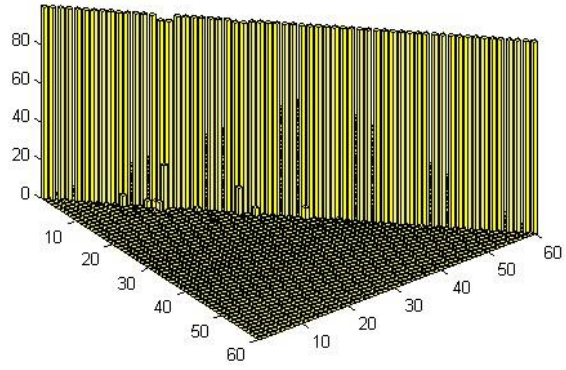
60

Baseline File: 1.1c.mat , Perturbed File: 1.5c.mat , tol=1e-005

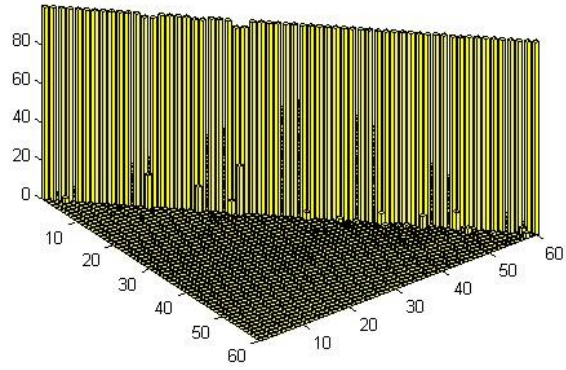


61

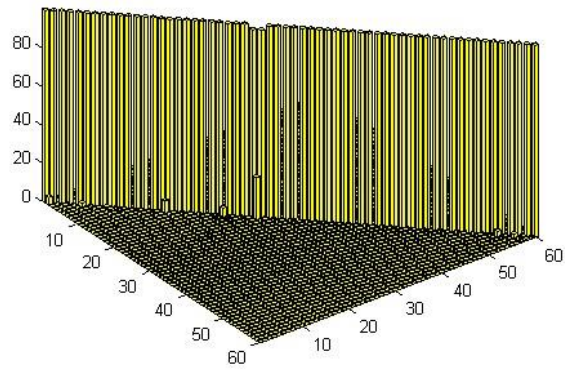
Baseline File: 1.1c.mat , Perturbed File: 1.6c.mat , tol=1e-005



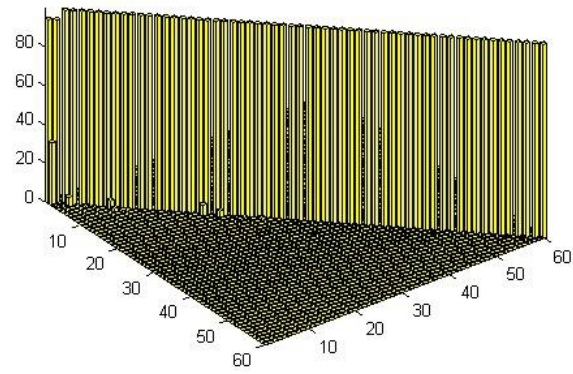
Baseline File: 1.1c.mat , Perturbed File: 1.7c.mat , tol=1e-005



Baseline File: 1.1c.mat , Perturbed File: 1.13c.mat, tol=1e-005

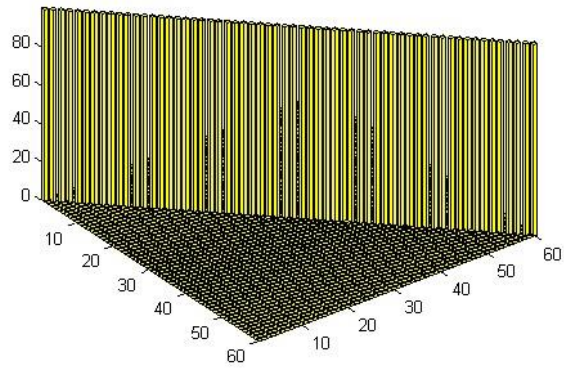


Baseline File: 1.1c.mat , Perturbed File: 1.14c.mat , tol=1e-005

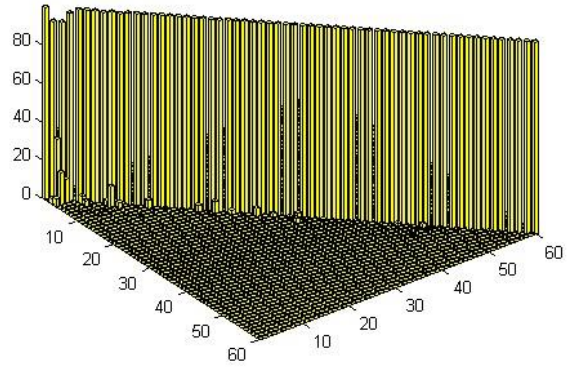


65

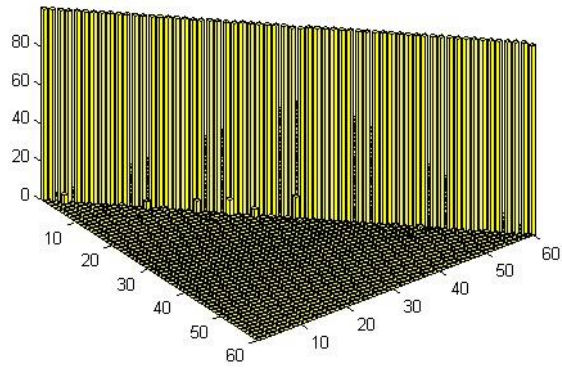
Baseline File: 1.1c.mat , Perturbed File: 1.18c.mat, tol=1e-005



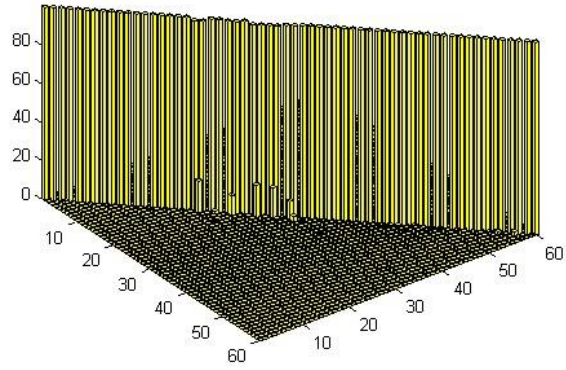
Baseline File: 1.1c.mat , Perturbed File: 1.20c.mat, tol=1e-005



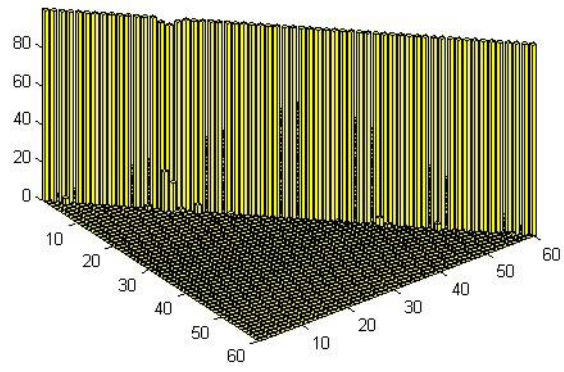
Baseline File: 1.1c.mat , Perturbed File: 1.21c.mat, tol=1e-005



Baseline File: 1.1c.mat , Perturbed File: 1.22c.mat, tol=1e-005

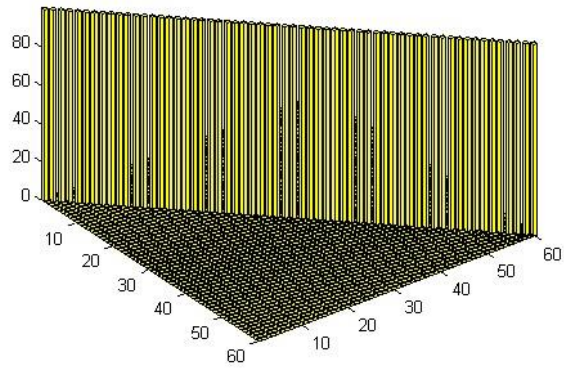


Baseline File: 1.1c.mat , Perturbed File: 1.23c.mat , tol=1e-005

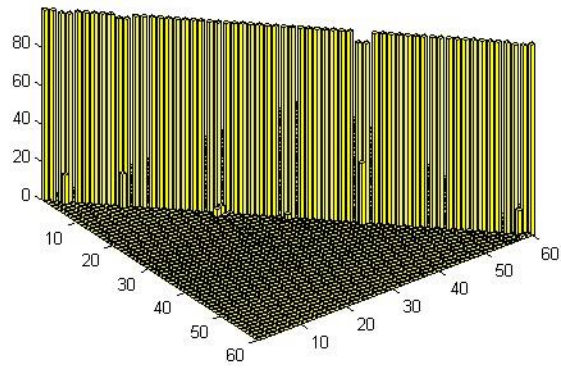


70

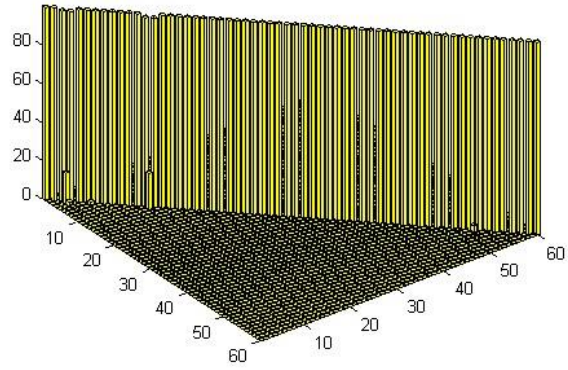
Baseline File: 1.1c.mat , Perturbed File: 1.24c.mat, tol=1e-005



Baseline File: 1.1c.mat , Perturbed File: 1.25c.mat , tol=1e-005



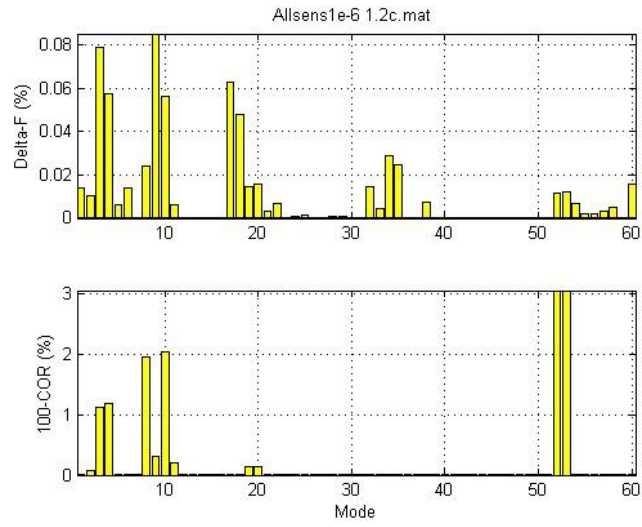
Baseline File: 1.1c.mat , Perturbed File: 1.26c.mat, tol=1e-005

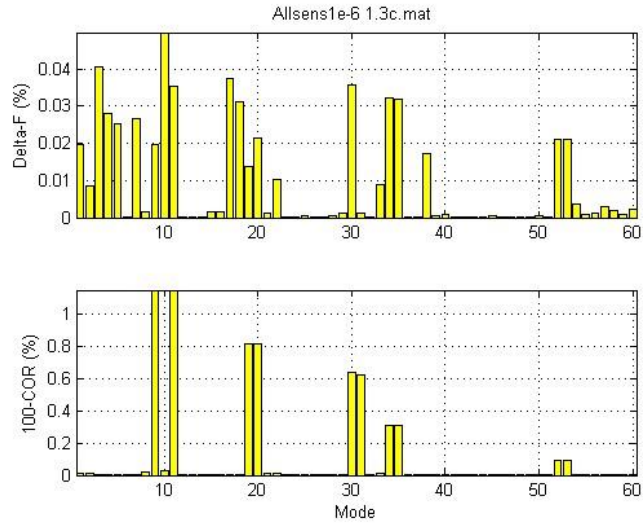


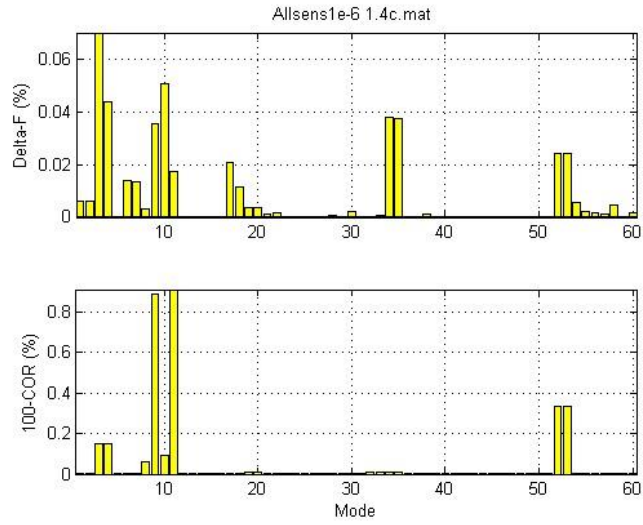
73

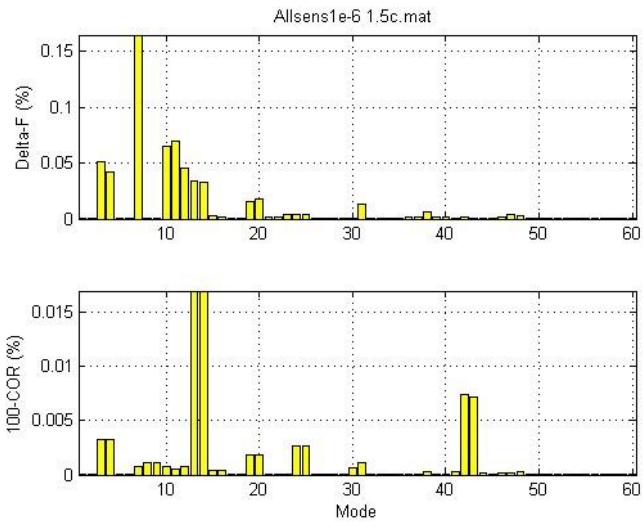
File: Allsens1e-6: Convergence Summary

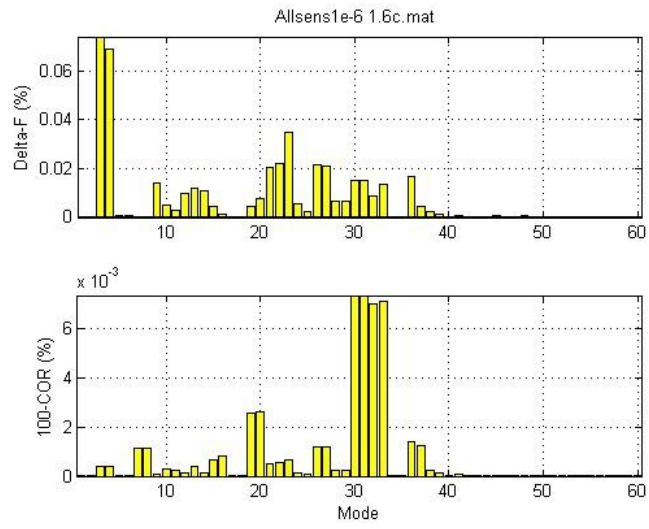
74

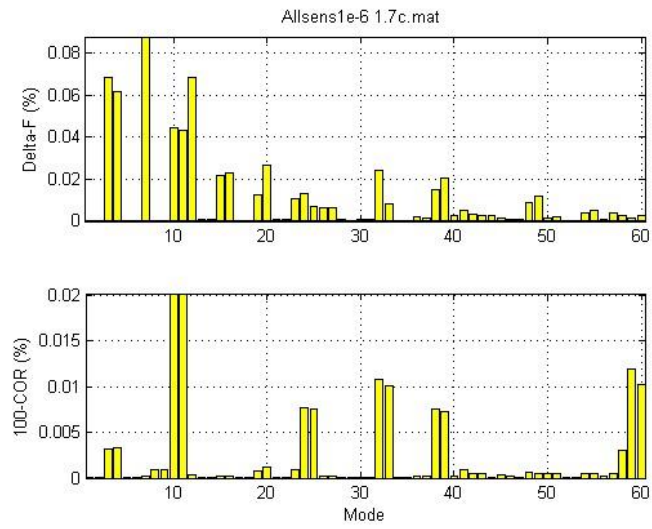


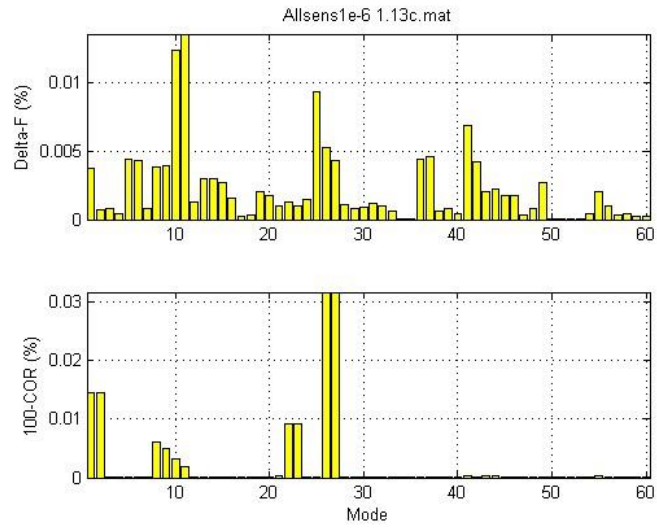


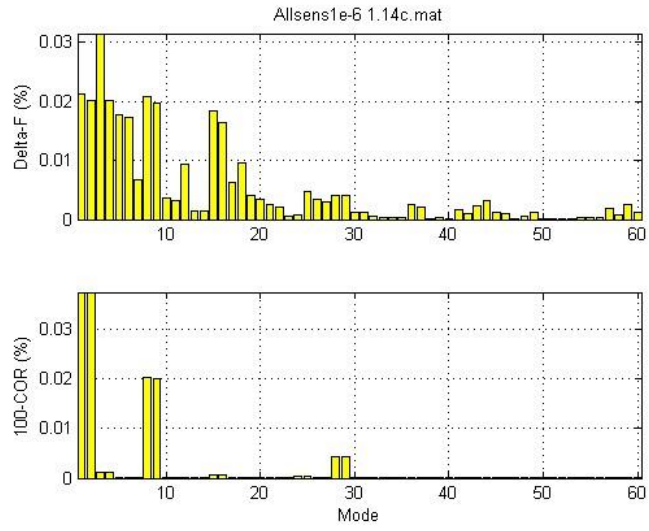


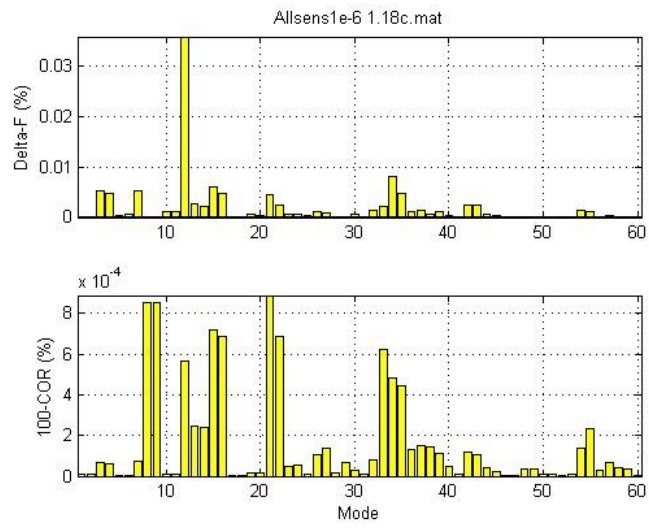


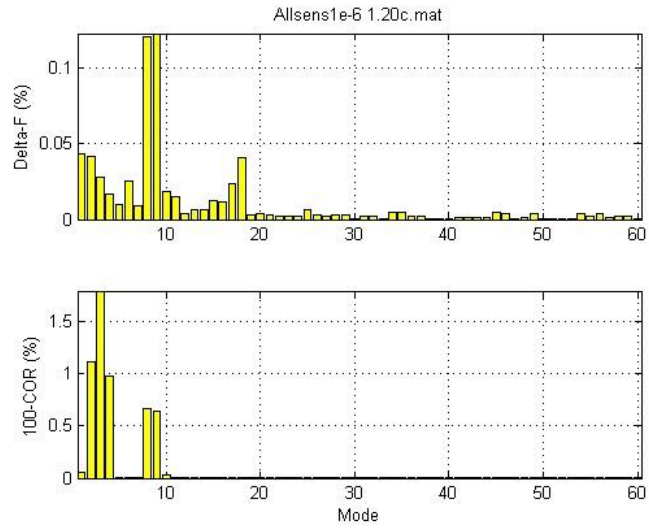


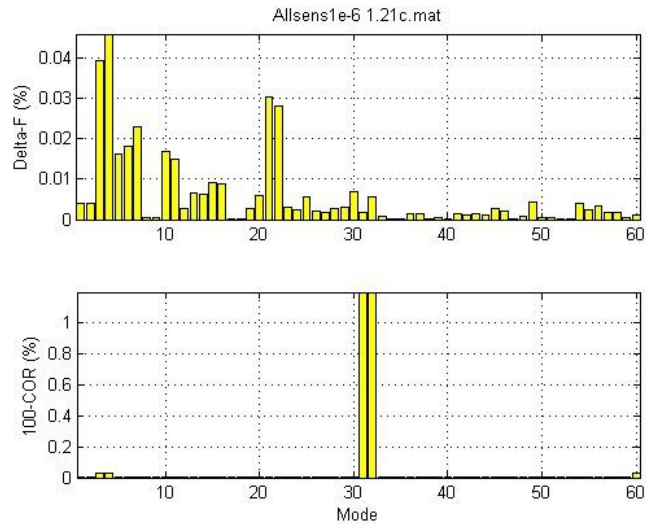


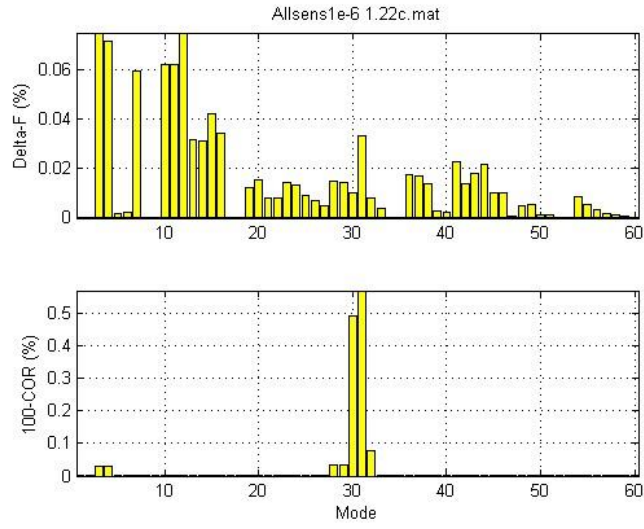


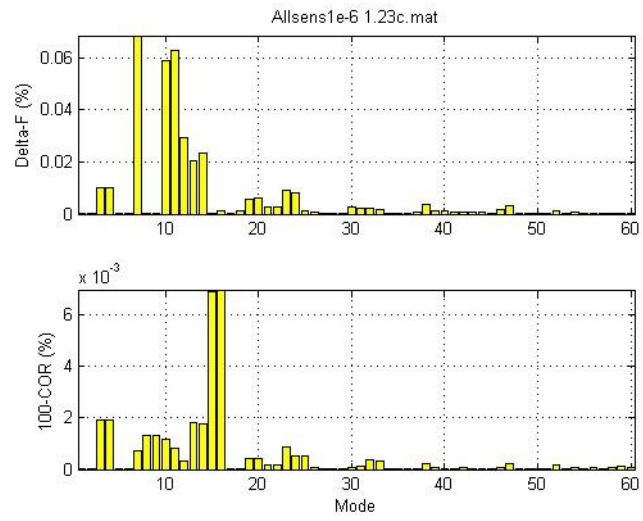


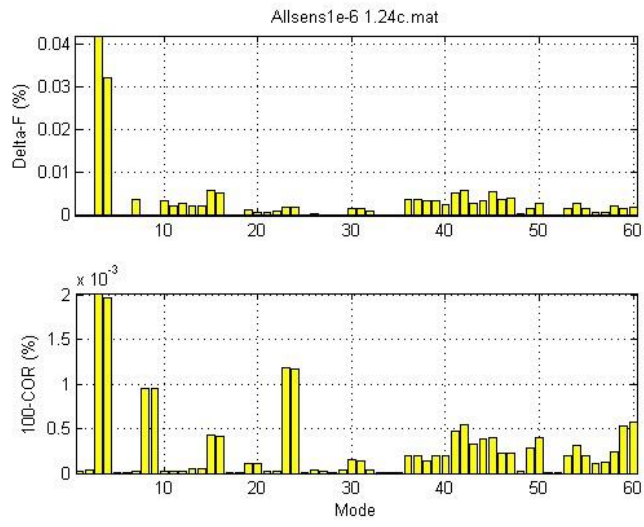


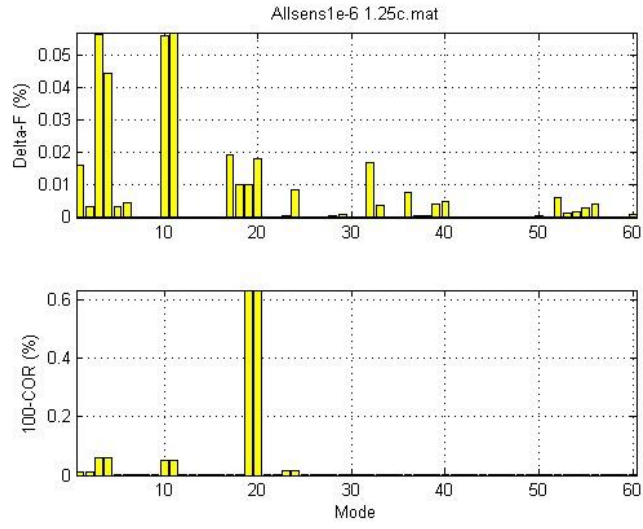


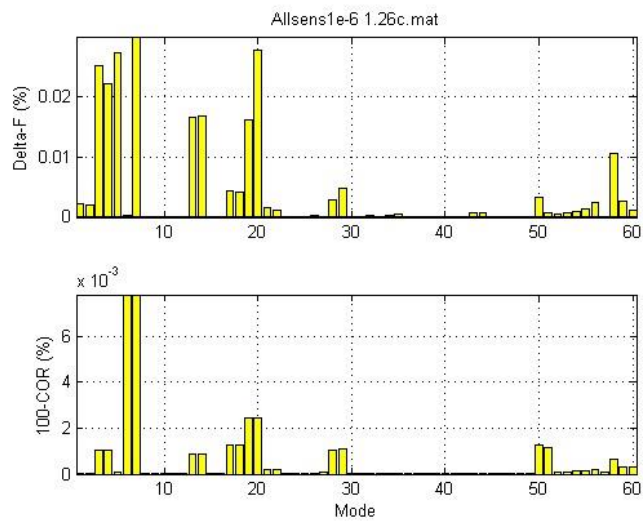








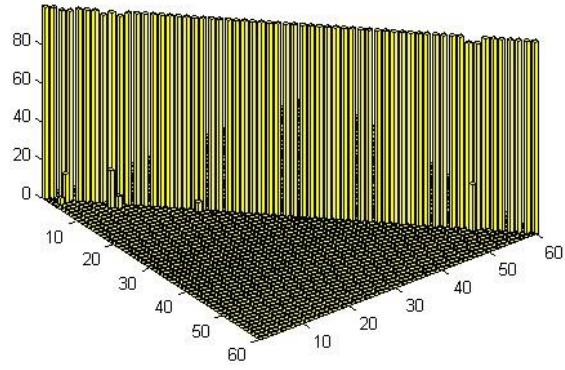




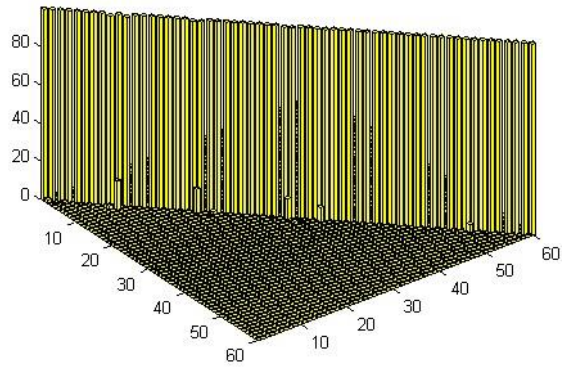
File: Allsens1e-6: Convergence Cross-Orthogonality

91

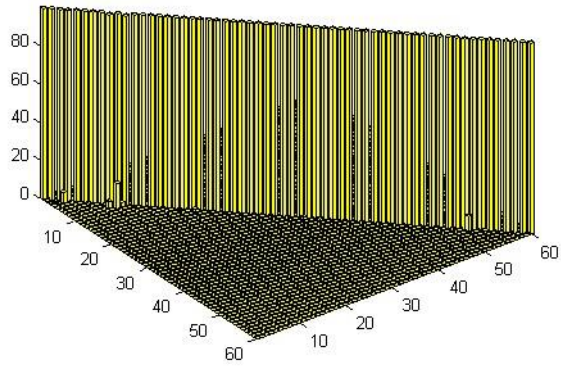
Baseline File: 1.1c.mat , Perturbed File: 1.2c.mat , tol=1e-006



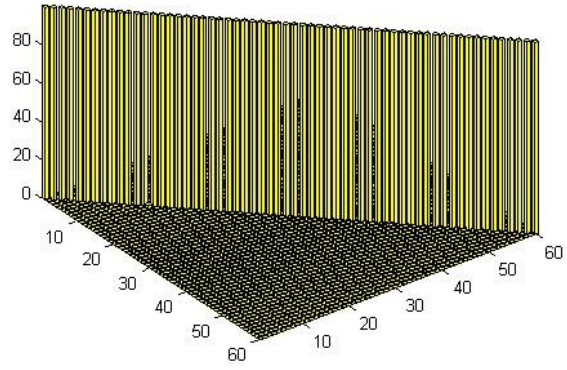
Baseline File: 1.1c.mat , Perturbed File: 1.3c.mat , tol=1e-006



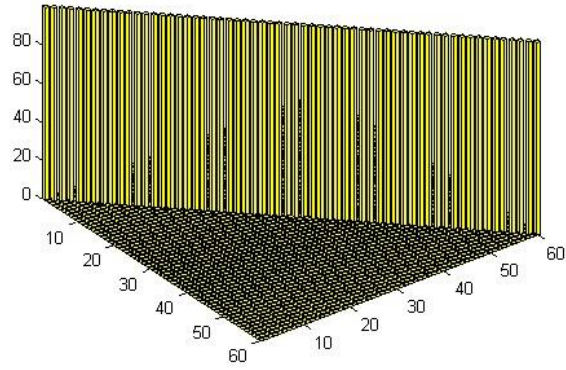
Baseline File: 1.1c.mat , Perturbed File: 1.4c.mat , tol=1e-006



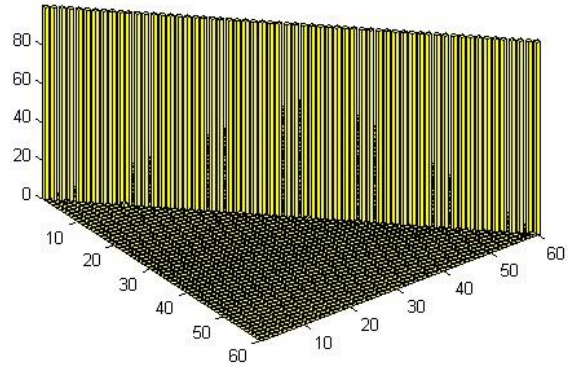
Baseline File: 1.1c.mat , Perturbed File: 1.5c.mat , tol=1e-006



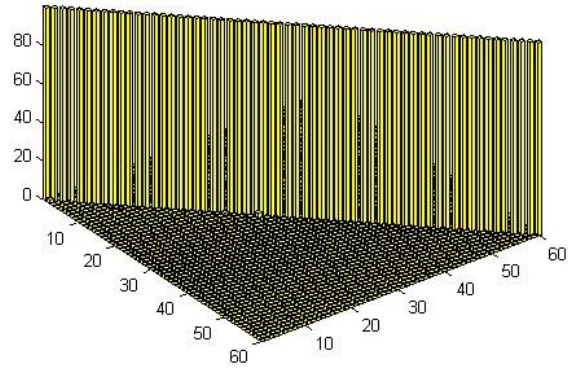
Baseline File: 1.1c.mat , Perturbed File: 1.6c.mat , tol=1e-006



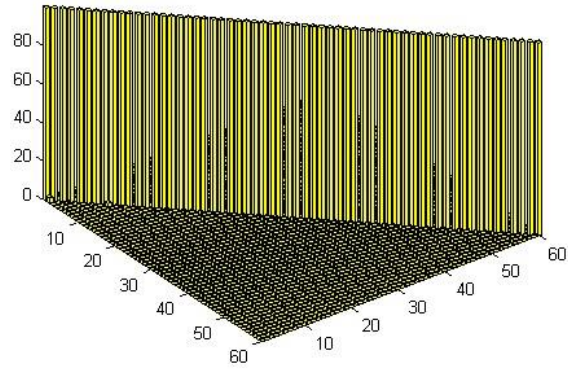
Baseline File: 1.1c.mat , Perturbed File: 1.7c.mat , tol=1e-006



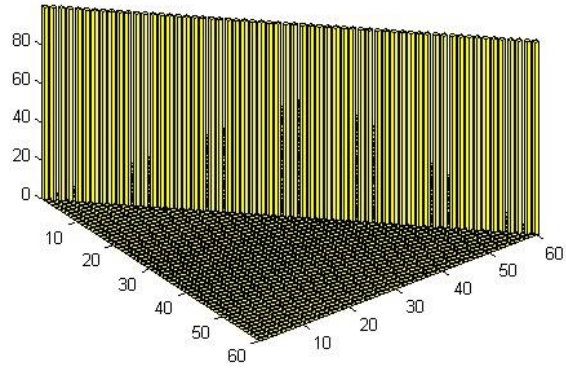
Baseline File: 1.1c.mat , Perturbed File: 1.13c.mat, tol=1e-006



Baseline File: 1.1c.mat , Perturbed File: 1.14c.mat, tol=1e-006

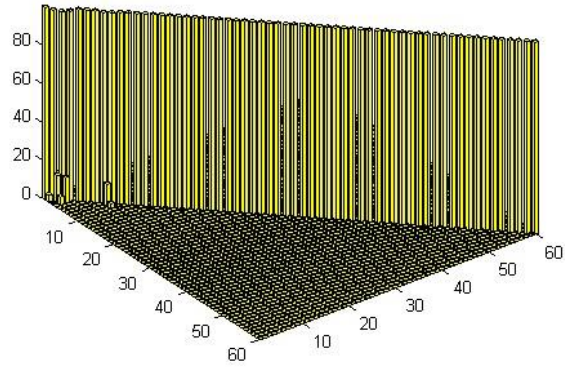


Baseline File: 1.1c.mat , Perturbed File: 1.18c.mat, tol=1e-006



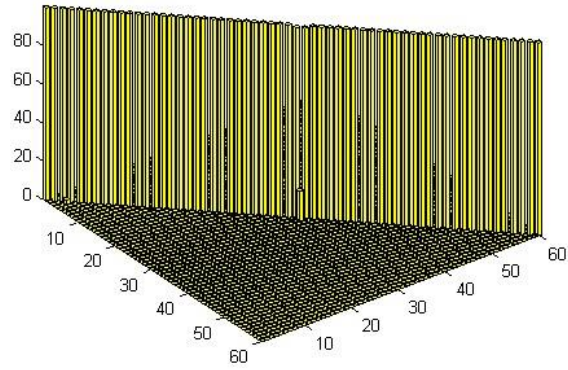
100

Baseline File: 1.1c.mat , Perturbed File: 1.20c.mat, tol=1e-006



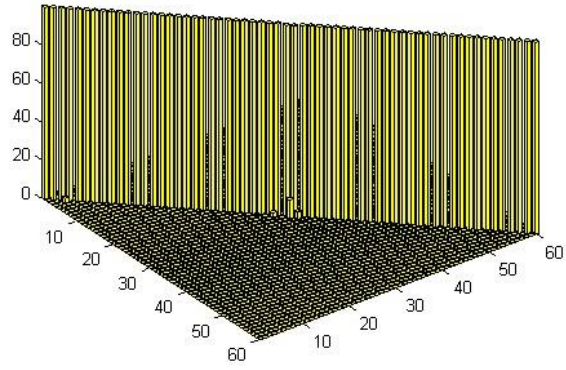
101

Baseline File: 1.1c.mat , Perturbed File: 1.21c.mat, tol=1e-006

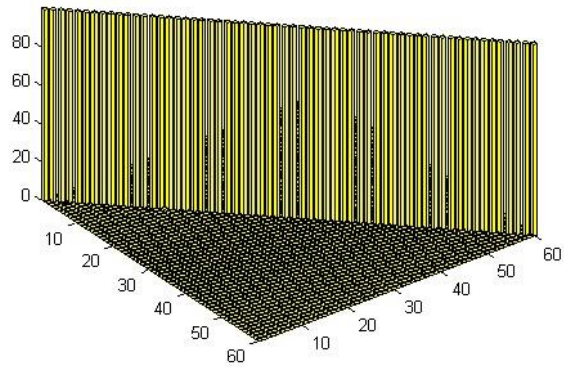


102

Baseline File: 1.1c.mat , Perturbed File: 1.22c.mat, tol=1e-006

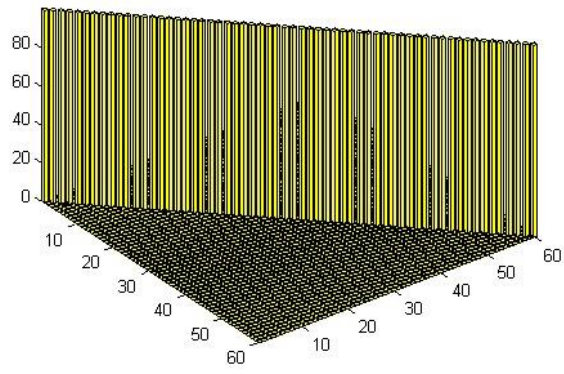


Baseline File: 1.1c.mat , Perturbed File: 1.23c.mat , tol=1e-006



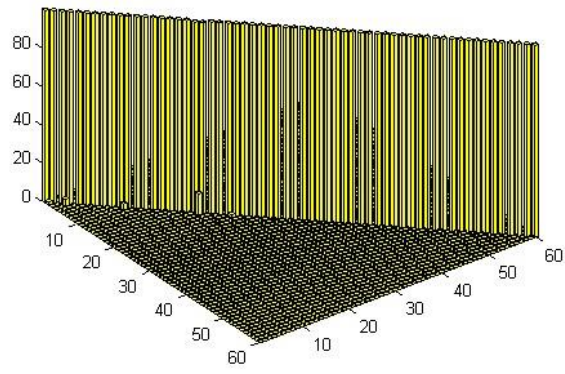
104

Baseline File: 1.1c.mat , Perturbed File: 1.24c.mat, tol=1e-006

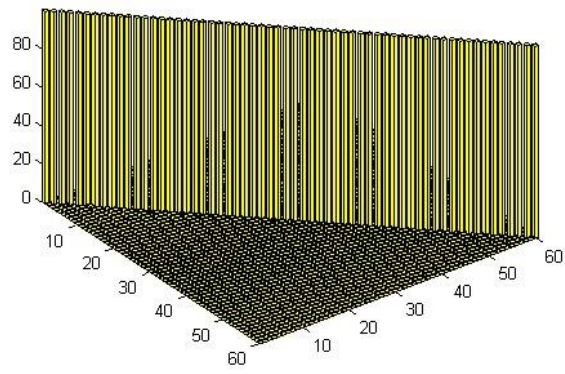


105

Baseline File: 1.1c.mat , Perturbed File: 1.25c.mat, tol=1e-006



Baseline File: 1.1c.mat , Perturbed File: 1.26c.mat, tol=1e-006



107

Appendix D. Consolidation of Body Modes for an “Axisymmetric” Shell Structure

Appendix D:
Consolidation of Body Modes
for an “Axisymmetric” Shell Structure

Robert N. Coppolino
Measurement Analysis Corporation
11 July 2017

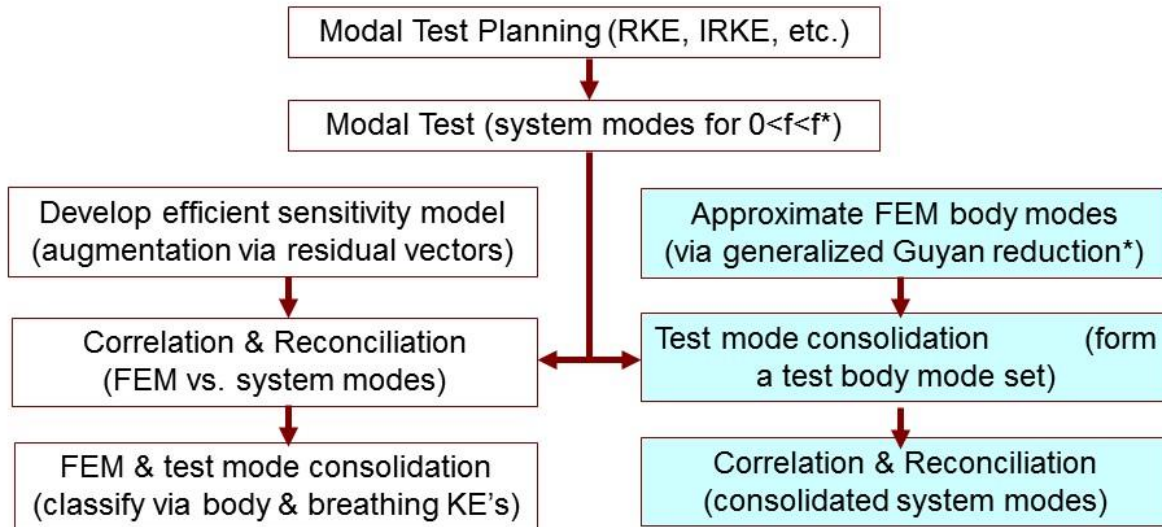
Introduction and Summary

- It is anticipated that the SLS Core Vehicle will have a high number of modes (on the order of 2000) over the 0-50 Hz frequency band. Many anticipated modes are of shell breathing character (which are sensitive to tank pressurization associated with fluid inertia and ullage). A smaller subset of modes are characterized by overall body deformation (e.g., bending, axial stretch, torsion, and n=0 bulge). Slight asymmetries and imperfections may cause some modes to be of mixed body and shell breathing character.
- A variety of modal quantities are examined to assist in interpretation of system modes and select a “target mode” subset, namely (a) directional kinetic energy, (b) “body” and “breathing” kinetic energies.
- “Body” dominant modes (which contain “breathing” components due to slight asymmetries and imperfections) may form modal clusters containing repeated body deflection patterns.
- Estimation of consolidated “pure body” modes of a corresponding perfectly axisymmetric structure is accomplished by employing SVD on body mode cluster generalized masses and system mode frequencies.

Introduction and Summary (cont'd)

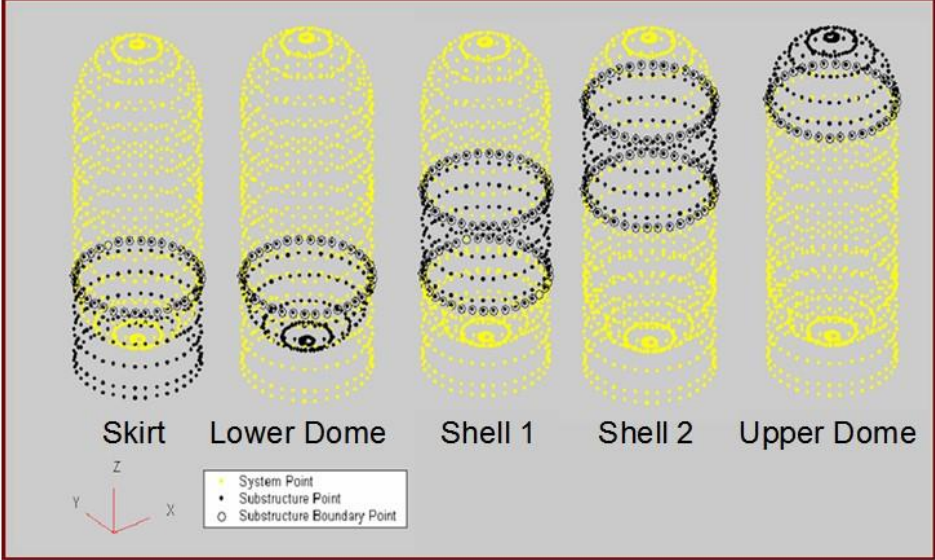
- While the present report serves the purpose of describing the mode consolidation process, it does not formally advocate how the concept is to be applied. Therefore, at this time it is anticipated that mode consolidation may be employed as back-up/new capability that is potentially useful in upcoming SLS modal tests.
- That being said, some preliminary thoughts on mode consolidation are provided in the next slide.

Potential Application of Mode Consolidation (a parallel process augmenting the conventional strategy)

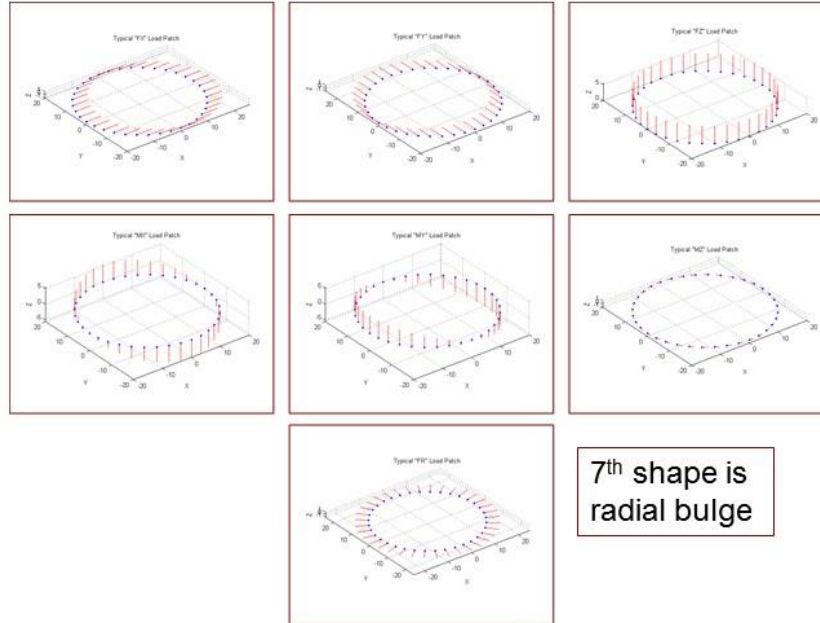


* An efficient generalized Guyan reduction sensitivity method has been defined, to be discussed in a subsequent report.

Illustrative Example: Segmented Shell Model (fixed base at the lower skirt bottom)



Body Displacement Pattern Shape Functions (for each "Z" station)



6

Body Displacement Pattern Shape Functions (separation of “body” and “breathing” modal patterns)

- Basic relationship

$$[\Phi_L] = [\Psi_b][\phi_b] + [\Phi_r]$$

- Least-squares analysis

$$[\Psi_b^T M \Phi_L] = [\Psi_b^T M \Psi_b][\phi_b] + [\cancel{\Psi_b^T M \Phi_r}^0]$$

$$[\phi_b] = [\Psi_b^T M \Psi_b]^{-1} [\Psi_b^T M \Phi_L]$$

- Modal pattern decomposition

$$[\Phi_b] = [\Psi_b][\phi_b] \quad , \quad [\Phi_r] = [\Phi_L] - [\Phi_b]$$

$$[\Phi_L] = [\Phi_b] + [\Phi_r]$$

Body Displacement Pattern Shape Functions (separation of “body” and “breathing” modal patterns)

- Modal kinetic energies

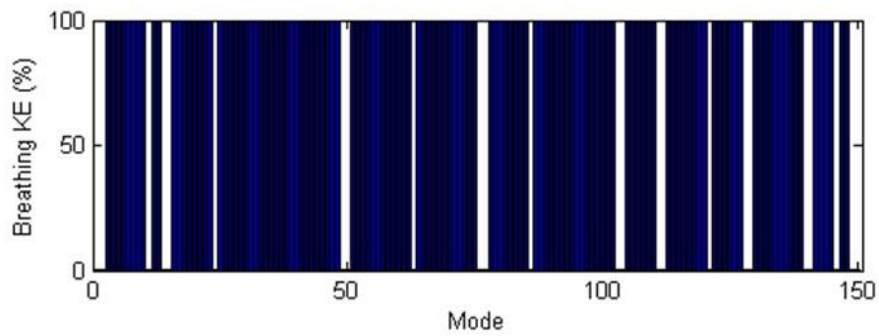
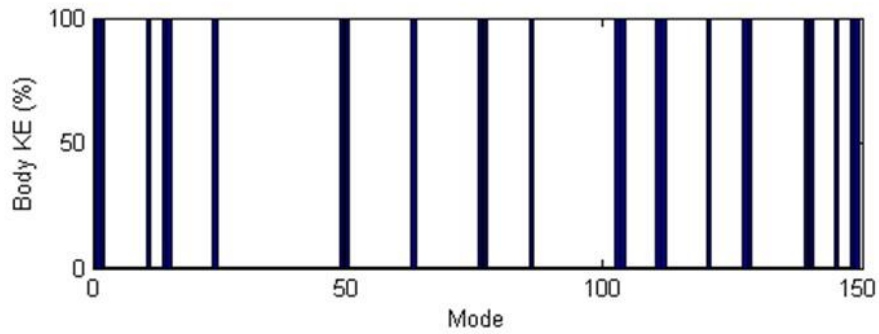
$$\begin{array}{c}
 \uparrow \\
 \text{“total KE”}
 \end{array}
 [M\Phi] \otimes [\Phi] =
 \begin{array}{c}
 \uparrow \\
 \text{“body KE”}
 \end{array}
 [M\Phi_b] \otimes [\Phi_b] +
 \begin{array}{c}
 \uparrow \\
 \text{“breathing KE”}
 \end{array}
 [M\Phi_r] \otimes [\Phi_r]$$

- Also....

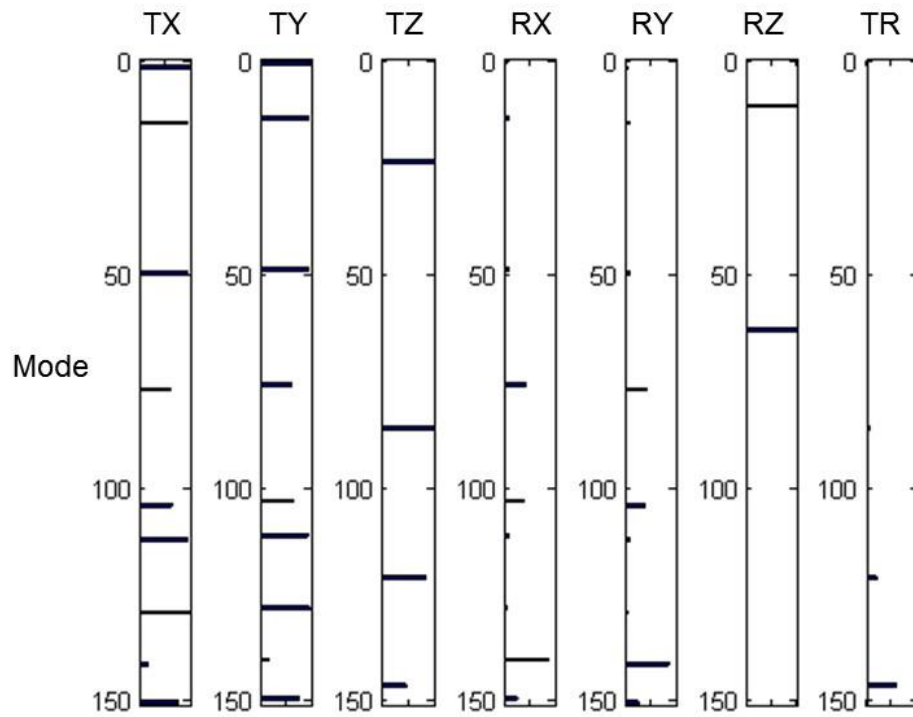
$$[\Phi_L^T M \Phi_L] = [I_L] = [\Phi_b^T M \Phi_b] + [\Phi_r^T M \Phi_r]$$

- Note: The “body” and “breathing” contributions are independent since the two groups are orthogonal to each other.

Overview of Body & Breathing Mode Kinetic Energies (for the baseline, axisymmetric structure)



Overview of Body Mode Kinetic Energies (for the baseline axisymmetric structure)



10

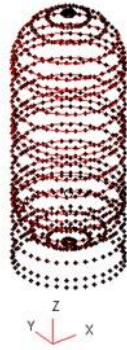
Typical Body Modes (for the baseline, axisymmetric structure)

Mode 1, Freq = 122.2 Hz



Lateral Y

Mode 11, Freq = 315.24 Hz



Torsion

Mode 24, Freq = 467.77 Hz



Axial

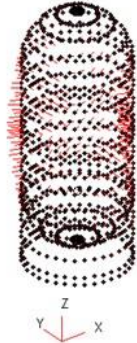
Mode 146, Freq = 1440.38 Hz



Bulge

Typical Breathing Modes (for the baseline, axisymmetric structure)

Mode 3, Freq = 176.086 Hz



Mode 3, Freq = 176.086 Hz



$n = 3$

Mode 5, Freq = 187.659 Hz

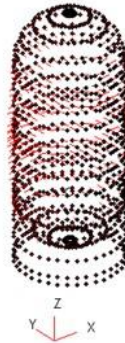


Mode 5, Freq = 187.659 Hz

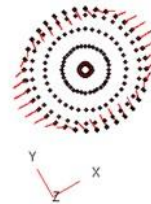


$n = 4$

Mode 7, Freq = 241.072 Hz

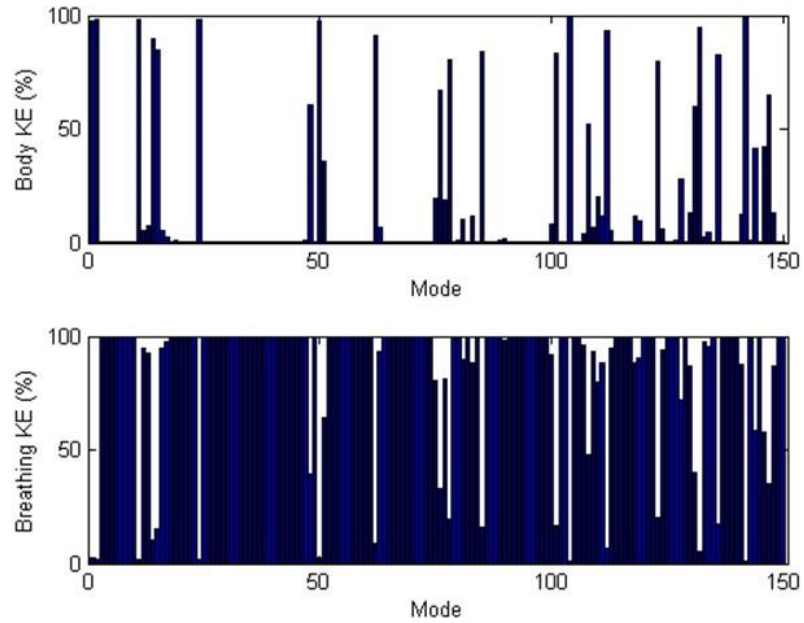


Mode 7, Freq = 241.072 Hz



$n = 2$

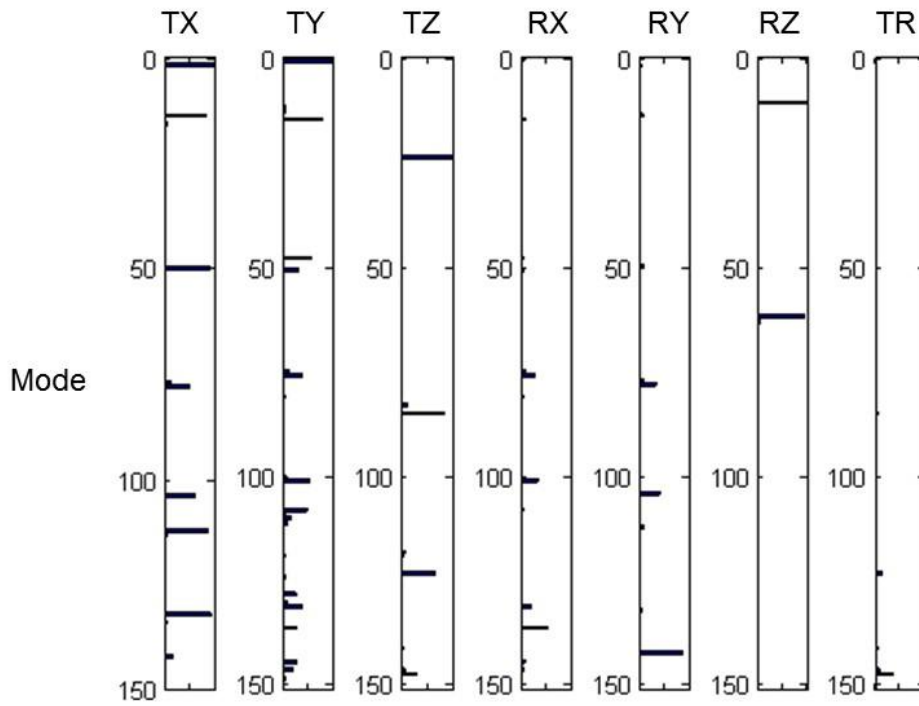
Overview of Body & Breathing Mode Kinetic Energies (for the perturbed*, axisymmetric structure)



* Finite mass perturbation introduced along the "X=0" line of grid points.

13

Overview of Body Mode Kinetic Energies (for the perturbed axisymmetric structure)

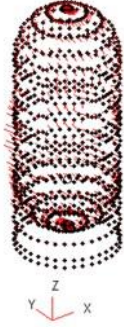


Typical Mixed Body & Breathing Modes (for the perturbed, axisymmetric structure)

Mode 14, Freq = 373.97 Hz



Mode 15, Freq = 374.65 Hz



Mode 16, Freq = 375.36 Hz



Mode 17, Freq = 377.43 Hz



Mode 14, Freq = 373.97 Hz



[KEB, KER] = [90, 10]

Mode 15, Freq = 374.65 Hz



[84, 16]

Mode 16, Freq = 375.36 Hz



[5, 95]

Mode 17, Freq = 377.43 Hz



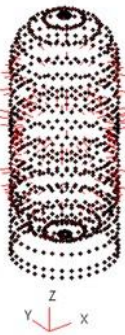
[3, 97]

Typical Mixed Body & Breathing Modes (for the perturbed, axisymmetric structure)

Mode 48, Freq = 695.39 Hz



Mode 49, Freq = 699.64 Hz



Mode 50, Freq = 701.56 Hz



Mode 51, Freq = 706.21 Hz



Mode 48, Freq = 695.39 Hz



[KEB, KER] = [61, 39]

Mode 49, Freq = 699.64 Hz



[1, 99]

Mode 50, Freq = 701.56 Hz



[98, 2]

Mode 51, Freq = 706.21 Hz



[36, 64]

16

Mode Consolidation Theory

(mode segmentation using shape matrix, $[\Psi_b]$)

$$[\Phi_L] = [\Psi_b][\phi_b] + [\Phi_r] \quad (\text{body, "b", and breathing, "r", segments})$$

$$[\Psi_b^T M \Phi_L] = [\Psi_b^T M \Psi_b][\phi_b] + \overset{0}{[\Psi_b^T M \Phi_r]} \Rightarrow [\phi_b] = [\Psi_b^T M \Psi_b]^{-1} [\Psi_b^T M \Phi_L]$$

↓

$$[\Phi_L] = [\Phi_b] + [\Phi_r], [\Phi_b] = [\Psi_b][\phi_b], [\Phi_r] = [\Phi_L] - [\Phi_b]$$

$$[\Phi_b^T M \Phi_b] = [OR_b] = [m_b], [\Phi_r^T M \Phi_r] = [OR_r] = [m_r], [\Phi_b^T M \Phi_r] = [0]$$

segmented (partial) modal kinetic energies

$$(\text{KE}_L)_i = (\text{KE}_b)_i + (\text{KE}_r)_i = 1, (\text{KE}_b)_i = (m_b)_{ii}, (\text{KE}_r)_i = (m_r)_{ii}$$

Mode Consolidation Theory (*motivational facts*)

$$[\mathbf{K}][\Phi] = [\mathbf{M}][\Phi][\lambda] \quad (\text{eigenvalue problem})$$

$$[\text{OR}] = [\mathbf{m}] = [\Phi^T \mathbf{M} \Phi] = [\mathbf{I}] \quad [\mathbf{k}] = [\Phi^T \mathbf{K} \Phi] = [\lambda]$$

- The orthogonality matrix is the sum of “body” and “breathing” components

$$[\text{OR}] = [\mathbf{m}] = [\mathbf{m}_b] + [\mathbf{m}_r]$$

- The “experimental” generalized stiffness matrix cannot be segmented
 - $[\mathbf{K}]$ is unknown, but $[\mathbf{k}] = [\lambda]$, which is experimentally “known”
 - therefore, a strategy based on $[\mathbf{m}_b]$ and $[\lambda]$ is required

Mode Consolidation Theory

(“body” mode segment cluster consolidation via SVD)

basic SVD operations

$$[\mathbf{m}_b][\tilde{\mathbf{v}}_b] = [\tilde{\mathbf{v}}_b][\boldsymbol{\gamma}_b] \quad \gamma_{b,1} \geq \gamma_{b,2} \geq \gamma_{b,3} \dots$$

$$[\tilde{\mathbf{v}}_b^T][\tilde{\mathbf{v}}_b] = [\mathbf{I}] \quad [\tilde{\mathbf{v}}_b^T \mathbf{m}_b \tilde{\mathbf{v}}_b] = [\boldsymbol{\gamma}_b]$$

Criterion for eigenvalue cut-off, $(\gamma_{b,i} / \gamma_{b,1}) \geq \text{tol}$

eigenvector rescaling

$$[\mathbf{v}_b] = [\tilde{\mathbf{v}}_b][\boldsymbol{\gamma}_b]^{1/2}$$

$$[\mathbf{v}_b^T \mathbf{v}_b] = [\boldsymbol{\gamma}_b] \quad [\mathbf{m}_b] = [\mathbf{v}_b][\mathbf{v}_b^T]$$

(Convenient step for KE based mode consolidation)

Mode Consolidation Theory

(“body” mode segment cluster consolidation via SVD)

consolidated modal frequencies as Rayleigh quotients

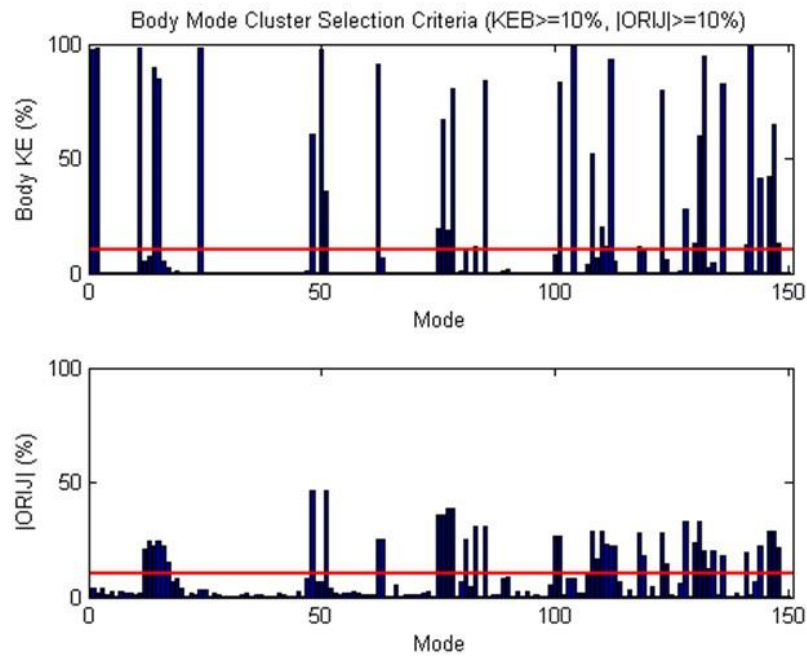
$$\lambda_{b,i} = \frac{\{\mathbf{v}_{b,i}\}^T [\lambda] \{\mathbf{v}_{b,i}\}}{\{\mathbf{v}_{b,i}\}^T \{\mathbf{v}_{b,i}\}} \quad \Rightarrow \quad f_{b,i} = \frac{\sqrt{\lambda_{b,i}}}{2\pi}$$

consolidated body modes via SVD transformation

$$\begin{aligned} [\tilde{\Phi}_c] &= [\Phi_b][\mathbf{v}_b] & m_{c,i} &= \{\Phi_{c,i}\}^T [M] \{\Phi_{c,i}\} \\ \{\Phi_{c,i}\} &= \{\tilde{\Phi}_{c,i}\} / \sqrt{m_{c,i}} & [\Phi_c^T M \Phi_c] &= [I] \end{aligned}$$

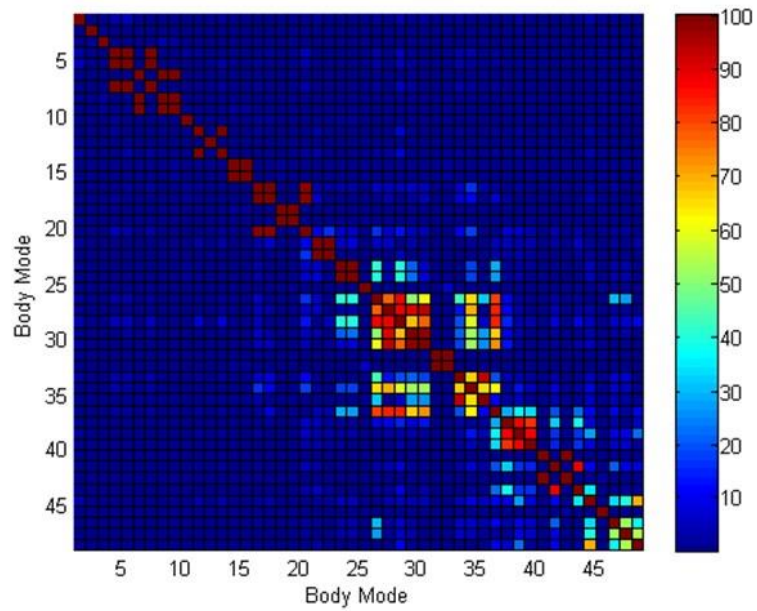
20

Body Mode Cluster Selection Criteria ($KE_B \geq 10\%$, $|OR_{IJ}| \geq 10\%$)



21

Orthogonality of Body Mode Clusters (normalized body modes indicating “repeated” body modes)



Overview of Body Mode Clusters (non-normalized body mode KE, selected modes 1-22)

Perturbed (Selected Modes)				Body Mode Orthogonality Matrix																						
Mode	Freq (Hz)	diag (OR)	coup(OR)	1	2	3	4	5	6	7	8	9	10	11	12	13	14	15	16	17	18	19	20	21	22	
1	120.97	98	2	98	0	0	1	-2	0	0	0	0	-1	1	0	1	0	0	0	0	0	0	0	0	-1	0
2	121.13	98	2	0	98	-2	0	0	0	0	0	0	0	0	0	0	0	0	0	0	0	0	0	0	0	0
11	312.43	98	2	0	-2	98	0	0	-1	0	-1	0	0	0	0	0	0	0	0	0	0	0	0	0	0	0
12	359.94	5	21	1	0	0	5	6	0	21	0	0	0	0	0	0	0	0	0	0	0	0	0	0	0	0
13	367.98	7	25	-2	0	0	6	7	0	25	0	0	0	0	0	1	0	0	0	0	0	0	0	0	0	0
14	373.97	90	22	0	0	-1	0	0	90	0	-22	-15	0	0	0	0	1	0	0	0	0	0	0	0	0	0
15	374.65	84	25	0	0	0	21	25	0	84	0	0	0	1	0	1	0	0	-1	0	0	0	-1	0	0	0
16	375.36	5	22	0	0	-1	0	0	-22	0	5	4	0	0	0	0	0	0	0	0	0	0	0	0	0	0
17	377.43	3	15	0	0	0	0	0	-15	0	4	3	0	0	0	0	0	0	0	0	0	0	0	0	0	0
24	463.45	98	2	-1	0	0	0	0	0	0	0	0	98	0	0	0	0	0	0	-1	-1	0	0	0	0	0
48	695.39	61	46	1	0	0	0	0	0	1	0	0	0	61	0	-46	0	0	-1	0	0	0	0	0	-1	0
50	701.56	98	0	0	0	0	0	0	0	0	0	0	0	0	98	0	0	0	0	0	0	0	0	0	0	0
51	706.21	36	46	1	0	0	0	1	0	1	0	0	0	-46	0	36	0	0	0	0	0	0	0	0	1	0
62	833.52	91	25	0	0	0	0	0	1	0	0	0	0	0	0	0	91	25	0	0	1	0	0	0	0	0
63	836.13	7	25	0	0	0	0	0	0	0	0	0	0	0	0	0	25	7	0	0	0	0	0	0	0	0
75	967.62	20	36	0	0	0	0	0	0	-1	0	0	-1	-1	0	0	0	0	20	36	0	0	-14	-1	1	1
76	986.08	67	36	0	0	0	0	0	0	0	0	0	-1	0	0	0	0	0	36	67	0	0	-25	-2	-1	
77	992.77	19	39	0	0	0	0	0	0	0	0	0	0	0	0	0	1	0	0	0	19	-39	0	0	0	
78	994.38	81	39	0	0	0	0	0	0	0	0	0	0	0	0	0	0	0	0	0	-39	81	0	0	0	
81	1001.81	10	25	0	0	0	0	0	0	-1	0	0	0	0	0	0	0	0	-14	-25	0	0	10	-1	-5	
83	1017.37	12	31	-1	0	0	0	0	0	0	0	0	0	-1	0	1	0	0	-1	-2	0	0	-1	12	31	
85	1020.38	84	31	0	0	0	0	0	0	0	0	0	0	0	0	0	0	0	1	-1	0	0	-5	31	84	

(There are eight selected clusters to analyze)

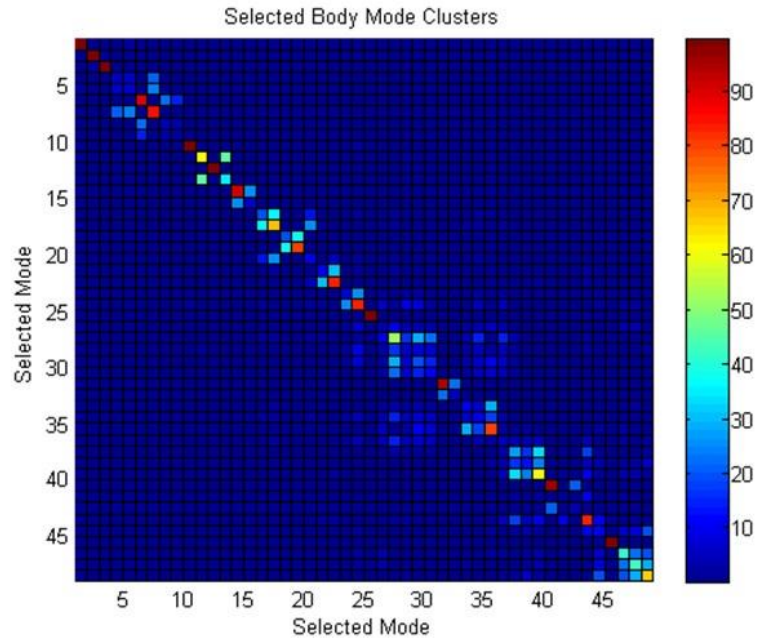
Overview of Body Mode Clusters

(non-normalized body mode KE, selected modes 23-49)

Perturbed (Selected Modes)				Body Mode Orthogonality Matrix																																													
Mode	Freq (Hz)	diag (OR)	coupl(OR)	23	24	25	26	27	28	29	30	31	32	33	34	35	36	37	38	39	40	41	42	43	44	45	46	47	48	49																			
100	1148.56	8	26	8	-26	0	2	1	-3	-3	-1	0	0	0	-2	0	-2	0	0	1	0	0	0	0	1	0	1	-1	0	0																			
101	1149.73	83	26	-26	83	0	-7	-2	10	9	3	0	0	0	5	-1	6	-1	-1	-1	0	0	0	0	-2	0	-2	3	1	1																			
104	1166.38	99	1	0	0	99	0	0	0	0	0	0	-1	0	0	0	0	0	0	0	0	0	0	0	0	0	0	0	0	0																			
107	1187.16	4	11	2	-7	0	4	11	-4	4	4	0	0	-3	4	-6	-4	-1	0	0	0	0	0	0	0	0	0	-4	3	0	-2																		
108	1200.07	52	29	1	-2	0	11	52	-17	29	23	0	0	-3	15	0	-15	-4	-1	-1	0	1	0	-2	-1	0	-1	1	-1	0																			
109	1205.54	7	17	-3	10	0	-4	-17	7	-8	-7	0	0	2	-5	2	5	2	0	-1	0	0	0	-2	0	0	1	1	-2	1																			
110	1210.18	20	29	-3	9	0	4	29	-8	20	15	0	0	3	7	11	-7	-2	-1	0	0	0	0	0	-1	0	1	-1	0	1																			
111	1212.47	12	23	-1	3	0	4	23	-7	15	12	0	0	2	6	8	-6	-2	0	0	0	0	0	1	-1	0	0	0	0	1																			
112	1219.50	93	22	0	0	0	0	0	0	0	0	93	22	0	0	0	0	0	0	0	0	0	0	0	0	0	0	0	0	0																			
113	1221.28	5	22	0	0	-1	0	0	0	0	0	22	5	0	0	0	0	0	0	0	0	0	0	0	0	0	0	0	0	0																			
118	1237.13	12	28	0	0	0	-3	-3	2	3	2	0	0	12	-7	28	2	1	1	1	0	0	0	0	1	0	1	-2	0	1																			
119	1252.53	10	18	-2	5	0	4	15	-5	7	6	0	0	-7	10	-18	-5	0	-2	1	0	0	0	-1	-1	0	1	-1	0	2																			
123	1266.47	80	28	0	-1	0	-6	0	2	11	8	0	0	28	-18	80	2	1	2	0	0	-1	0	-1	2	0	-2	1	-1	-2																			
124	1275.81	6	15	-2	6	0	-4	-15	5	-7	-6	0	0	2	-5	2	6	-4	3	-6	0	-1	0	5	-1	0	2	0	-2	1																			
128	1322.55	28	33	0	1	0	-1	-4	2	-2	-2	0	0	1	0	1	-4	28	-17	33	0	3	0	-18	2	0	-1	0	-3	1																			
130	1352.82	13	24	0	-1	0	0	-1	0	-1	0	0	0	1	-2	2	3	-17	13	-24	0	-1	0	5	3	0	-2	-3	7	-2																			
131	1363.11	60	33	1	-1	0	0	-1	-1	0	0	0	0	1	1	0	-6	33	-24	60	0	-2	0	11	-2	0	-3	-3	2	-1																			
132	1366.26	95	20	0	0	0	0	0	0	0	0	0	0	0	0	0	0	0	0	0	95	0	20	0	0	0	0	0	0	0																			
133	1366.43	2	12	0	0	0	0	1	0	0	0	0	0	0	0	-1	-1	3	-1	-2	0	2	0	-12	1	0	2	-1	-1	1																			
134	1368.84	4	20	0	0	0	0	0	0	0	0	0	0	0	0	0	0	0	0	0	20	0	4	0	0	0	0	0	0	0																			
136	1373.70	83	18	0	0	0	0	-2	-2	0	1	0	0	0	-1	-1	5	-18	5	11	0	-12	0	83	-11	0	0	-1	-2	-1																			
141	1395.25	12	20	1	-2	0	0	-1	0	-1	-1	0	0	1	-1	2	-1	2	3	-2	0	1	0	-11	12	0	-8	-9	20	-5																			
142	1402.03	99	0	0	0	0	0	0	0	0	0	0	0	0	0	0	0	0	0	0	0	0	0	0	0	99	0	0	0	0																			
144	1419.64	42	22	1	-2	0	-4	-1	1	1	0	0	0	1	1	-2	2	-1	-2	-3	0	2	0	0	-8	0	42	-22	-19	22																			
146	1422.59	42	29	-1	3	0	3	1	1	-1	0	0	0	-2	-1	1	0	0	-3	-3	0	-1	0	-1	-9	0	-22	42	-29	-9																			
147	1433.20	65	29	0	1	0	0	-1	-2	0	0	0	0	0	0	-1	-2	-3	7	2	0	-1	0	-2	20	0	-19	-29	65	-14																			
148	1434.82	13	22	0	1	0	-2	0	1	1	1	0	0	1	2	-2	1	1	-2	-1	0	1	0	-1	-5	0	22	-9	-14	13																			

(There are eight selected clusters to analyze)

Overview of Body Mode Clusters (*non-normalized body mode KE*)



25

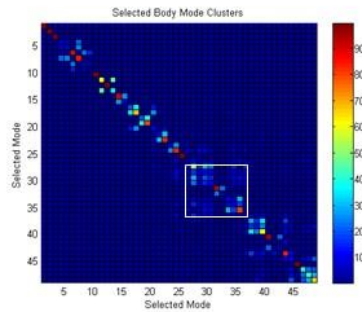
Mode Consolidation Theory

(process summary for each modal cluster)

1. Mode segmentation

- $[\Phi_L] = [\Phi_b] + [\Phi_r]$

2. Identify distinct “body” mode clusters

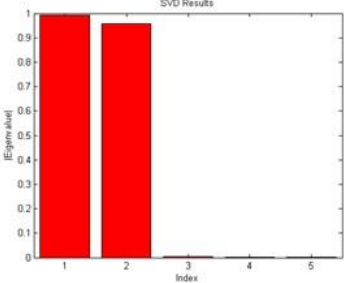
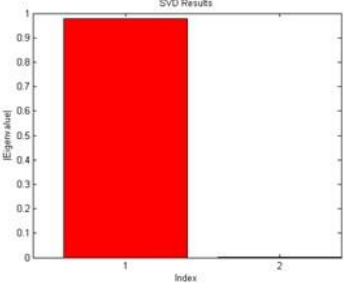
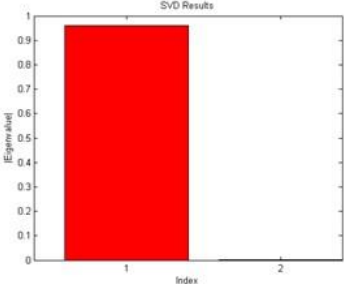
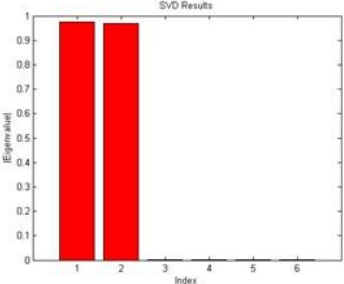


Requires judgment and intuition with experimental modal data

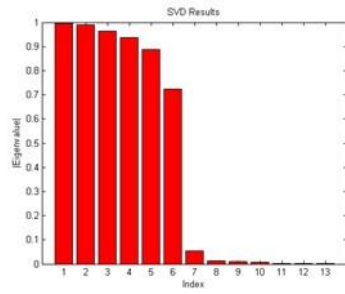
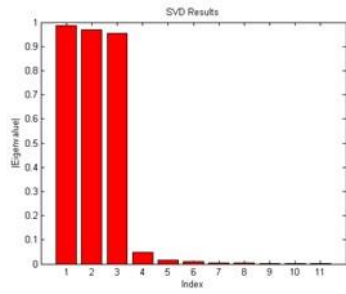
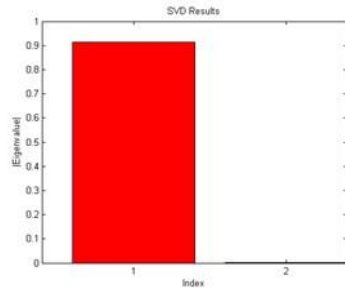
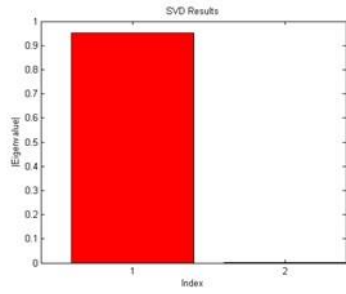
3. Consolidate “body” mode clusters

- SVD process results in $[\Phi_c]$, $[\lambda_c]$ for successive clusters

Cluster Analysis



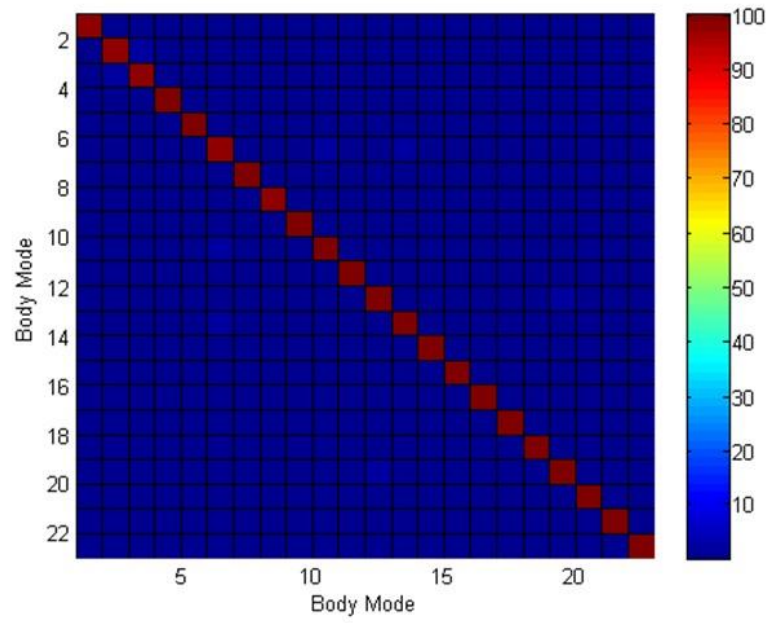
Cluster Analysis



Consolidated Body Mode Orthogonality

Mode	Freq (Hz)	1	2	3	4	5	6	7	8	9	10	11	12	13	14	15	16	17	18	19	20	
		Orthogonality (%)																				
1	120.97	100	0	0	0	0	-1	0	0	0	0	0	0	0	0	0	0	0	0	0	0	0
2	121.13	0	100	-2	0	0	0	0	0	0	0	0	0	0	0	0	0	0	0	0	0	0
3	312.43	0	-2	100	0	1	0	0	0	0	0	0	0	0	0	0	0	0	0	0	0	0
4	373.36	0	0	0	100	0	1	0	0	0	1	0	0	0	0	0	0	0	-1	0	0	0
5	374.14	0	0	1	0	100	0	0	0	-1	0	0	0	0	0	0	0	0	0	0	0	0
6	463.45	-1	0	0	1	0	100	0	0	0	-2	0	0	-2	0	1	0	0	0	0	0	0
7	699.42	0	0	0	0	0	0	100	0	0	0	0	1	0	0	0	0	0	0	0	1	0
8	701.56	0	0	0	0	0	0	0	100	0	0	0	0	0	0	0	0	0	0	0	0	0
9	833.71	0	0	0	0	-1	0	0	0	100	0	-1	0	0	0	0	0	0	0	0	0	0
10	983.97	0	0	0	1	0	-2	0	0	0	100	0	-1	-1	0	0	0	0	-1	0	0	0
11	994.07	0	0	0	0	0	0	0	0	-1	0	100	0	0	0	0	0	0	0	0	0	0
12	1020.02	0	0	0	0	0	0	1	0	0	-1	0	100	1	0	1	0	0	0	0	3	0
13	1149.62	0	0	0	0	0	-2	0	0	0	-1	0	1	100	0	0	0	-1	-1	0	0	0
14	1166.38	0	0	0	0	0	0	0	0	0	0	0	0	0	100	0	0	0	0	0	0	0
15	1210.08	0	0	0	0	0	1	0	0	0	0	0	1	0	0	100	0	0	0	0	0	0
16	1219.59	0	0	0	0	0	0	0	0	0	0	0	0	0	0	0	100	0	0	0	0	0
17	1260.33	0	0	0	-1	0	0	0	0	0	-1	0	0	-1	0	0	0	100	0	0	0	0
18	1359.92	0	0	0	0	0	0	0	0	0	0	0	0	-1	0	0	0	0	0	100	0	0
19	1375.75	0	0	0	0	0	0	1	0	0	0	0	3	0	0	0	0	0	0	0	100	0
20	1381.47	0	0	0	0	0	0	0	0	0	0	0	0	0	0	0	0	0	0	0	0	100
21	1387.15	0	0	0	0	0	0	0	0	0	0	0	0	0	0	0	0	0	0	0	0	0
22	1415.87	0	0	0	0	0	0	1	0	0	0	0	-1	0	0	0	0	0	0	0	0	0
23	1422.53	0	0	0	0	0	-1	0	0	0	0	0	0	-4	0	1	0	2	0	0	0	0

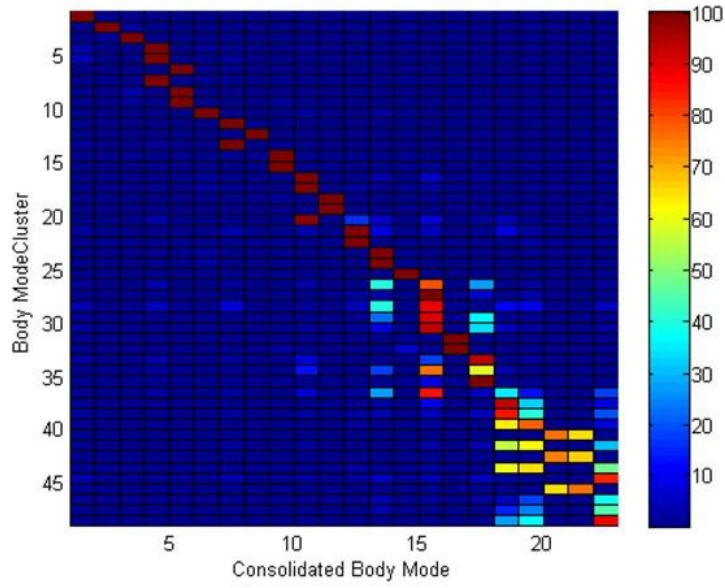
Consolidated Body Mode Orthogonality



30

Cross-Orthogonality

(Body Mode Clusters vs. Consolidated Body Modes)



31

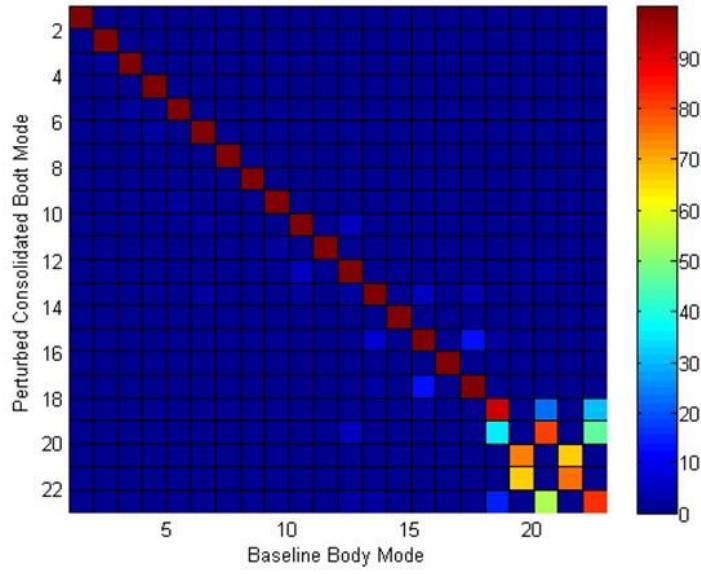
Cross-Orthogonality

(Consolidated Body Modes vs. Baseline Body Modes)

		Baseline Structure																						
Mode	Freq (Hz)	1	2	3	4	5	6	7	8	9	10	11	12	13	14	15	16	17	18	19	20	21	22	23
Perturbed Structure	1	120.97	99	0	0	0	0	0	0	0	0	0	0	0	0	0	0	0	0	0	0	0	0	0
	2	121.13	0	99	0	0	0	0	0	0	0	0	0	0	0	0	0	0	0	0	0	0	0	0
	3	312.43	0	2	99	0	1	0	0	0	0	0	0	0	0	0	0	0	0	0	0	0	0	0
	4	373.36	0	0	0	100	0	1	0	0	0	0	0	0	0	0	0	0	0	0	0	0	0	0
	5	374.14	0	0	2	0	100	0	0	0	0	0	0	0	0	0	0	0	0	0	0	0	0	0
	6	463.45	1	0	0	2	0	99	0	0	0	0	0	0	0	0	0	0	0	0	0	0	0	0
	7	699.42	0	0	0	0	0	1	100	0	0	0	1	0	0	0	0	0	0	0	0	0	0	0
	8	701.56	0	0	0	0	0	0	0	99	1	0	0	0	0	0	0	0	0	0	0	0	0	0
	9	833.71	0	0	0	0	2	0	0	1	100	0	1	0	0	0	0	0	0	0	0	0	0	0
	10	983.97	0	0	0	1	0	2	0	0	0	100	0	5	1	0	1	0	1	0	0	0	0	0
	11	994.07	0	0	0	0	0	0	0	0	2	0	100	0	0	1	0	0	0	0	0	0	0	0
	12	1020.02	0	0	0	0	0	1	0	0	6	0	100	1	0	1	0	0	0	0	0	3	0	0
	13	1149.62	0	0	0	0	0	2	0	0	0	2	0	100	0	6	0	3	0	0	0	0	0	2
	14	1166.38	0	0	0	0	0	0	0	0	0	1	0	0	99	0	1	0	0	0	0	0	0	0
	15	1210.08	0	0	0	0	0	1	0	0	0	1	0	1	7	0	99	0	14	2	0	0	0	1
	16	1219.59	0	0	0	0	0	0	0	0	0	0	1	0	0	1	0	100	0	0	0	0	0	0
	17	1260.33	0	0	0	1	0	0	0	0	1	0	0	0	3	0	14	0	99	0	0	0	0	3
	18	1359.92	0	0	0	0	0	0	0	0	0	0	0	1	0	3	0	0	92	0	23	0	31	1
	19	1375.75	0	0	0	0	0	0	1	0	0	1	0	5	1	0	1	0	0	35	0	80	0	46
	20	1381.47	0	0	0	0	0	0	0	0	0	0	0	0	0	0	0	0	0	0	75	0	56	0
	21	1387.15	0	0	0	0	0	0	0	0	0	0	0	0	0	0	0	0	0	0	66	0	75	0
	22	1415.87	0	0	0	0	0	0	1	0	0	0	0	3	2	0	1	0	1	14	0	54	0	82
	23	1422.53	0	0	0	0	0	1	0	0	0	0	0	0	4	0	2	0	5	1	0	0	0	7

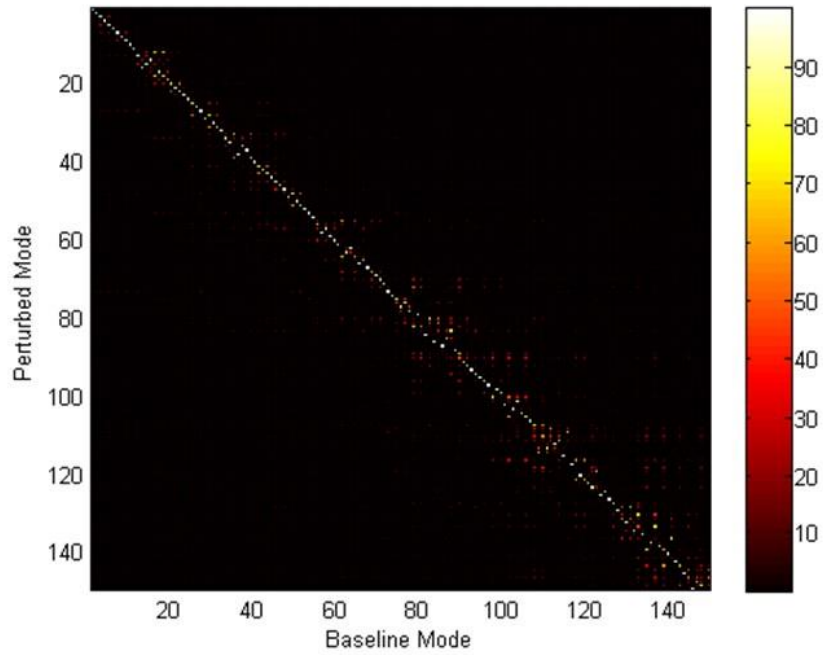
Cross-Orthogonality

(Consolidated Body Modes vs. Baseline Body Modes)



Cross-Orthogonality

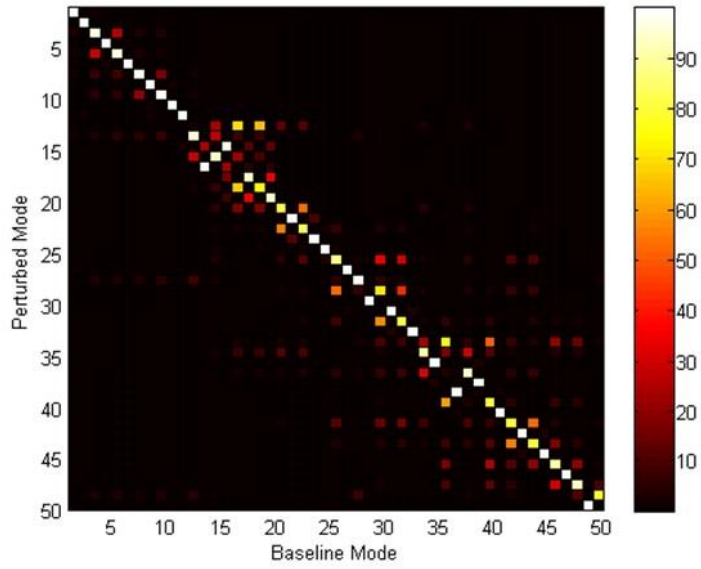
(150 Perturbed Modes vs. 150 Baseline Modes)



34

Cross-Orthogonality

(50 Perturbed Modes vs. 50 Baseline Modes)



35

Comparison of Shell Body Mode Approximations (Modal Frequencies)

Baseline (O)		Perturbed (P)		Consolidated (C)		Modified Guyan Reduction (MGR)			Harmonic Reduction (HR)		
Mode	Freq (Hz)	Mode	Freq (Hz)	Mode	Freq (Hz)	Mode	Freq (Hz)	COR	Mode	Freq (Hz)	COR
1	122.20	1	120.97	1	120.97	1	121.02	100	1	121.02	100
2	122.20	2	121.13	2	121.13	2	121.14	100	2	121.13	100
11	315.24	11	312.43	3	312.43	3	312.38	100	3	312.38	100
14	377.21	15	374.65	4	373.36	4	373.37	100	4	373.35	100
15	377.21	14	373.97	5	374.14	5	374.19	100	5	374.17	100
24	467.77	24	463.45	6	463.45	6	463.50	100	6	463.50	100
49	706.65	48	695.39	7	699.42	7	698.99	100	7	698.99	100
50	706.65	50	701.56	8	701.56	8	701.74	100	8	701.70	100
63	841.31	62	833.52	9	833.71	9	833.72	100	9	833.72	100
76	997.48	76	986.08	10	983.97	10	983.00	100	10	984.52	100
77	997.50	78	994.38	11	994.07	11	994.38	100	11	995.48	100
86	1029.94	85	1020.38	12	1020.02	12	1020.47	100	12	1021.74	100
103	1169.56	101	1149.73	13	1149.62	13	1151.88	100	13	1156.45	100
104	1169.59	104	1166.38	14	1166.38	14	1166.83	100	14	1170.61	100
111	1223.46	108	1200.07	15	1210.08	15	1205.31	99	15	1215.82	99
112	1223.49	112	1219.50	16	1219.59	16	1220.14	100	16	1228.84	100
121	1273.43	123	1266.47	17	1260.33	17	1261.37	99	17	1268.71	99
128	1368.34	131	1363.11	18	1359.92	18	1344.84	94	18	1371.89	91
129	1368.41	132	1366.26	19	1375.75	20	1379.78	84	19	1391.51	80
140	1402.79	136	1373.70	20	1381.47	19	1367.05	76	20	1391.78	74
141	1402.83	142	1402.03	21	1387.15	21	1403.83	76	21	1415.61	74
146	1440.38	147	1433.20	22	1415.87	23	1427.86	78	23	1453.68	82
149	1452.66	144	1419.64	23	1422.53	22	1426.94	88	22	1453.35	9
(O) = Baseline System Body Modes						Cross-Orthogonality (COR) : Reference Modes= Consolidated (C)					
(P) = Perturbed System Body-Dominant Modes (p=1)						Reference Mass = Baseline [MFF]					
(C) = Perturbed System Consolidated Body Modes (Reference)											
(MGR) = Modified Guyan Reduction (Perturbed System)											
(HR) = Harmonic Reduction (Perturbed System)											

Comparison of Shell Body Mode Approximations (Kinetic Energy Distribution: Baseline & Consolidated)

Baseline										Consolidated									
Mode	Direction	Freq (Hz)	TX	TY	TZ	RX	RY	RZ	TR	Mode	Direction	Freq (Hz)	TX	TY	TZ	RX	RY	RZ	TR
1	TY	122.20	0	96	0	4	0	0	0	1	TY	120.97	0	94	0	4	0	0	0
2	TX	122.20	96	0	0	0	4	0	0	2	TX	121.13	95	0	0	0	4	0	0
3	RZ	315.24	0	0	0	0	0	100	0	3	RZ	312.43	0	0	0	0	0	98	0
4	TY	377.21	0	91	0	9	0	0	0	4	TY	373.36	0	91	0	9	0	0	0
5	TX	377.21	91	0	0	0	9	0	0	5	TX	374.14	91	0	0	0	9	0	0
6	TZ	467.77	0	0	100	0	0	0	0	6	TZ	463.45	0	0	98	0	0	0	0
7	TY	706.65	0	90	0	10	0	0	0	7	TY	699.42	0	90	0	10	0	0	0
8	TX	706.65	90	0	0	0	10	0	0	8	TX	701.56	89	0	0	0	9	0	0
9	RZ	841.31	0	0	0	0	0	100	0	9	RZ	833.71	0	0	0	0	0	100	0
10	TY-RX	997.48	0	59	0	41	0	0	0	10	TY-RX	983.97	0	58	0	42	0	0	0
11	TX-RY	997.50	59	0	0	0	41	0	0	11	TX-RY	994.07	60	0	0	0	40	0	0
12	TZ	1029.94	0	0	96	0	0	0	4	12	TZ	1020.02	0	0	95	0	0	0	4
13	TY-RX	1169.56	0	61	0	39	0	0	0	13	TY-RX	1149.62	0	61	0	39	0	0	0
14	TX-RY	1169.59	61	0	0	0	39	0	0	14	TX-RY	1166.38	59	0	0	0	39	0	0
15	TY	1223.46	0	90	0	10	0	0	0	15	TY	1210.08	0	90	2	8	0	0	0
16	TX	1223.49	90	0	0	0	10	0	0	16	TX	1219.59	90	0	0	0	10	0	0
17	TZ-TR	1273.43	0	0	81	0	0	0	19	17	TZ-TR	1260.33	0	2	80	1	0	0	18
18	TY	1368.34	0	94	0	6	0	0	0	18	TY	1359.92	0	85	4	6	0	0	6
19	TX	1368.41	94	0	0	0	6	0	0	19	RX-TY-TR	1375.75	0	17	12	61	0	0	10
20	RX	1402.79	0	16	0	83	0	0	0	20	TX-RY	1381.47	70	0	0	0	30	0	0
21	RY	1402.83	16	0	0	0	83	0	0	21	TX-RY	1387.15	41	0	0	0	59	0	0
22	TR-TZ	1440.38	0	0	45	0	0	0	55	22	TR-TZ-RX	1415.87	0	9	31	23	0	0	37
23	TY-RX	1452.66	0	74	0	25	0	0	0	23	TY-RX	1422.53	0	74	2	23	0	0	1

Comparison of Shell Body Mode Approximations (Kinetic Energy Distribution: Body-Dominant Perturbed & Consolidated)

Selected Body-Dominant Perturbed										Consolidated									
Mode	Direction	Freq (Hz)	TX	TY	TZ	RX	RY	RZ	TR	Mode	Direction	Freq (Hz)	TX	TY	TZ	RX	RY	RZ	TR
1	TY	120.97	0	94	0	4	0	0	0	1	TY	120.97	0	94	0	4	0	0	0
2	TX	121.13	95	0	0	0	4	0	0	2	TX	121.13	95	0	0	0	4	0	0
3	RZ	312.43	0	0	0	0	0	0	98	3	RZ	312.43	0	0	0	0	0	98	0
4	TY	374.65	0	77	0	8	0	0	0	4	TY	373.36	0	91	0	9	0	0	0
5	TX	373.97	81	0	0	0	8	0	0	5	TX	374.14	91	0	0	0	9	0	0
6	TZ	463.45	0	0	98	0	0	0	0	6	TZ	463.45	0	0	98	0	0	0	0
7	TY	695.39	0	55	0	6	0	0	0	7	TY	699.42	0	90	0	10	0	0	0
8	TX	701.56	89	0	0	0	9	0	0	8	TX	701.56	89	0	0	0	9	0	0
9	RZ	833.52	0	0	0	0	0	91	0	9	RZ	833.71	0	0	0	0	0	100	0
10	TY-RX	986.08	0	38	0	28	0	0	0	10	TY-RX	983.97	0	58	0	42	0	0	0
11	TX-RY	994.38	48	0	0	0	32	0	0	11	TX-RY	994.07	60	0	0	0	40	0	0
12	TZ	1020.38	0	0	80	0	0	0	4	12	TZ	1020.02	0	0	95	0	0	0	4
13	TY-RX	1149.73	0	51	0	32	0	0	0	13	TY-RX	1149.62	0	61	0	39	0	0	0
14	TX-RY	1166.38	59	0	0	0	39	0	0	14	TX-RY	1166.38	59	0	0	0	39	0	0
15	TY	1200.07	0	47	0	4	0	0	0	15	TY	1210.08	0	90	2	8	0	0	0
16	TX	1219.50	84	0	0	0	9	0	0	16	TX	1219.59	90	0	0	0	10	0	0
17	TZ-TR	1266.47	0	0	65	0	0	0	14	17	TZ-TR	1260.33	0	2	80	1	0	0	18
18	TY-RX	1363.11	0	38	1	21	0	0	0	18	TY	1359.92	0	85	4	6	0	0	6
19	TX	1366.26	89	0	0	0	5	0	0	19	RX-TY-TR	1375.75	0	17	12	61	0	0	10
20	RX-TY	1373.70	0	28	1	53	0	0	0	20	TX-RY	1381.47	70	0	0	0	30	0	0
21	RY-TX	1402.03	16	0	0	0	83	0	0	21	TX-RY	1387.15	41	0	0	0	59	0	0
22	TR-TZ	1433.20	0	1	29	1	0	0	34	22	TR-TZ-RX	1415.87	0	9	31	23	0	0	37
23	TY	1419.64	0	27	3	8	0	0	3	23	TY-RX	1422.53	0	74	2	23	0	0	1

Comparison of Shell Body Mode Approximations

(Kinetic Energy Distribution: Generalized Guyan Reduction & Consolidated)

Perturbed "PsiF"									Consolidated										
Mode	Direction	Freq (Hz)	TX	TY	TZ	RX	RY	RZ	TR	Mode	Direction	Freq (Hz)	TX	TY	TZ	RX	RY	RZ	TR
1	TY	121.02	0	94	0	4	0	0	0	1	TY	120.97	0	94	0	4	0	0	0
2	TX	121.14	95	0	0	0	4	0	0	2	TX	121.13	95	0	0	0	4	0	0
3	RZ	312.38	0	0	0	0	0	98	0	3	RZ	312.43	0	0	0	0	0	98	0
4	TY	373.37	0	89	0	9	0	0	0	4	TY	373.36	0	91	0	9	0	0	0
5	TX	374.19	90	0	0	0	9	0	0	5	TX	374.14	91	0	0	0	9	0	0
6	TZ	463.50	0	0	98	0	0	0	0	6	TZ	463.45	0	0	98	0	0	0	0
7	TY	698.99	0	88	0	9	0	0	0	7	TY	699.42	0	90	0	10	0	0	0
8	TX	701.74	89	0	0	0	9	0	0	8	TX	701.56	89	0	0	0	9	0	0
9	RZ	833.72	0	0	0	0	0	98	0	9	RZ	833.71	0	0	0	0	0	100	0
10	TY-RX	983.00	0	56	0	40	0	0	0	10	TY-RX	983.97	0	58	0	42	0	0	0
11	TX-RY	994.38	59	0	0	0	40	0	0	11	TX-RY	994.07	60	0	0	0	40	0	0
12	TZ	1020.47	0	0	93	0	0	0	4	12	TZ	1020.02	0	0	95	0	0	0	4
13	TY-RX	1151.88	0	60	0	37	0	0	0	13	TY-RX	1149.62	0	61	0	39	0	0	0
14	TX-RY	1166.83	60	0	0	0	40	0	0	14	TX-RY	1166.38	59	0	0	0	39	0	0
15	TY	1205.31	0	87	0	9	0	0	0	15	TY	1210.08	0	90	2	8	0	0	0
16	TX	1220.14	89	0	0	0	10	0	0	16	TX	1219.59	90	0	0	0	10	0	0
17	TZ-TR	1261.37	0	0	79	0	0	0	18	17	TZ-TR	1260.33	0	2	80	1	0	0	18
18	TY	1344.84	0	89	0	6	0	0	1	18	TY	1359.92	0	85	4	6	0	0	6
19	TX	1367.05	94	0	0	0	6	0	0	19	RX-TY-TR	1375.75	0	17	12	61	0	0	10
20	RX-TY	1379.78	0	16	1	79	0	0	0	20	TX-RY	1381.47	70	0	0	0	30	0	0
21	RY-TX	1403.83	16	0	0	0	83	0	0	21	TX-RY	1387.15	41	0	0	0	59	0	0
22	TY-RX	1426.94	0	59	8	19	0	0	9	22	TR-TZ-RX	1415.87	0	9	31	23	0	0	37
23	TR-TZ-TY	1427.86	0	13	37	4	0	0	44	23	TY-RX	1422.53	0	74	2	23	0	0	1

Comparison of Shell Body Mode Approximations (Kinetic Energy Distribution: Rigid Cross-Section & Consolidated)

Perturbed "PsiFR"									Consolidated										
Mode	Direction	Freq (Hz)	TX	TY	TZ	RX	RY	RZ	TR	Mode	Direction	Freq (Hz)	TX	TY	TZ	RX	RY	RZ	TR
1	TY	121.02	0	94	0	4	0	0	0	1	TY	120.97	0	94	0	4	0	0	0
2	TX	121.13	95	0	0	0	4	0	0	2	TX	121.13	95	0	0	0	4	0	0
3	RZ	312.38	0	0	0	0	0	98	0	3	RZ	312.43	0	0	0	0	0	98	0
4	TY	373.35	0	89	0	9	0	0	0	4	TY	373.36	0	91	0	9	0	0	0
5	TX	374.17	90	0	0	0	9	0	0	5	TX	374.14	91	0	0	0	9	0	0
6	TZ	463.50	0	0	98	0	0	0	0	6	TZ	463.45	0	0	98	0	0	0	0
7	TY	698.99	0	88	0	9	0	0	0	7	TY	699.42	0	90	0	10	0	0	0
8	TX	701.70	89	0	0	0	9	0	0	8	TX	701.56	89	0	0	0	9	0	0
9	RZ	833.72	0	0	0	0	0	98	0	9	RZ	833.71	0	0	0	0	0	100	0
10	TY-RX	984.52	0	56	0	41	0	0	0	10	TY-RX	983.97	0	58	0	42	0	0	0
11	TX-RY	995.48	59	0	0	0	40	0	0	11	TX-RY	994.07	60	0	0	0	40	0	0
12	TZ	1021.74	0	0	94	0	0	0	4	12	TZ	1020.02	0	0	95	0	0	0	4
13	TY-RX	1156.45	0	60	0	37	0	0	0	13	TY-RX	1149.62	0	61	0	39	0	0	0
14	TX-RY	1170.61	59	0	0	0	40	0	0	14	TX-RY	1166.38	59	0	0	0	39	0	0
15	TY	1215.82	0	90	0	7	0	0	0	15	TY	1210.08	0	90	2	8	0	0	0
16	TX	1228.84	91	0	0	0	8	0	0	16	TX	1219.59	90	0	0	0	10	0	0
17	TZ-TR	1268.71	0	0	82	0	0	0	16	17	TZ-TR	1260.33	0	2	80	1	0	0	18
18	TY	1371.89	0	91	0	5	0	0	0	18	TY	1359.92	0	85	4	6	0	0	6
19	RX-TY	1391.51	0	17	1	79	0	0	0	19	RX-TY-TR	1375.75	0	17	12	61	0	0	10
20	TX	1391.78	96	0	0	0	4	0	0	20	TX-RY	1381.47	70	0	0	0	30	0	0
21	RY-TX	1415.61	16	0	0	0	84	0	0	21	TX-RY	1387.15	41	0	0	0	59	0	0
22	RZ	1453.35	0	0	0	0	0	98	0	22	TR-TZ-RX	1415.87	0	9	31	23	0	0	37
23	TZ-TR	1453.68	0	2	59	1	0	0	36	23	TY-RX	1422.53	0	74	2	23	0	0	1

Appendix E. Verification of Experimental Modes (*ISPE case study using SFD modes*)

Appendix E:
Verification of Experimental Modes
(*ISPE case study using SFD modes*)

Bob Coppolino
Measurement Analysis Corporation
15 August 2017

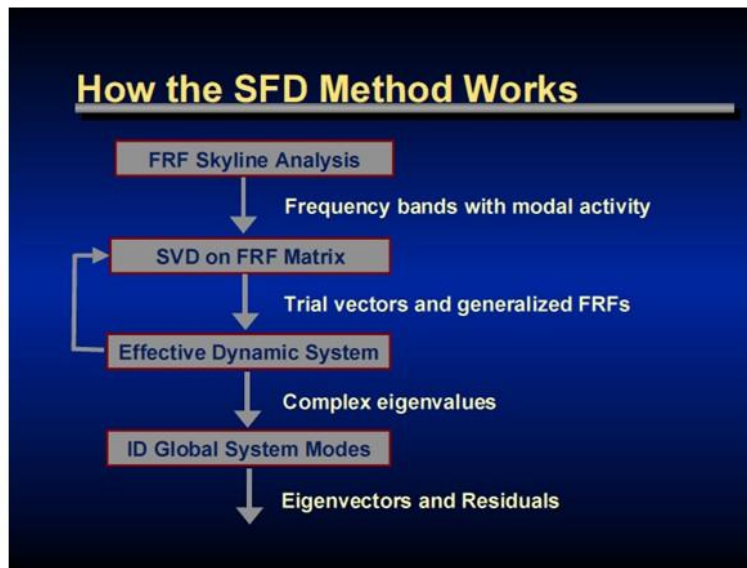
Executive Summary

In view of difficulties encountered by NASA/MSFC with analysis of ISPE modal test data, recorded on its B&K modal test system, the following preliminary development of an objective strategy for modal test data verification and validation was pursued. The presently defined strategy is (1) independent of mathematical model predictions and orthogonality checks, and (2) requires estimation of “left-hand” eigenvectors. The second attribute may be problematic as the author employed the SFD method of test mode estimation, which readily computes “left-hand” eigenvectors for an estimated effective dynamic system. The user of other well-established test mode estimators (e.g., AFPoly) are encouraged to implement similar verification methodology that employs “left-hand” eigenvectors.

The new verification strategy offers objective means for evaluation of estimated modes (acceptable-to-unacceptable figures of merit) based on properties of (a) estimated SDOF modal FRFs and (b) modal FRF coherence factors.

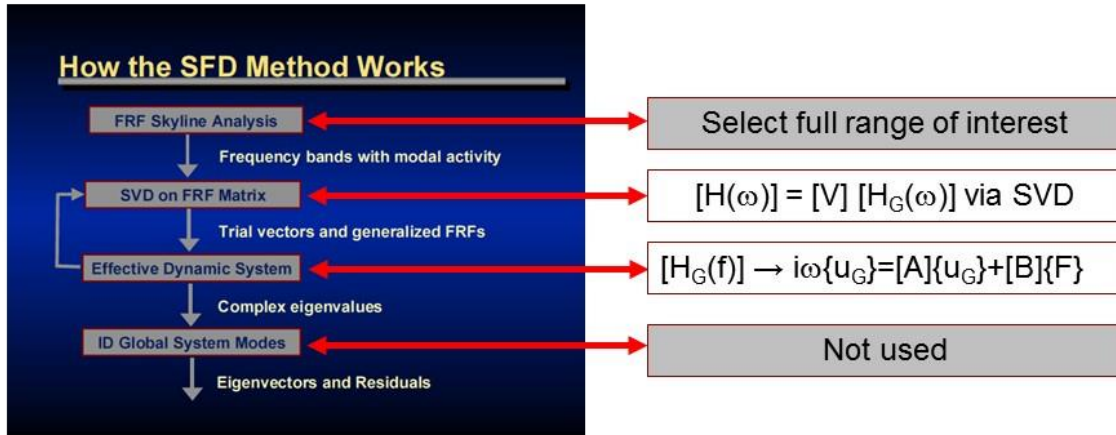
General Overview of the SFD Method

(as published in IMAC XXI, 2003)



Numerous variations of SFD have been defined, but not employed herein.

Nuanced Application of SFD (with Embedded Experimental Mode Verification)



Experimental mode verification focuses on the effective dynamic system

SFD Effective Dynamic System Development

- Organization of MI/MO FRF data

$$\begin{bmatrix} [\ddot{u}_1(t)] \\ [\ddot{u}_2(t)] \\ \dots \\ [\ddot{u}_m(t)] \end{bmatrix} = \begin{bmatrix} [H_1(t)] \\ [H_2(t)] \\ \dots \\ [H_m(t)] \end{bmatrix} = \begin{bmatrix} [V_1] \\ [V_2] \\ \dots \\ [V_m] \end{bmatrix} \cdot [H_g(t)] \Rightarrow \begin{matrix} \text{“shorthand”} \\ [\ddot{U}(t)] = [H(t)] = [V] \cdot [H_g(t)] = [V] \cdot [\ddot{\xi}(t)] \\ [V^T] \cdot [V] = [I] \end{matrix}$$

- Effective dynamic system (physical dof)

$$\begin{matrix} [\ddot{u}_1] + [M^{-1}B][\dot{u}_1] + [M^{-1}K][u_1] = [M^{-1}\Gamma_1][F] \\ [\ddot{u}_2] + [M^{-1}B][\dot{u}_2] + [M^{-1}K][u_2] = [M^{-1}\Gamma_2][F] \\ \dots \end{matrix} \Rightarrow \begin{matrix} \text{“shorthand”} \\ [\ddot{U}] + [M^{-1}B][\dot{U}] + [M^{-1}K][U] = [M^{-1}\Gamma][F] \end{matrix}$$

- Effective dynamic system (generalized dof)

$$[V^T][V][\ddot{\xi}] + [V^T][M^{-1}B][V][\dot{\xi}] + [V^T][M^{-1}K][V][\xi] = [V^T][M^{-1}\Gamma][F]$$

$$\Downarrow$$

$$[\ddot{\xi}] + [\tilde{B}][\dot{\xi}] + [\tilde{K}][\xi] = [\tilde{\Gamma}][F]$$

Effective Dynamic System Verification Operations

- Effective dynamic system

$$\begin{bmatrix} \dot{\xi} \\ \xi \end{bmatrix} = \begin{bmatrix} -\tilde{B} & -\tilde{K} \\ I & 0 \end{bmatrix} \begin{bmatrix} \dot{\xi} \\ \xi \end{bmatrix} + \begin{bmatrix} \tilde{\Gamma} \\ 0 \end{bmatrix} [F] \quad \Rightarrow \quad \{\dot{\eta}\} = [A]\{\eta\} + [B]\{F\}$$

- Complex system modes & “model” based modal FRFs

$$\{\eta\} = [\Phi]\{q\} \quad \Rightarrow \quad \begin{array}{l} [\Phi_L] = [\Phi]^{-1} \\ [\Phi_L][\Phi] = [I] \\ [\Phi_L][A][\Phi] = [\lambda] \end{array} \quad \Rightarrow \quad \begin{array}{l} \dot{q}_n - \lambda_n q_n = [\Phi_{L,n} B]\{F\} \\ \boxed{h_{n,model} = \dot{q}_n} \end{array}$$

- Construction of experimental modal FRFs

$$\begin{bmatrix} \dot{\xi} \\ \xi \end{bmatrix} = \begin{bmatrix} H_G(f) \\ H_G(f)/(i2\pi f) \end{bmatrix} \quad \Rightarrow \quad \boxed{h_n(f) = [\Phi_{L,n}] \cdot \begin{bmatrix} H_G(f) \\ H_G(f)/(i2\pi f) \end{bmatrix}}$$

6

Attributes of the Modal FRFs

- Model-based FRFs, ($h_{n,model}$)
 - Based on exact frequency domain response of the “SFD” effective dynamic system to unit loading, $F(f)=1$.
- Experimental modal FRFs (h_n)
 - Left hand experimental complex mode, $[\Phi_n]$ serves as a scale factor for combining experimental generalized FRFs, $[H_G(f)]$ that are linear combinations of MI/MO FRFs, $[H(f)]$.
 - The modal FRFs (h_n) do not necessarily constrain experimental data to behave as “theoretical” SDOF systems.
- Validity of experimental modes
 - Objectively evaluated based on attributes of $h_n(f)$ and...
 - A coherence metric (defined in the next slide).

7

Modal FRF and Coherence Metric

- Definition

$$\text{COH}_n = \frac{|\mathbf{h}_{n,\text{model}}^* \cdot \mathbf{h}_n|^2}{|\mathbf{h}_n^* \cdot \mathbf{h}_n| \cdot |\mathbf{h}_{n,\text{model}}^* \cdot \mathbf{h}_{n,\text{model}}|}$$

- Properties and attributes (of $h_n(f)$ and COH_n)
 - values $0.0 \leq \text{COH}_n \leq 1.0$
 - Completely independent of TAM mass matrix (FEM model)
 - Performs modal isolation reminiscent of multi-shaker tuning

ISPE Results

Candidate Experimental Modes 1-45

EV	Eigenvalue		Excitation (PHIL*GAM)		Evaluation Criteria & Assessment		
	FREQ (Hz)	Zeta (%)	Gain (%)	Phase (deg)	max h (%)	Coherence (%)	Is it a mode?
1	16.74	2.42	9	6.9	2.11	100	Y
2	17.10	2.37	8	-11.0	2.04	100	Y
3	18.13	0.12	2	-169.2	6.99	97	Y
4	18.16	0.11	1	-174.2	4.72	96	Y
5	18.79	-0.03	0	137.5	6.00	63	N
6	18.79	0.11	6	-4.0	24.72	98	Y
7	18.90	0.01	0	161.1	7.71	58	N
8	19.28	0.08	1	-2.6	2.31	88	Y
9	20.38	2.81	6	165.7	1.31	99	Y
10	20.90	0.03	0	-158.2	4.25	58	N
11	20.96	0.07	2	-8.9	10.86	88	Y?
12	21.02	0.07	2	156.2	11.47	91	Y?
13	21.25	0.05	1	163.7	1.72	2	N
14	22.43	-2.12	1	13.0	0.86	4	N
15	24.02	0.10	1	-2.1	2.44	86	Y?
16	24.07	0.46	12	-175.5	15.21	100	Y
17	24.27	0.44	12	175.0	15.52	100	Y
18	25.82	0.14	4	4.5	13.89	100	Y
19	25.88	-0.01	0	-58.7	2.99	10	N
20	25.89	0.12	4	-0.2	16.30	99	Y
21	26.75	-0.85	1	153.8	0.50	1	N
22	27.53	1.65	7	26.3	2.66	100	Y
23	27.81	1.54	9	159.8	3.15	100	Y
24	28.41	-0.34	0	67.2	0.43	0	N
25	30.14	-0.01	1	138.7	4.35	8	N
26	30.15	0.33	2	-167.1	3.31	62	Y?
27	31.00	-0.83	1	61.0	1.33	2	N
28	31.78	-0.43	1	-55.9	0.63	0	N
29	32.32	1.08	3	-163.5	1.31	95	Y?
30	33.15	1.03	7	80.9	3.46	95	N
31	33.42	0.32	5	-113.0	8.72	96	Y?
32	33.70	-0.07	1	-39.2	1.66	0	N
33	34.19	2.23	20	148.4	5.00	100	Y
34	34.22	0.03	0	-116.1	0.51	3	N
35	34.64	-0.23	0	-101.3	0.44	0	N
36	35.42	0.53	10	-165.1	8.94	99	Y
37	35.77	-10.73	7	72.0	0.68	32	N
38	35.96	-0.23	1	106.1	1.57	1	N
39	35.97	1.16	12	157.8	6.04	100	Y
40	36.21	0.14	5	163.3	18.03	98	Y
41	36.30	0.09	1	13.2	4.01	67	N
42	36.47	0.31	54	137.4	99.69	100	Y
43	36.51	0.00	0	-151.1	2.74	28	N
44	36.55	-0.05	0	103.5	4.34	1	N
45	36.61	0.56	100	-159.1	100.00	100	Y

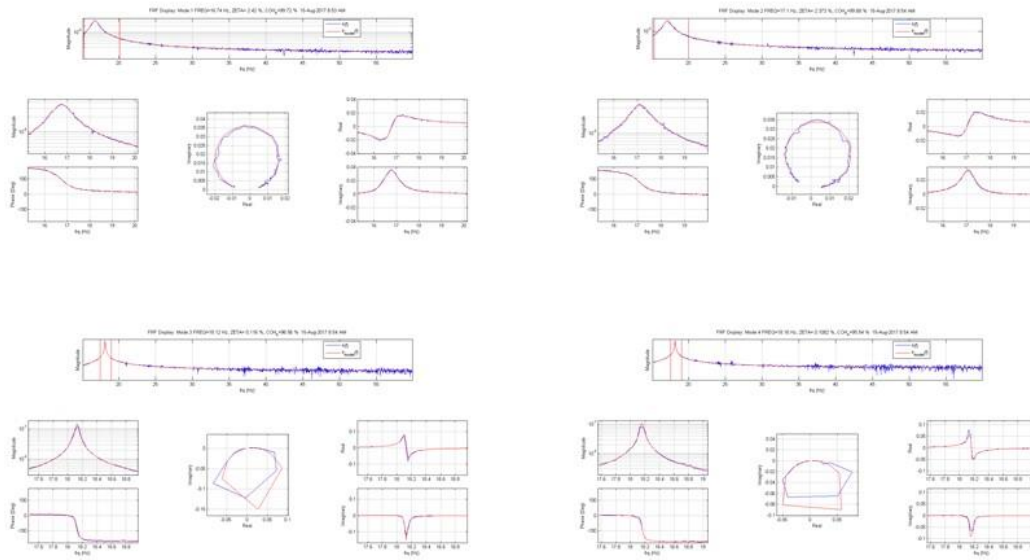
Candidate Experimental Modes 46-90

EV	Eigenvalue		Excitation (PHIL*GAM)		Evaluation Criteria & Assessment		
	FREQ(Hz)	Zeta (%)	Gain (%)	Phase(deg)	max h (%)	Coherence (%)	Is it a mode?
46	36.76	-0.07	0	45.4	1.34	3	N
47	36.92	0.17	2	109.1	4.65	73	N
48	37.03	0.25	7	8.1	16.80	99	Y?
49	37.24	-0.13	1	-70.8	3.68	0	N
50	37.27	0.47	18	-101.4	22.79	99	Y?
51	37.36	0.30	20	-161.4	36.59	100	Y
52	37.69	0.36	19	158.1	30.11	100	Y
53	37.99	-0.07	0	24.2	1.06	0	N
54	38.13	0.09	1	-15.9	1.13	20	N
55	38.30	1.22	17	-57.8	7.97	99	Y
56	38.55	-0.09	1	-65.5	0.92	0	N
57	38.71	0.04	0	160.9	1.85	23	N
58	38.81	0.12	2	13.2	4.98	62	N
59	38.92	2.14	37	-77.3	10.35	99	Y
60	39.35	-0.41	1	103.4	0.83	1	N
61	39.41	0.62	18	-38.9	15.34	99	Y?
62	39.54	0.16	4	-161.5	14.33	98	Y?
63	39.68	0.70	15	-80.4	12.27	96	Y?
64	39.90	0.31	2	115.1	2.46	38	N
65	40.40	-0.03	0	-0.5	0.40	0	N
66	40.95	0.03	0	86.9	1.85	8	N
67	41.18	-0.98	4	-139.2	2.61	2	N
68	41.22	-0.17	1	8.1	1.84	0	N
69	41.71	0.78	46	166.6	32.62	99	Y
70	41.88	0.04	4	73.0	8.51	31	N
71	42.02	0.95	36	22.2	22.07	99	Y
72	42.57	0.03	0	-42.6	0.64	3	N
73	42.93	0.01	1	-46.7	0.78	1	N
74	43.11	-0.01	0	-35.1	1.00	0	N
75	43.45	0.99	92	-2.3	52.01	100	Y
76	43.51	-8.62	11	-43.5	1.83	32	N
77	43.63	0.03	1	55.5	1.56	16	N
78	43.73	0.49	8	148.6	8.23	98	Y?
79	43.98	0.08	1	152.6	1.63	33	N
80	44.49	-0.14	1	-15.3	0.70	0	N
81	44.70	0.04	1	17.5	2.61	12	N
82	45.00	0.39	10	178.3	13.83	99	Y
83	45.02	0.04	1	-97.9	4.04	41	N
84	45.35	-0.10	1	-178.5	1.77	0	N
85	45.54	0.15	2	-17.5	8.13	90	Y?
86	45.72	2.10	49	-158.7	13.36	100	Y
87	45.77	0.00	0	-64.1	2.20	2	N
88	45.87	-0.96	3	46.2	2.24	2	N
89	45.92	0.05	1	-159.1	5.97	15	N
90	46.11	0.00	0	-9.3	38.44	22	N

Candidate Experimental Modes 91-133

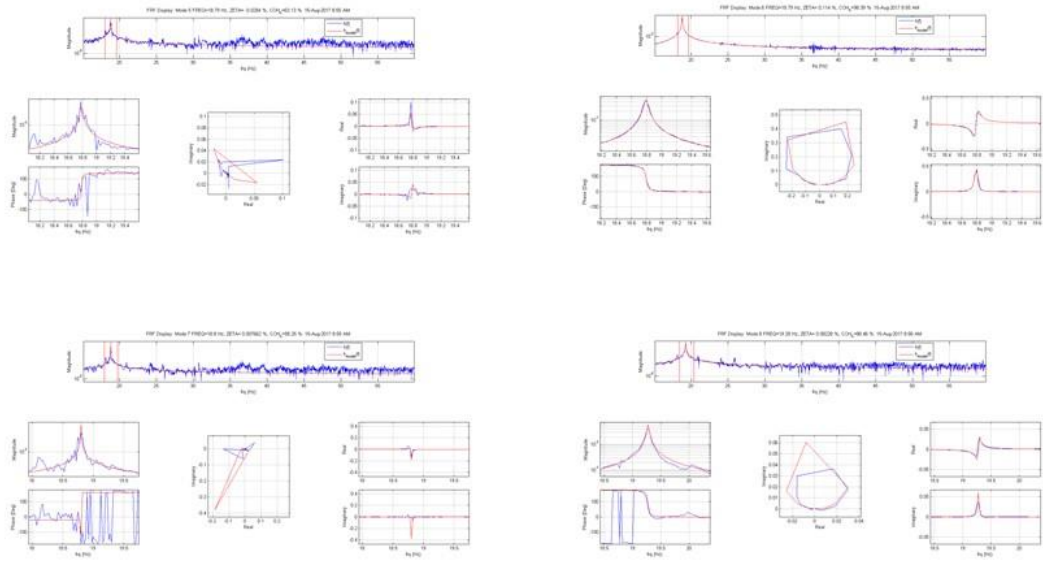
EV	Eigenvalue		Excitation (PHIL*GAM)		Evaluation Criteria & Assessment		
	FREQ (Hz)	Zeta (%)	Gain (%)	Phase (deg)	max h (%)	Coherence (%)	Is it a mode?
91	46.13	-0.01	1	-115.3	4425	76	N
92	46.24	0.13	4	-142.3	13.66	52	Y
93	46.49	0.50	18	81.7	21.27	99	Y
94	46.65	0.76	49	175.6	36.27	100	Y
95	46.96	-0.01	0	-166.0	4.44	2	N
96	46.98	0.23	6	99.8	12.53	91	N
97	47.48	0.22	7	-135.1	17.45	99	Y
98	47.62	0.85	64	-30.8	44.04	100	Y
99	47.78	-0.23	1	75.0	1.43	0	N
100	47.85	0.37	7	-8.8	10.03	98	Y?
101	48.11	1.54	56	15.4	21.03	100	Y
102	48.38	0.24	3	-99.5	4.45	86	N
103	48.58	-0.04	0	161.7	1.04	0	N
104	48.89	-0.11	1	135.8	1.11	0	N
105	49.18	0.75	20	-26.6	14.84	100	Y
106	50.05	0.75	11	-141.6	8.99	99	Y?
107	50.20	0.10	1	-19.4	2.30	53	N
108	50.44	0.33	6	85.7	9.16	97	Y?
109	50.69	0.18	3	141.2	8.62	91	Y?
110	50.95	0.49	16	156.3	17.32	99	Y?
111	51.26	0.19	3	99.0	7.05	85	N
112	51.32	0.46	23	33.8	23.71	99	Y
113	51.45	1.47	56	-173.8	21.49	100	Y
114	52.28	0.03	0	67.6	1.33	4	N
115	52.73	-0.07	1	30.4	0.99	0	N
116	53.43	0.57	12	79.8	12.76	99	Y?
117	53.62	1.64	54	3.4	18.42	100	Y
118	53.80	0.23	5	58.8	9.09	96	Y?
119	54.18	0.01	3	169.1	3.52	10	N
120	54.32	0.52	15	-115.7	15.63	99	Y?
121	55.11	-0.39	1	-31.7	1.00	1	N
122	55.26	1.04	44	15.3	23.55	100	Y
123	55.44	0.62	19	-26.6	16.11	99	Y
124	55.99	0.00	1	82.6	1.24	1	N
125	56.38	0.58	13	-149.9	12.06	99	Y
126	57.33	0.99	30	142.0	18.25	100	Y
127	57.88	0.36	6	-157.6	8.80	98	Y
128	58.03	-0.03	0	68.5	1.66	0	N
129	58.40	0.38	11	143.9	15.37	99	Y
130	58.56	1.25	64	12.5	28.51	100	Y
131	58.77	0.09	1	-22.1	5.50	59	N
132	59.43	0.02	1	61.9	4.76	26	N
133	59.65	0.13	4	-154.0	13.25	96	Y?

Candidate Experimental Modes 1-4

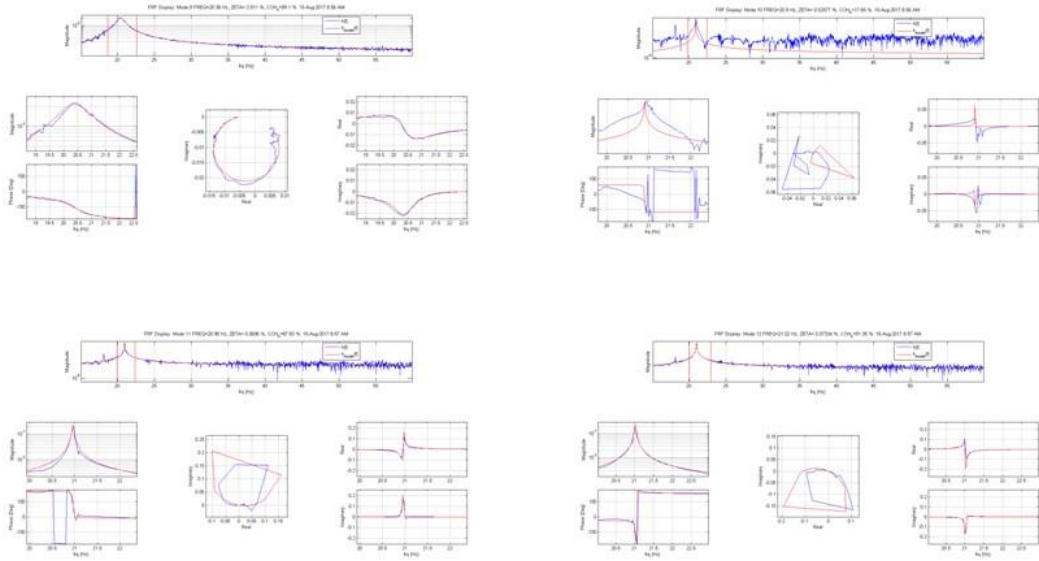


13

Candidate Experimental Modes 5-8

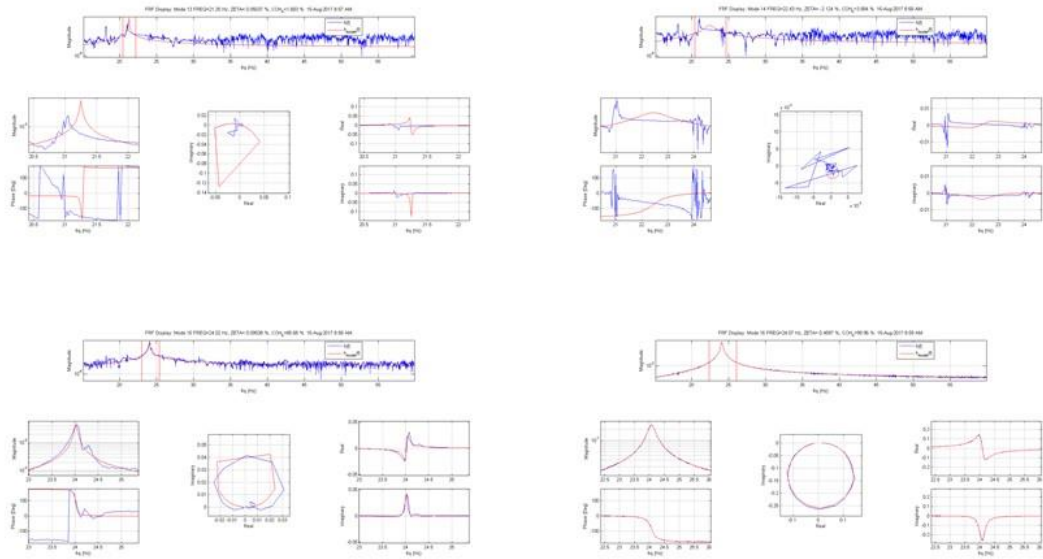


Candidate Experimental Modes 9-12



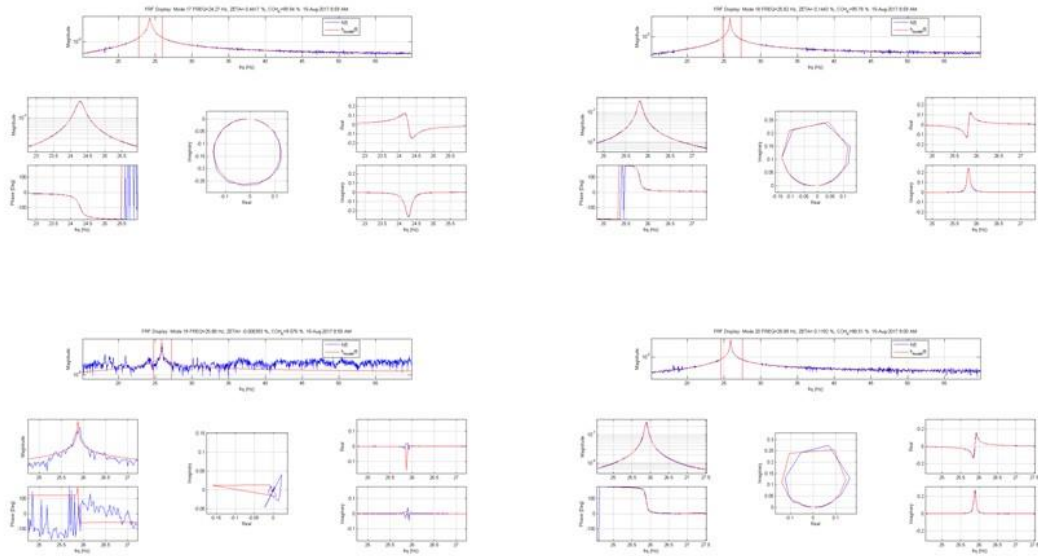
15

Candidate Experimental Modes 13-16



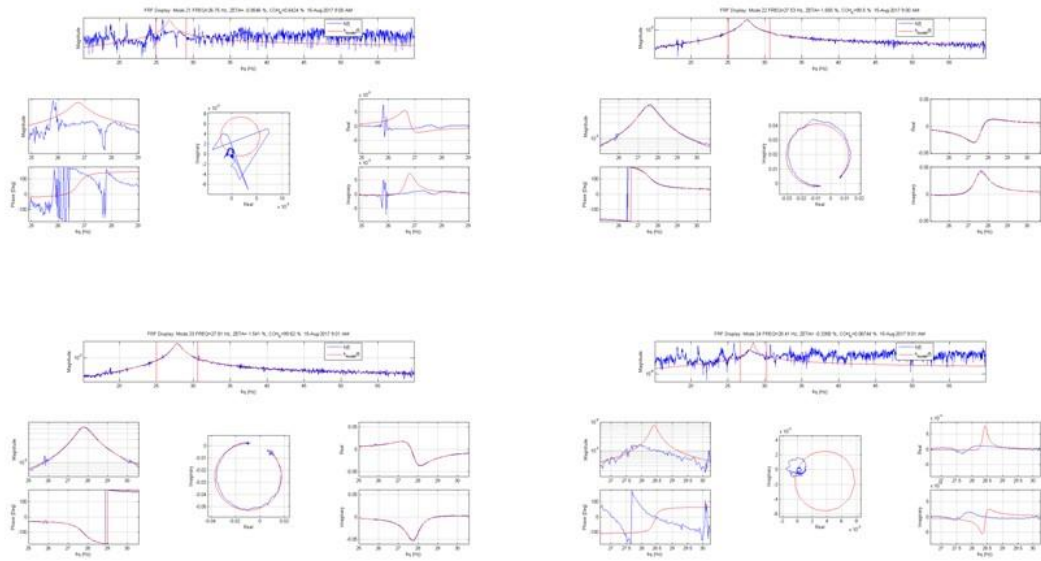
16

Candidate Experimental Modes 17-20

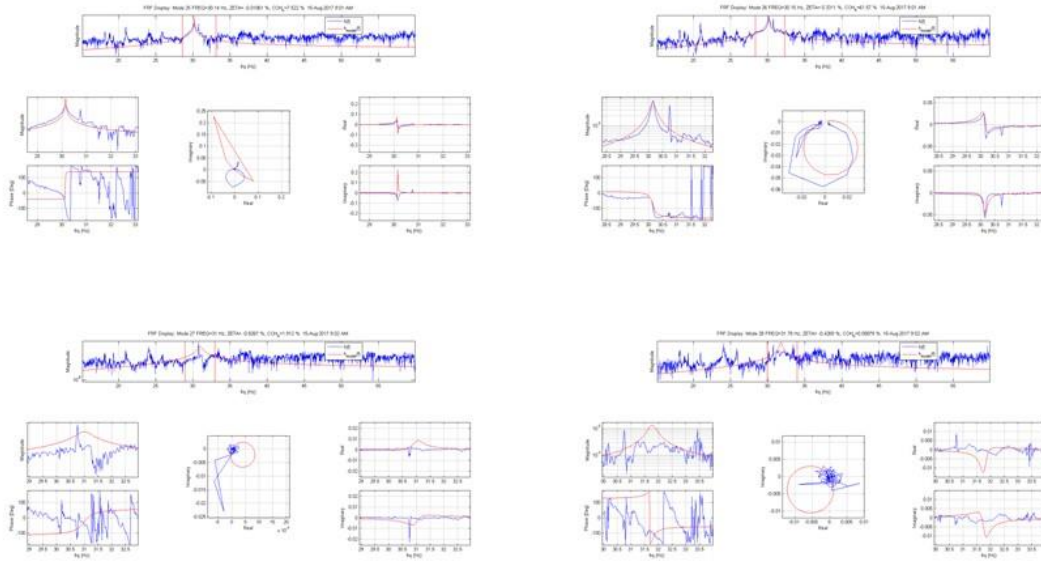


17

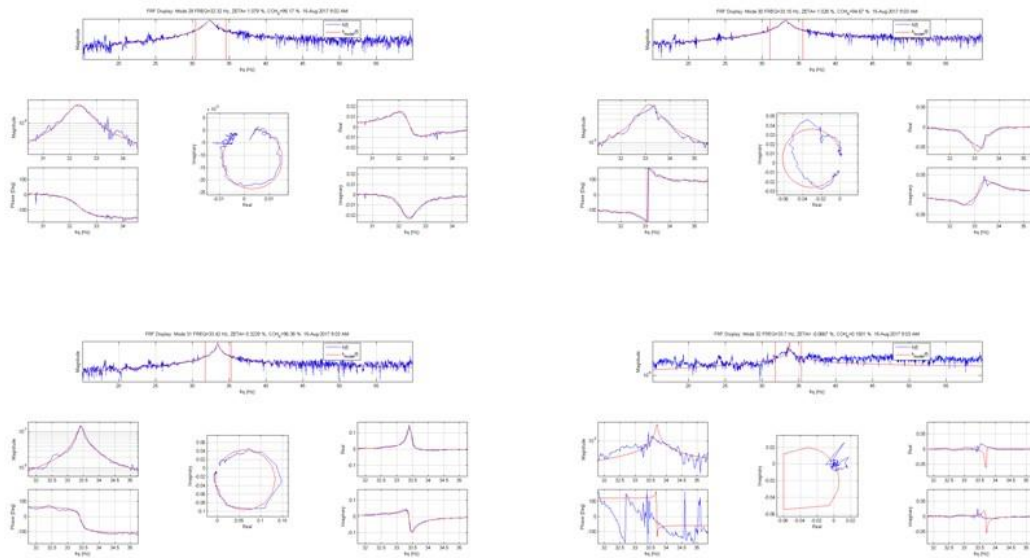
Candidate Experimental Modes 21-24



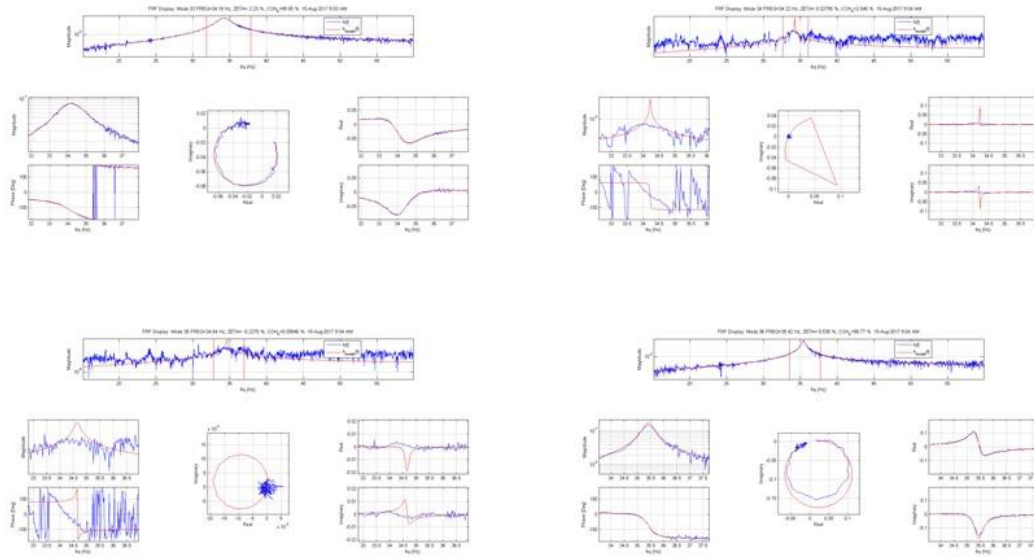
Candidate Experimental Modes 25-28



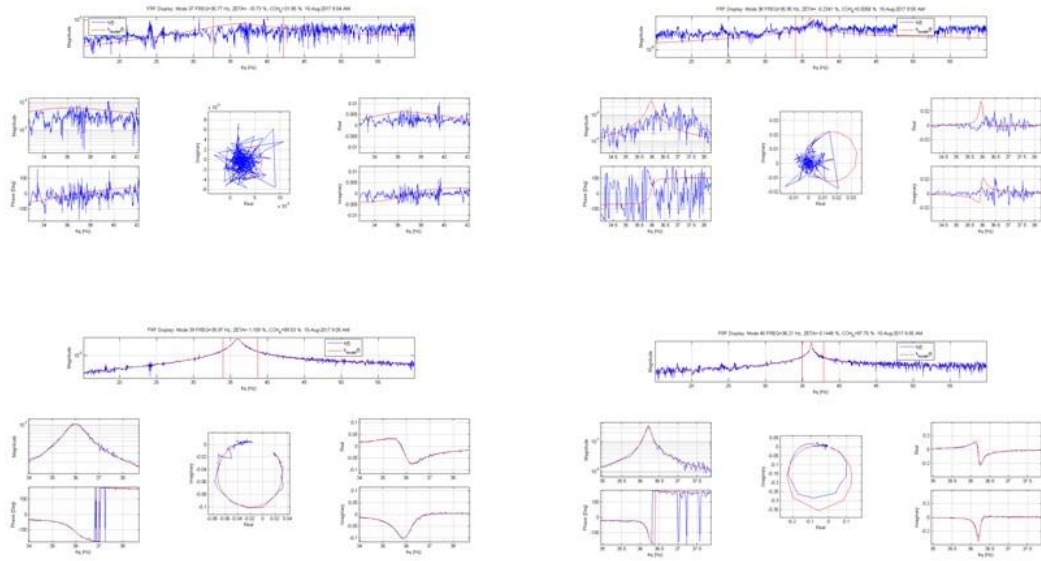
Candidate Experimental Modes 29-32



Candidate Experimental Modes 33-36

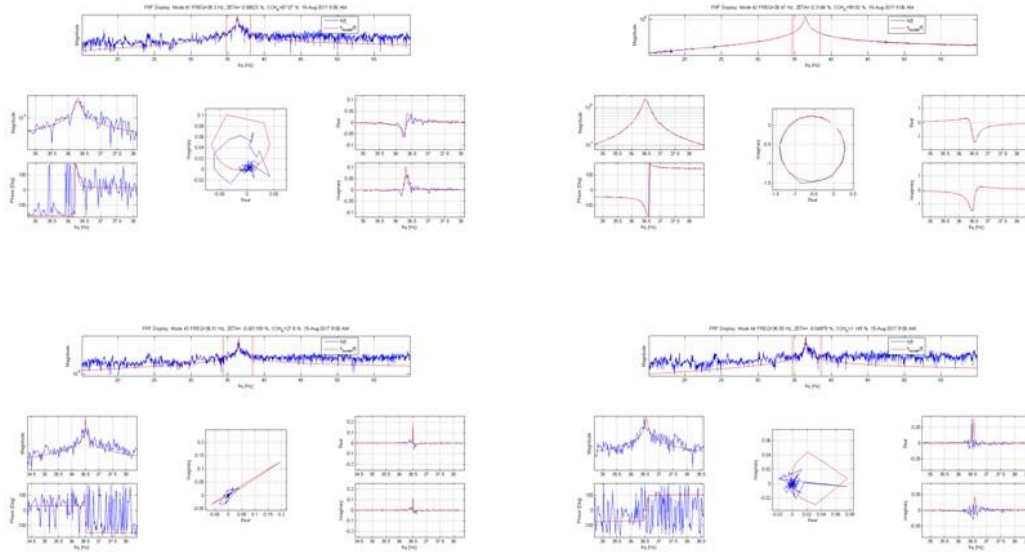


Candidate Experimental Modes 37-40



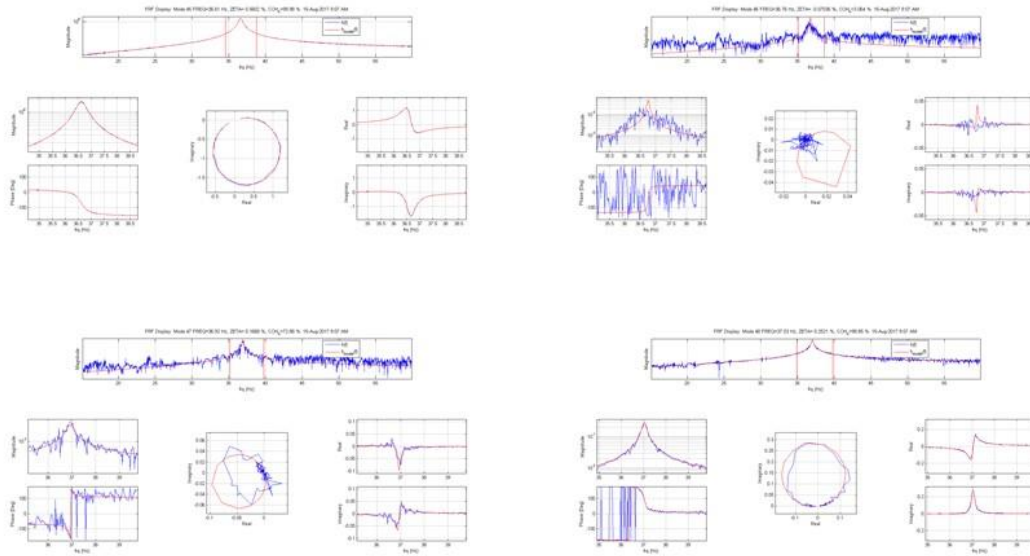
22

Candidate Experimental Modes 41-44

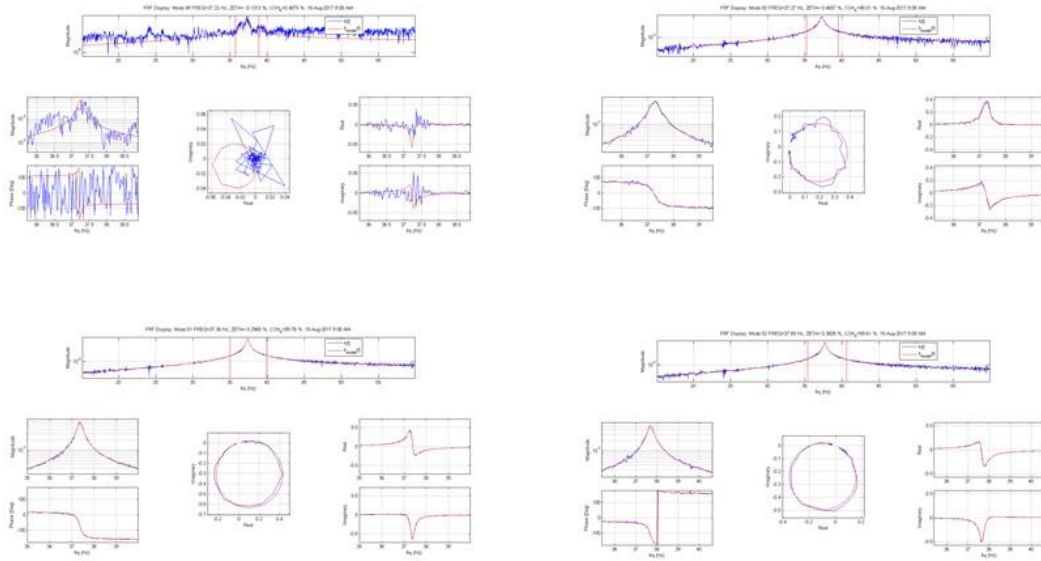


23

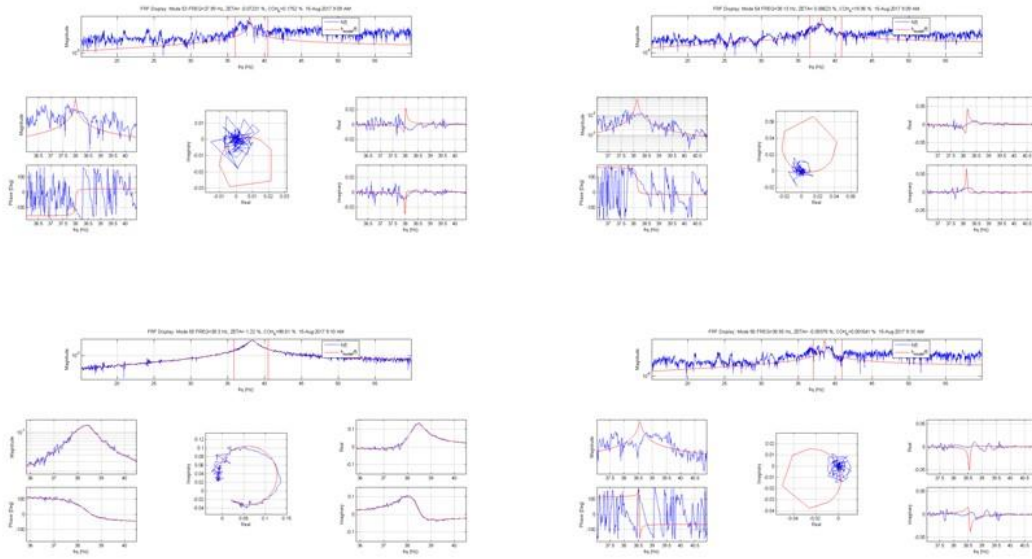
Candidate Experimental Modes 45-48



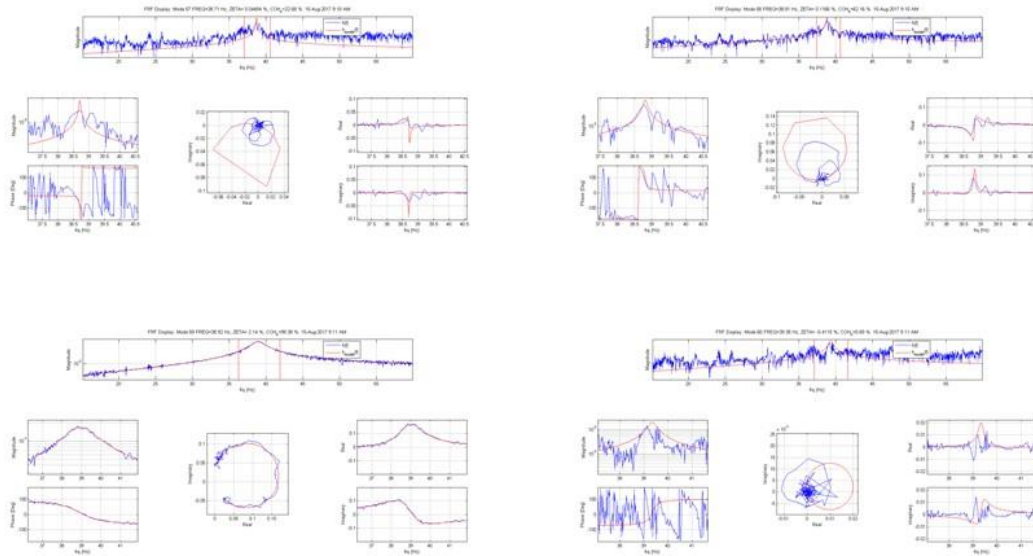
Candidate Experimental Modes 49-52



Candidate Experimental Modes 53-56

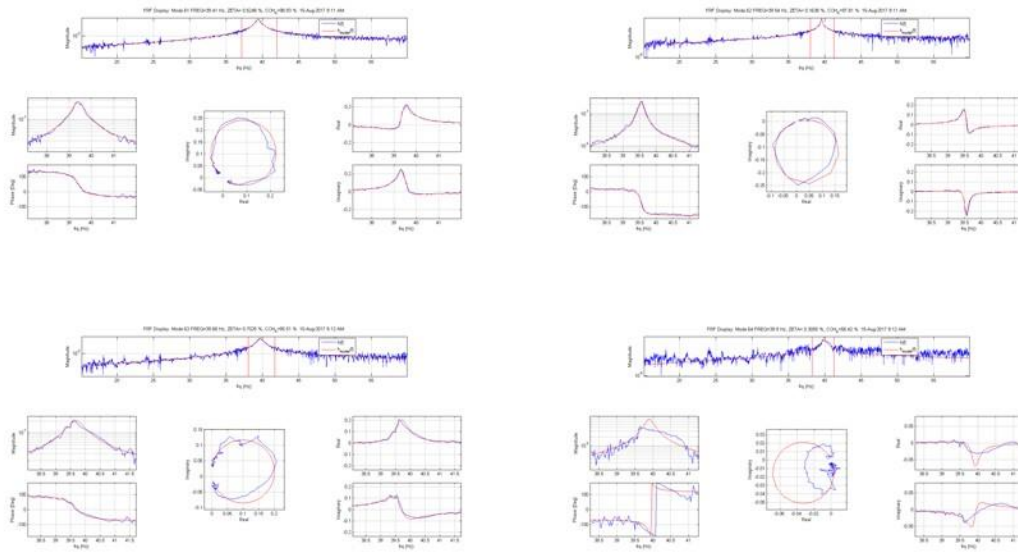


Candidate Experimental Modes 57-60



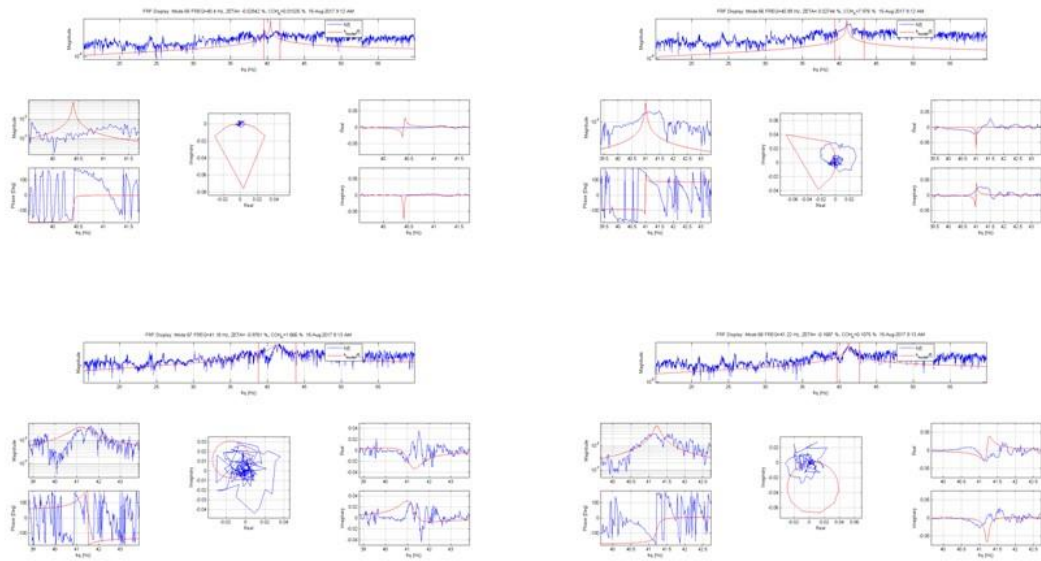
27

Candidate Experimental Modes 61-64

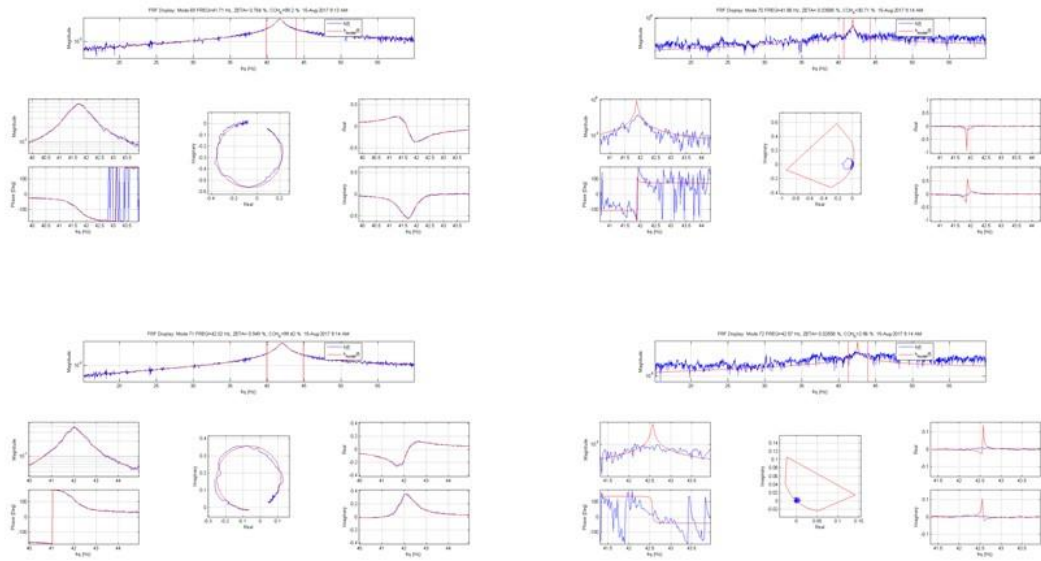


28

Candidate Experimental Modes 65-68

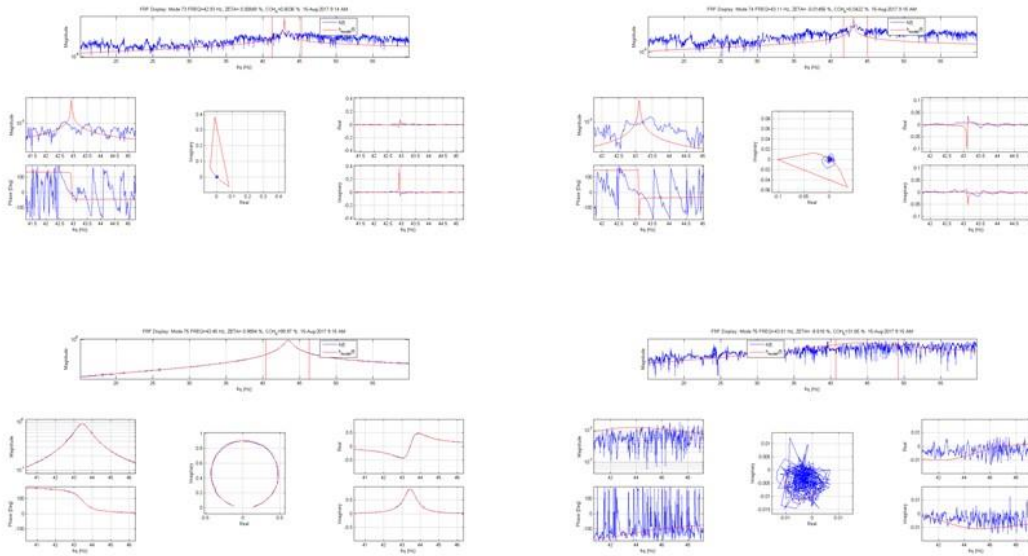


Candidate Experimental Modes 69-72



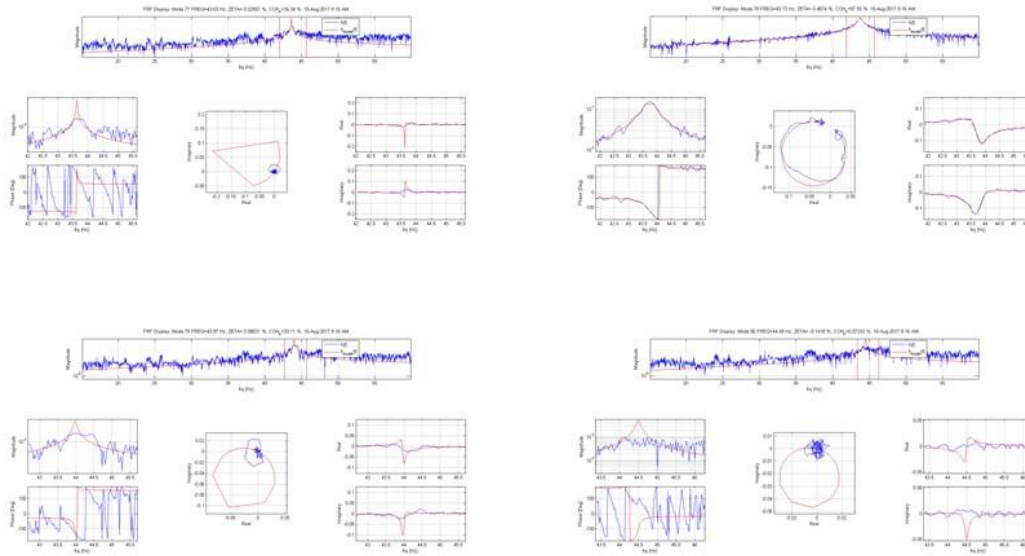
30

Candidate Experimental Modes 73-76



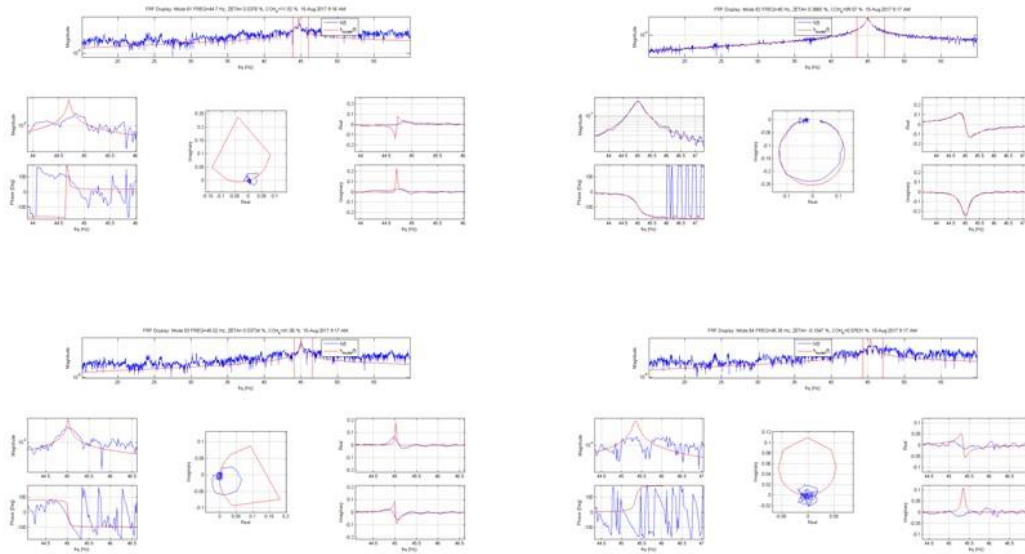
31

Candidate Experimental Modes 77-80



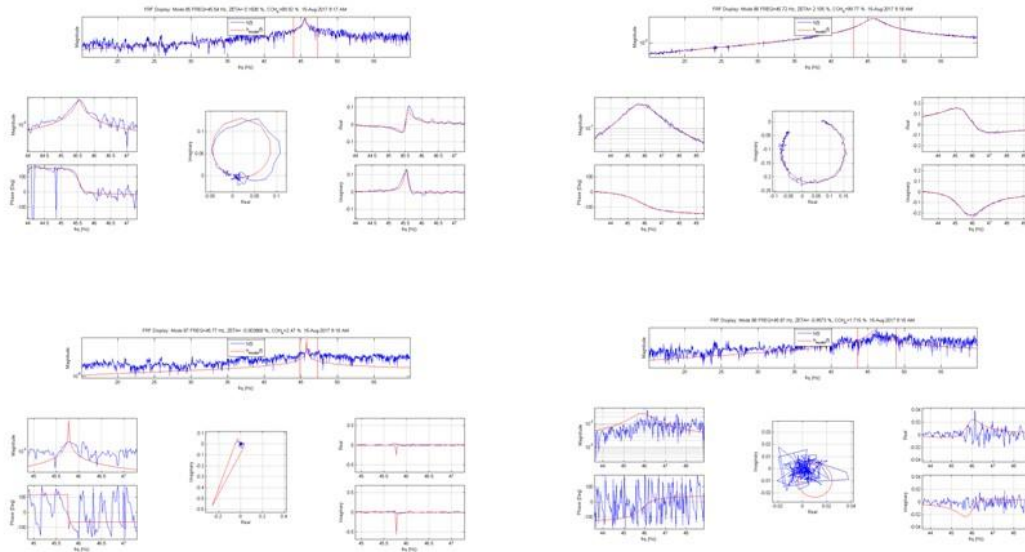
32

Candidate Experimental Modes 81-84



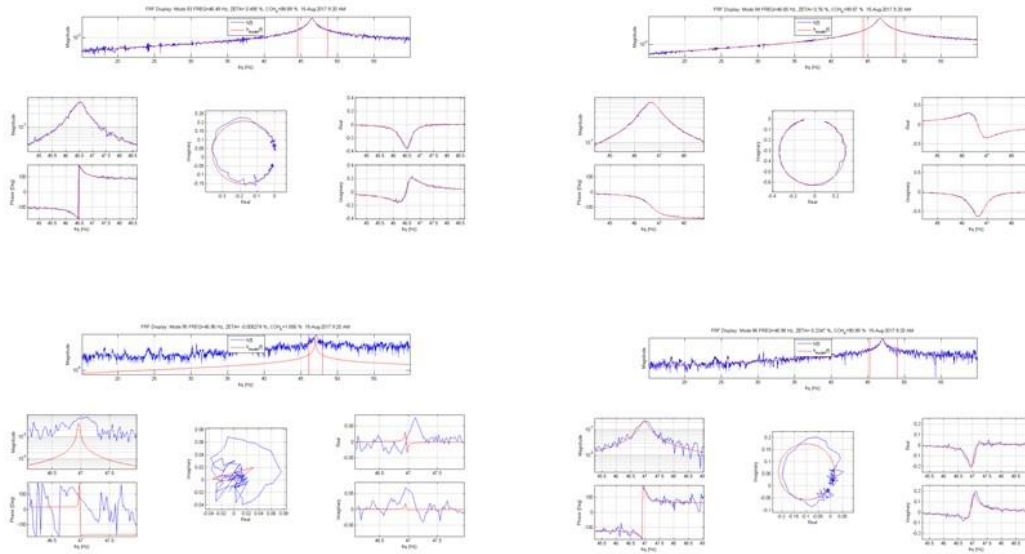
33

Candidate Experimental Modes 85-88



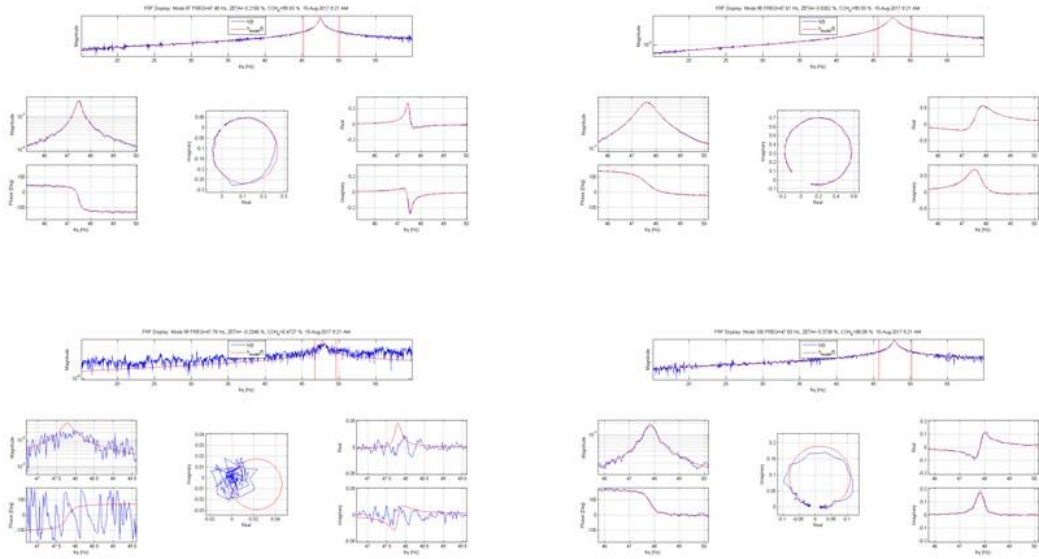
34

Candidate Experimental Modes 93-96



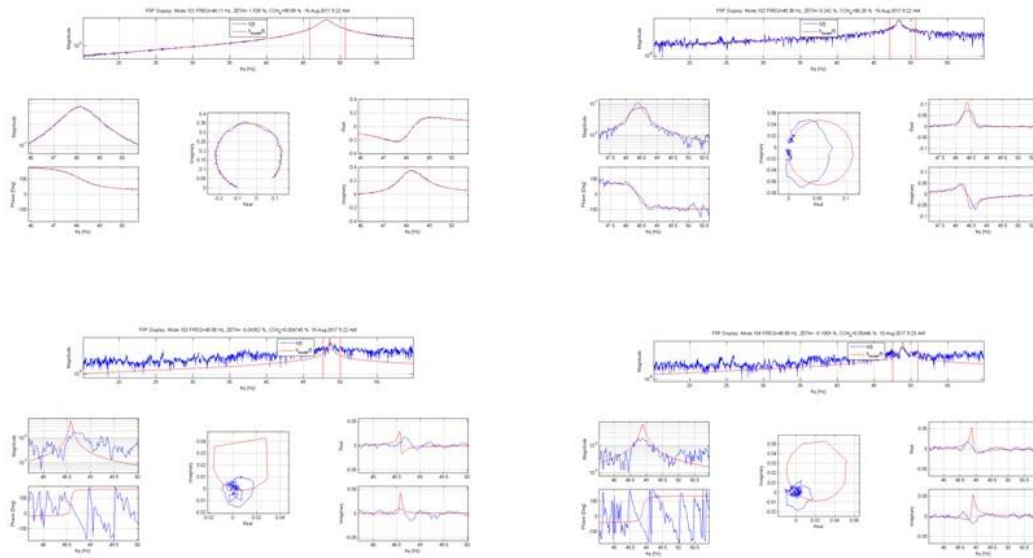
36

Candidate Experimental Modes 97-100



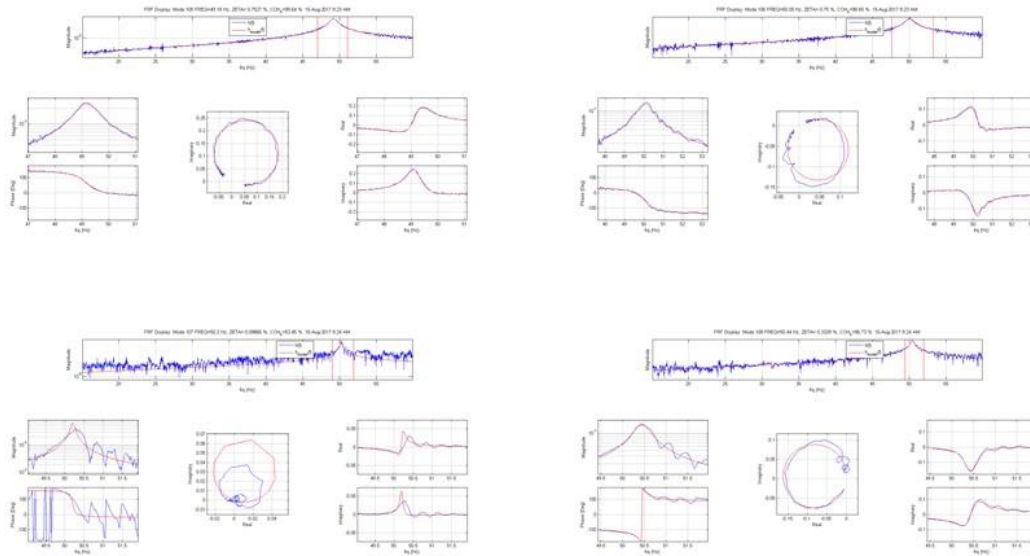
37

Candidate Experimental Modes 101-104

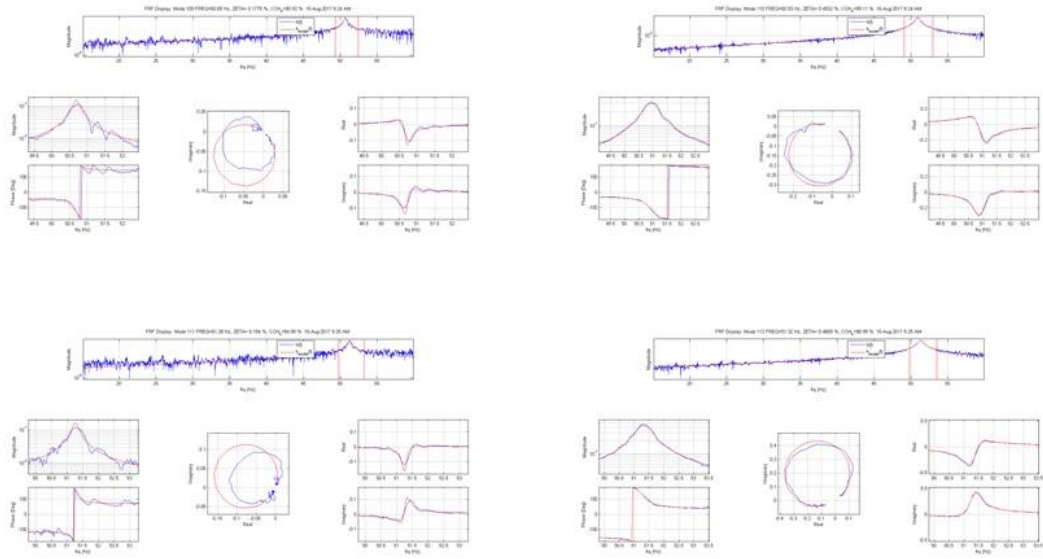


38

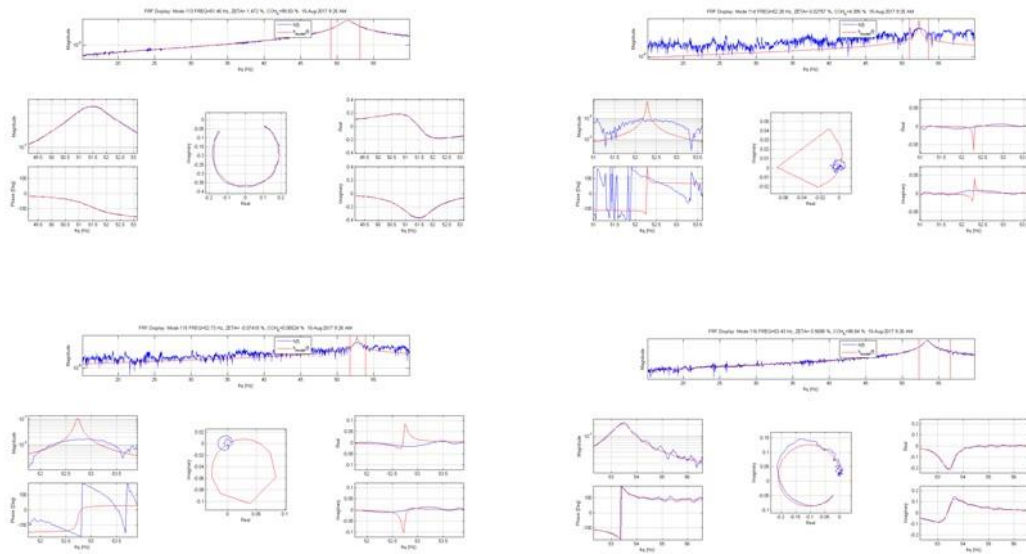
Candidate Experimental Modes 105-108



Candidate Experimental Modes 109-112

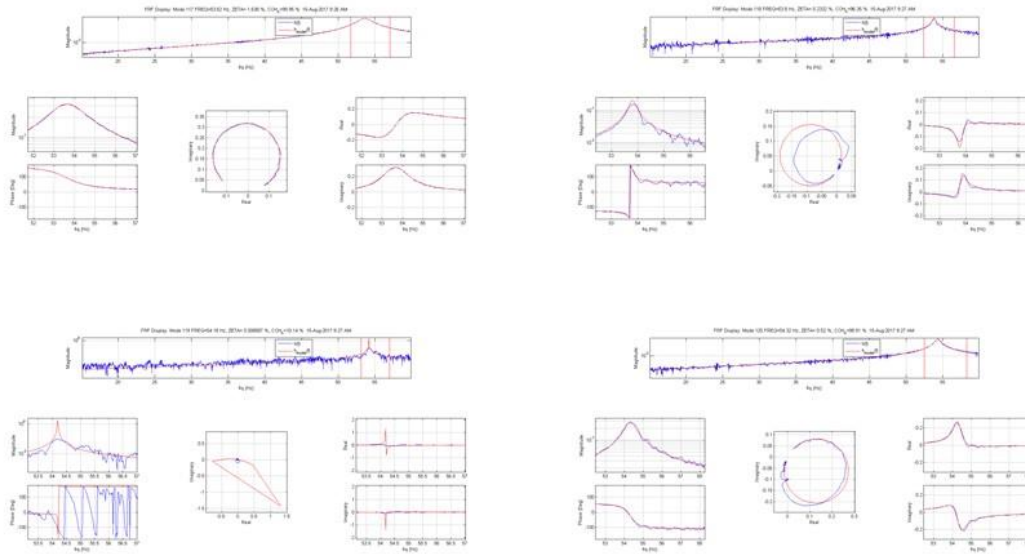


Candidate Experimental Modes 113-116



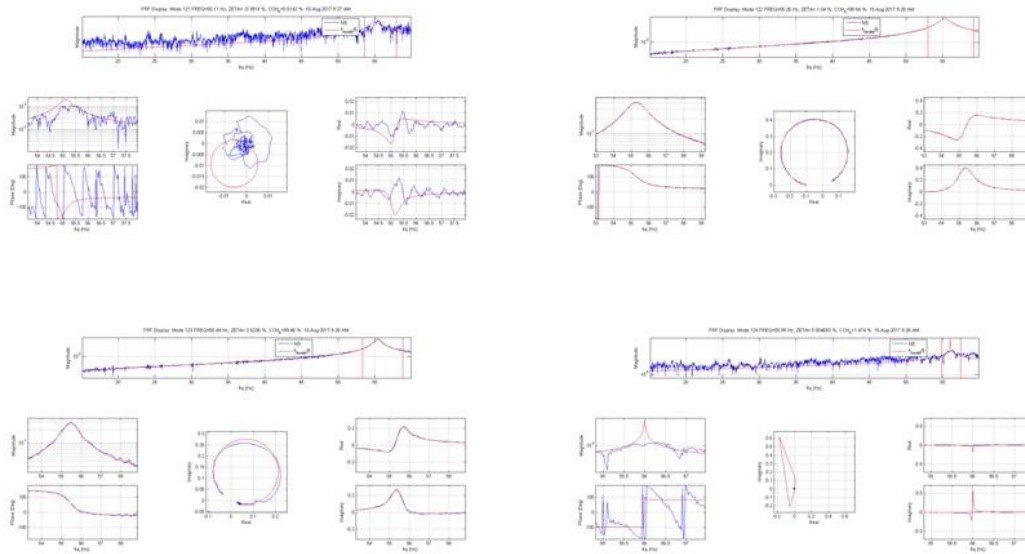
41

Candidate Experimental Modes 117-120



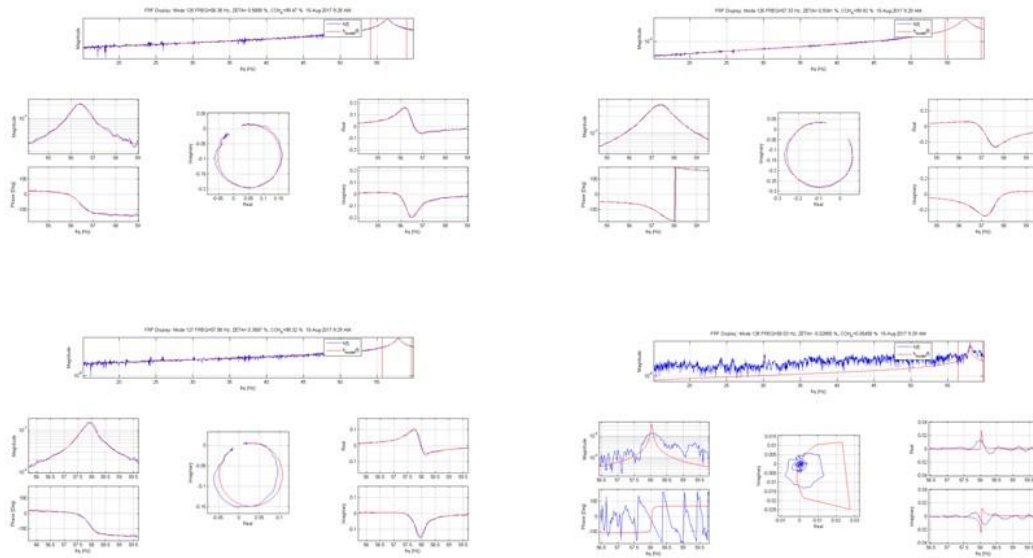
42

Candidate Experimental Modes 121-124

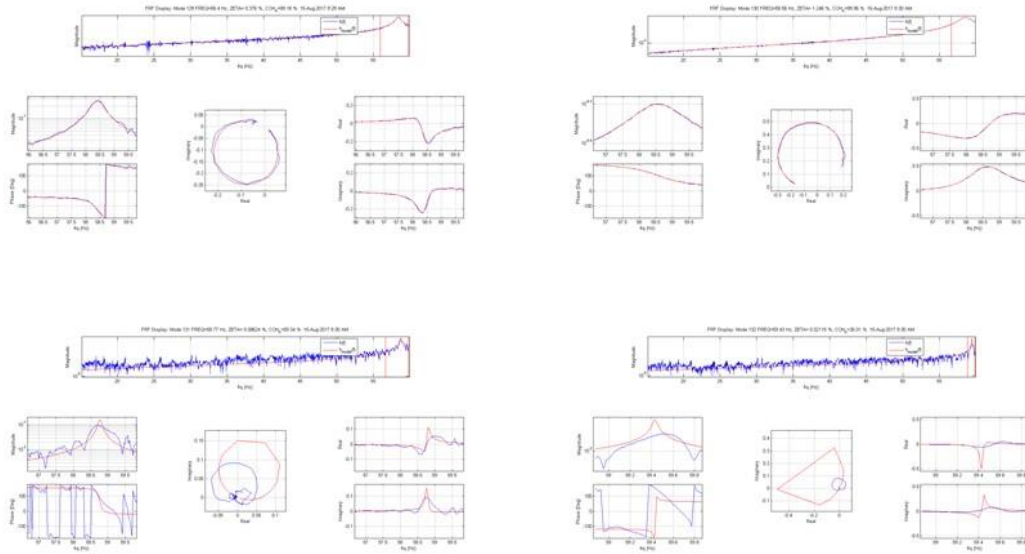


43

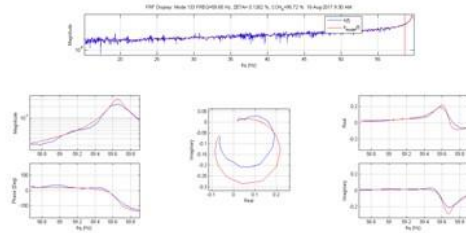
Candidate Experimental Modes 125-128



Candidate Experimental Modes 129-132



Candidate Experimental Mode 133



REPORT DOCUMENTATION PAGE

Form Approved
OMB No. 0704-0188

The public reporting burden for this collection of information is estimated to average 1 hour per response, including the time for reviewing instructions, searching existing data sources, gathering and maintaining the data needed, and completing and reviewing the collection of information. Send comments regarding this burden estimate or any other aspect of this collection of information, including suggestions for reducing the burden, to Department of Defense, Washington Headquarters Services, Directorate for Information Operations and Reports (0704-0188), 1215 Jefferson Davis Highway, Suite 1204, Arlington, VA 22202-4302. Respondents should be aware that notwithstanding any other provision of law, no person shall be subject to any penalty for failing to comply with a collection of information if it does not display a currently valid OMB control number.
PLEASE DO NOT RETURN YOUR FORM TO THE ABOVE ADDRESS.

1. REPORT DATE (DD-MM-YYYY) 01/22/2018	2. REPORT TYPE Contractor Report	3. DATES COVERED (From - To)
--	--	-------------------------------------

4. TITLE AND SUBTITLE Methodologies for Verification and Validation of Space Launch System (SLS) Structural Dynamic Models Appendices	5a. CONTRACT NUMBER NNL12AA09C
	5b. GRANT NUMBER
	5c. PROGRAM ELEMENT NUMBER

6. AUTHOR(S) Coppolino, Robert N.	5d. PROJECT NUMBER
	5e. TASK NUMBER
	5f. WORK UNIT NUMBER 869021.03.07.01.03

7. PERFORMING ORGANIZATION NAME(S) AND ADDRESS(ES) NASA Langley Research Center Hampton, VA 23681-2199	8. PERFORMING ORGANIZATION REPORT NUMBER
---	---

9. SPONSORING/MONITORING AGENCY NAME(S) AND ADDRESS(ES) National Aeronautics and Space Administration Washington, DC 20546-0001	10. SPONSOR/MONITOR'S ACRONYM(S) NASA
	11. SPONSOR/MONITOR'S REPORT NUMBER(S) NASA/CR-2018-219800/Vol II

12. DISTRIBUTION/AVAILABILITY STATEMENT
Unclassified - Unlimited
Subject Category 16 Space Transportation and Safety
Availability: NASA STI Program (757) 864-9658

13. SUPPLEMENTARY NOTES
This report was prepared for the NASA Engineering and Safety Center by Measurement Analysis Corporation, Reston, Virginia. under NASA contract number NNL12AA09C.

14. ABSTRACT
Verification and validation (V&V) is a highly challenging undertaking for SLS structural dynamics models due to the magnitude and complexity of SLS subassemblies and subassemblies. Responses to challenges associated with V&V of Space Launch System (SLS) structural dynamics models are presented in Volume I of this paper. Four methodologies addressing specific requirements for V&V are discussed. (1) Residual Mode Augmentation (RMA). (2) Modified Guyan Reduction (MGR) and Harmonic Reduction (HR, introduced in 1976). (3) Mode Consolidation (MC). Finally, (4) Experimental Mode Verification (EMV). This document contains the appendices to Volume I.

15. SUBJECT TERMS
Verification and Validation; Space Launch System; Residual Mode Augmentation; Modified Guyan Reduction; Mode Consolidation; Experimental Mode Verification

16. SECURITY CLASSIFICATION OF:			17. LIMITATION OF ABSTRACT	18. NUMBER OF PAGES	19a. NAME OF RESPONSIBLE PERSON	
a. REPORT	b. ABSTRACT	c. THIS PAGE			STI Help Desk (email: help@sti.nasa.gov)	
U	U	U	UU	238	19b. TELEPHONE NUMBER (Include area code) (443) 757-5802	